

A doctoral thesis

Development of porous biomaterials prepared
by using spontaneous emulsification

Shinnosuke NISHIMURA

Tokyo University of Agriculture and Technology

<u>Chapter 1</u>	
<u>Introduction of emulsions and porous materials: Basic theory and their applications as a biomaterial</u>	1
1. Emulsions and its applications	1
1.1. The basic theory of emulsions	1
1.2. Application of emulsions	2
1.2.1. <i>O/w emulsions as drug carrier</i>	2
1.2.2. <i>Solvent evaporation</i>	4
1.2.3. <i>Pickering emulsions</i>	4
1.2.4. <i>Emulsion polymerization</i>	4
1.2.5. <i>Salting-out</i>	5
2. Low energy emulsification	5
2.1. Phase inversion method	5
2.1.1. <i>PIT method</i>	6
2.1.2. <i>PIC method</i>	7
2.2. Spontaneous emulsification	7
2.2.1. <i>Ouzo effect</i>	8
2.2.2. <i>Spontaneous emulsification with polymers</i>	9
2.3. Application of spontaneous emulsification for microparticle preparation	10
2.3.1. <i>Spontaneous emulsification-solvent diffusion (SESD)</i>	10
2.3.2. <i>Porous particles</i>	10
3. Porous Materials used in the medical field	13
3.1. Porous particles	13
3.1.1. <i>Tissue regeneration scaffold</i>	13
3.1.2. <i>High speed chromatography</i>	14
3.1.3. <i>Drug carrier for pulmonary delivery</i>	15
3.2. Two-dimensional porous materials	18
3.2.1. <i>Scaffold for tissue regeneration</i>	18
3.2.2. <i>Cell culture substrate</i>	19
3.2.3. <i>Drug delivery systems</i>	21
3.2.4. <i>Biosensors</i>	21
3.2.5. <i>Membrane for material separation</i>	22
3.3. Porous microneedle	22
3.3.1. <i>Biological fluid collectors</i>	23
3.3.2. <i>Drug delivery</i>	23

4. The aim of this thesis	24
----------------------------------	-----------

5. References	26
----------------------	-----------

Chapter 2

<u>Preparation of the porous particles prepared via spontaneous emulsification and evaluation of the aerodynamic performance of the particles for pulmonary delivery</u>	41
---	-----------

1. Introduction	41
------------------------	-----------

2. Materials and Methods	42
---------------------------------	-----------

2.1. Materials	43
----------------	----

2.2. Synthesis of methoxy-terminated PEG-PLA	43
--	----

2.3. Preparation of the porous and non-porous PLGA particles	43
--	----

2.4. Observation of the surface morphology of the porous and non-porous PLGA particles	44
--	----

2.5. Determination the amount of the RFP loaded on the particles	44
--	----

2.6. Determination of the tapped density of the porous and non-porous PLGA particles	44
--	----

2.7. Evaluation of in vitro aerosol-dispersion performance of the porous and non-porous PLGA particles	45
--	----

2.8. Observation of the morphology of the particles after inhalation	47
--	----

3. Results and Discussion	47
----------------------------------	-----------

3.1. Characterization of synthesized methoxy-terminated PEG-PLA	47
---	----

3.2. The morphology of the porous and non-porous particles	48
--	----

3.3. Determination the quantity of RFP in the porous and non-porous particles	49
---	----

3.4. Determination of the tapped density of the porous and non-porous particles	50
---	----

3.5. In vitro aerosol dispersion performance of the porous and non-porous particles	51
---	----

3.6. Observation of the porous and non-porous particles after inhalation	55
--	----

4. Conclusions	60
-----------------------	-----------

5. References	60
----------------------	-----------

Chapter 3

<u>Effect of the composition of organic solvent on pore formation for porous particles prepared with emulsification-solvent evaporation method</u>	63
1. Introduction	63
2. Material and Methods	64
2.1. Materials	64
2.2. Measurement of the interfacial tension between water and organic solutions	64
2.3. Preparation of the multiple emulsions and porous particles	64
2.4. Observation of the morphology of the obtained emulsions and particles	65
2.5. Evaluation of the residual organic solvent	66
2.6. Determination of the composition of the porous particles	66
3. Results and Discussion	66
3.1. Interfacial tension between water and organic phase	66
3.2. Effect of the composition of TD-OS on the morphology of w/o/w emulsions	67
3.3. Effect of the composition of TD-OS on the surface morphology and internal structure of the resulting particles	69
3.4. Effect of solvent evaporation rate on the morphology of the particles	72
3.4.1. <i>Liquid-gas interfacial area</i>	72
3.4.2. <i>Temperature</i>	74
3.5. Evaluation of solvent evaporation rate	76
3.5.1. <i>Monitoring the amount of the residual organic solvent with GC-MS</i>	76
3.5.2. <i>Comparison of solvent evaporation rate with UV-vis spectrophotometer</i>	77
3.6. Strategy to control the surface and internal morphology of porous particles	79
4. Conclusion	81
5 References	81
<u>Chapter 4</u>	
<u>Establishment of a novel method for preparing a film-type biomaterial with highly porous structure by using spontaneous emulsification</u>	85
1. Introduction	85

2. Material and Methods	86
2.1. Materials	86
2.2. Preparation of the polymeric films on the surface of water	86
2.3. Observation of the surface morphology of the films	86
2.4. Observation of the internal structure of the films	87
2.5. Determination of the composition of the porous films	87
2.6. Evaluation of the effect of temperature and humidity on the morphology of the films	87
3. Results and Discussion	87
3.1. Observation of the appearance and the morphology of the films	88
3.2. Evaluation of the composition of the porous films	90
3.3. Effect of the combination of hydrophobic block and material-forming polymer on the morphology of the materials	91
3.4. Effect of temperature on the morphology of the films	92
3.5. Effect of humidity on the morphology of the films	94
4. Conclusion	98
5 References	99
<u>Chapter 5</u>	
<u>General conclusion of this thesis</u>	102
<u>Acknowledgement</u>	105

Chapter 1

Introduction of emulsions and porous materials: Basic theory and their applications as a biomaterial

This doctoral thesis is a study to propose a novel material preparation method using specific emulsification technique and to evaluate the feasibility of applying the obtained materials as a biomaterial. In this chapter, the methods for preparing materials through emulsification are introduced and the possibility of applying these materials as biomaterials is described.

1. Emulsions and its applications

1.1. The basic theory of emulsions

An emulsion is a state in which one immiscible liquid that is not soluble in each other is dispersed in the other as small droplets. The interfacial free energy G exists at the interface between these immiscible liquids, which can be expressed as follows,

$$G = \gamma S \quad (\text{Eq. 1})$$

Where γ is the interfacial tension and S is the total area of the interface. Emulsions can be formed by artificially applying energy, such as high speed agitation or sonication. In this case, however, the dispersed phase exists as droplets, which results in large S ; that is thermodynamically unstable because of high energy state of the entire system. Therefore, the system would spontaneously separate into two phases again when the system is statically placed after emulsification. In order to maintain this thermodynamically unstable emulsion state, a surfactant is needed. Surfactants are oriented at the interface between the two immiscible liquids, thereby decreasing the interfacial tension γ and keeping the interfacial free energy G low even with an increase in S . In such a system, emulsions can be kept static to inhibit the coalescence of the droplets and maintain the dispersion state. In order to apply emulsions for our life, it is common to prepare emulsions by water and organic solvents that are immiscible with water. Such emulsions have several types depending on whether the water or organic phase is the dispersed phase (Fig. 1).

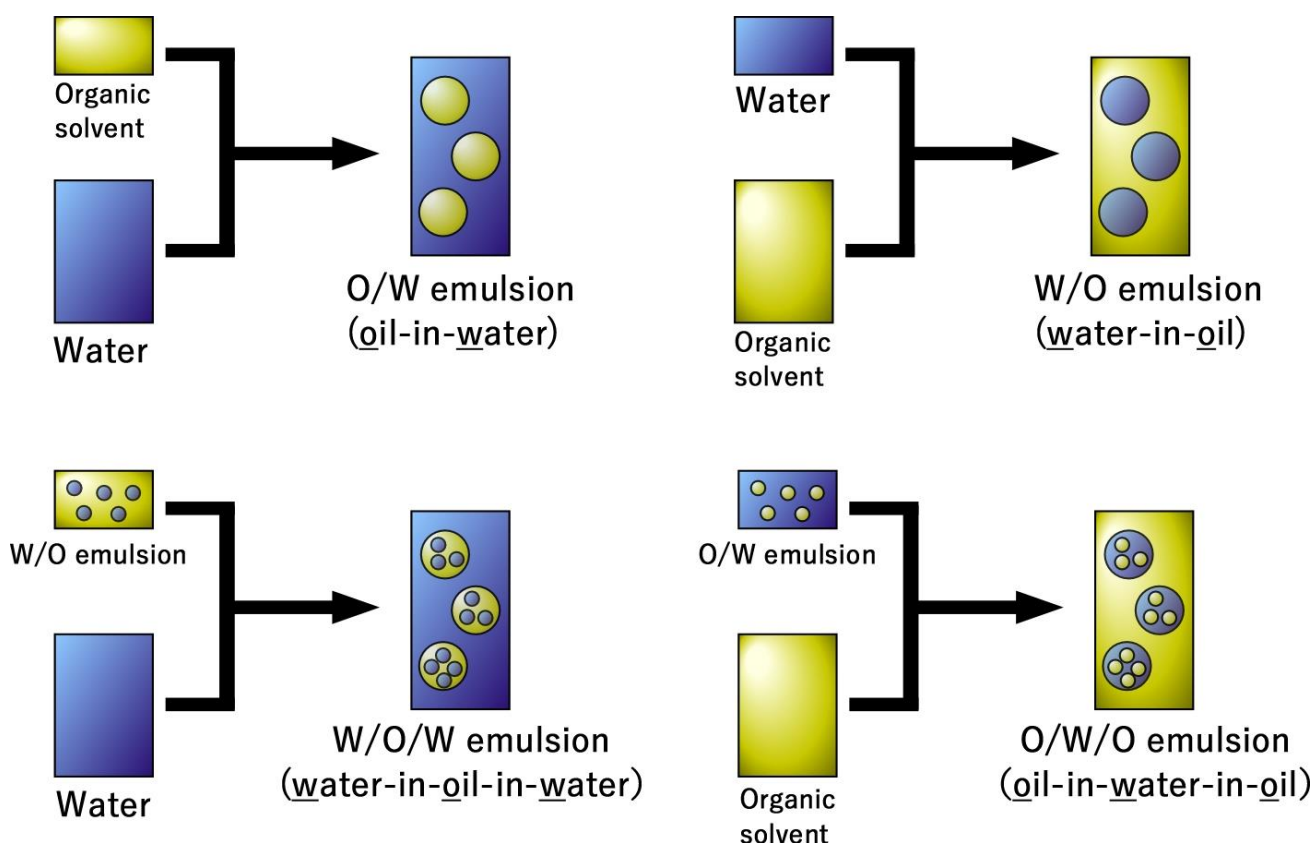


Fig. 1 Types of emulsions composed of water and organic solvent.

1.2. Application of emulsions

Emulsions have been used for cosmetics and food products for a long time, and they have also been applied to the medical field by using emulsions as templates for further processing. The following will introduce some examples of such applications and methods for preparing nano- or microcarrier of compounds.

1.2.1. *O/w emulsions as drug carrier*

It is difficult to incorporate nutraceutical encapsulations into foods with high water content because most nutraceutical encapsulations are hydrophobic molecules. Therefore, encapsulation in o/w emulsions is an effective approach (Fig. 2 (a)) [1,2]. As an example, β -carotene, a type of provitamin A, has been studied for incorporation into foods in o/w emulsions due to its low water solubility [3]. However, in o/w emulsions protected by an outer layer composed of only surfactants, it is difficult to prevent chemical degradation of β -carotene due to environmental stresses such as heat, free radicals, light, and oxygen [4]. Therefore, some improved approaches to inhibit the degradation of β -carotene by multi-layered protection of emulsion droplets by macromolecules of opposite charge, such as “chitosan and milk-protein” [5] and “lactoferrin and β -lactoglobulin” [6], have been proposed. Some cationic surfactants such as lauric arginate [7] and essential oil components [8,9] are known to have antibacterial properties. However, their antimicrobial activity is lost when they bind to anionic polymers such as pectin [7], so their use as

surfactants oriented to emulsions is expected to enable them to maintain their activity and to be delivered into the body. In recent years, it has been found that high antibacterial activity can be obtained in systems with electrostatic complexes formed by using several surfactants [2,10–12].

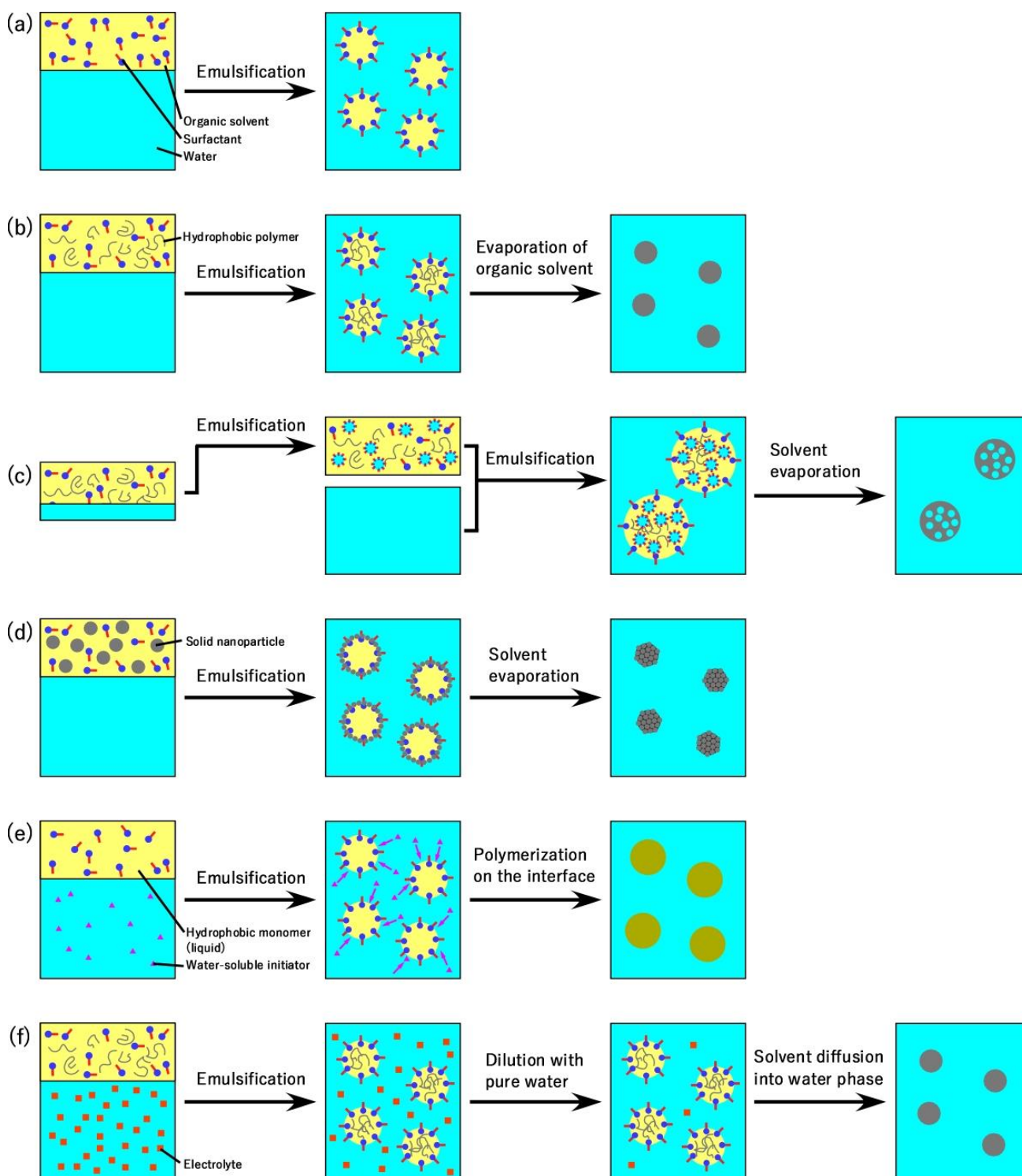


Fig. 2 Various preparation methods for nano- or micro-carrier: (a) emulsification for o/w emulsion, (b), emulsion-solvent evaporation for spherical particle, (c), double emulsion-solvent evaporation for porous particle, (d) pickering emulsion, (e) emulsion polymerization, and (f) salting-out.

1.2.2. Solvent evaporation

In solvent evaporation, polymer nano or microspheres are obtained by dispersing a polymer solution in the continuous phase and subsequent evaporation of the solvent of polymer (Fig. 2 (b)). Since volatile solvents are needed as the dispersion phase solvent in order to remove from the system, o/w type emulsions are generally used for this method [13–15]. Hydrophobic drugs are encapsulated in the resulting polymer particles by dissolving the drug in the organic solvent. It has been suggested that the efficiency of drug encapsulation and release rate from the particles depends on the rate of solvent evaporation; Izumikawa *et al.* reported that the faster the solvent was removed, the lower the crystallinity of the particle-forming polymer, polylactic acid (PLA), resulting in the formation of particles with higher drug encapsulation efficiency and slower release rate [16].

On the other hand, nano or microspheres formed from o/w emulsions are not suitable for encapsulating hydrophilic substances such as peptides and proteins. Therefore, “double emulsion-solvent evaporation” method was proposed (Fig. 2 (c)) [17,18]. In this method, $w_1/o/w_2$ emulsions (w_1 : inner water phase; w_2 : outer continuous water phase) are prepared by emulsifying pure water and w_1/o emulsions which are composed of organic polymer solution and aqueous drug solution. After preparing them, the organic solvent is removed from $w_1/o/w_2$ emulsions and the hydrophilic drug is encapsulated in the hydrophobic particles. The particles prepared via this method are generally porous ones because w_1 phase works as porogens.

1.2.3. Pickering emulsions

Pickering emulsions are emulsions containing solid particles working as stabilizers (Fig. 2 (d)). The solid particles accumulate on the water-oil interface, which inhibits the coalescence of emulsion droplets, resulting in increasing their stability [19]. Various functions can be given to the surface of emulsion by using various materials of which solid particles are composed. For example, pickering emulsions coated by chitosan, cyclodextrin, silica or starch have been reported as a drug carrier because the solid particles work as a dense barrier which controlled the release rate of the encapsulated compounds [20,21]. Hydroxyapatite particles, which is part of the components of bone, has been applied as a bone regeneration scaffold [22]. By using cyclodextrin, which is one of the host molecules for including a specific molecule, or light-responsive inorganic particles, catalytic microparticles can be obtained [23,24]. Thus, the advantage of pickering emulsions is that they can be given various functions depending on the materials of solid particles.

1.2.4. Emulsion polymerization

The preparation methods for microparticles introduced so far using aggregation of pre-synthesized polymers by increasing the concentration of them through diffusion and evaporation of organic solvents. In contrast, “emulsion polymerization” is a method of which polymers are synthesized on the water-oil interface and subsequently formed microparticles in the process (Fig. 2 (e)) [25,26]. It generally consists of water, a water-immiscible monomer, a water-soluble initiator, and a surfactant. After the preparation of the emulsion, polymerization begins when the

monomer molecules in the dispersed phase collide with the initiator molecules in the ionic or free radical state at the water-oil interface. The solvent evaporation method uses biodegradable polymers such as PLA as particle forming agents, while styrene and methyl methacrylate are often used in this method. More recently, the system not containing any surfactant, has also been proposed [27,28]. “Surfactant-free emulsion polymerization” uses ionizable initiators and ionic monomers to stabilize the emulsions without surfactants and to reduce the cost by eliminating the process of removing surfactants from the particles after polymerization [27,28]. However, there are still challenges such as monodisperse and precisely controlled particle sizes [29].

1.2.5. Salting-out

Since the solvent evaporation method uses volatile and water-immiscible organic solvents such as dichloromethane and chloroform, it is necessary to pay attention to the amount of residual solvents because of their toxicity. Therefore, the salting-out method was devised to obtain nano or microparticles using less toxic solvents such as acetone (Fig. 2 (f)) [30–32]. Acetone is essentially a water-miscible solvent and therefore cannot form emulsions with water. However, its miscibility can be adjusted by dissolving a high concentration of salt in water. In other words, it is possible to prepare o/w emulsions with acetone as the organic phase. By diluting the resulting o/w emulsions with water, the salt concentration decreases and the acetone becomes miscible in water again, and the polymer dissolved in the acetone can be precipitated as nano or microparticles.

2. Low energy emulsification

The higher the energy applied externally, the smaller the droplet size of the emulsion. Therefore, they have been prepared by high-energy methods using mechanical devices such as high-shear agitators, high-pressure homogenizers, and ultrasonic generators. However, the energy required to obtain nano-droplets is extremely high and only a small amount (about 0.1%) of the energy generated by mechanical devices is used for emulsification [33]; that is not cost-effective way. In addition, the use of the system in the medical field remains a challenge because hydrophilic biopolymers such as nucleic acids and proteins can be easily broken by high-energy input [34]. Therefore, low energy methods that reduce the externally applied energy by using the internal chemical energy of the system have begun to be reported. Low-energy emulsification methods can be classified into two categories: the emulsification method in which the sign of the spontaneous curvature of the surfactant inverts is referred to as the phase inversion method, while the emulsification method in which no reversal of the sign occurs is referred to as spontaneous emulsification [33]. While the phase inversion method requires the application of low energy such as weak agitation in addition to changes in temperature and phase composition, spontaneous emulsification occurs by contacting two immiscible liquids in a non-equilibrium state.

2.1. Phase inversion method

Phase inversion method is an emulsification phenomenon caused by the spontaneous curvature of the non-ionic surfactant oriented at the interface changing from zero to positive or negative in a three-component system, mainly water, oil and surfactant. This method has been the most widely studied and applied among various low-energy emulsification methods since it was invented by Shinoda *et al.* in 1968 [35]. Phase inversion method can be broadly classified into two types depending on the factors that change the spontaneous curvature: the phase inversion temperature (PIT) and the phase inversion composition (PIC). The emulsification processes common to them are shown in Fig. 3. Both methods allow the formation of emulsion droplets from a dispersed state opposite to the desired emulsions via a bi-continuous phase (*i.e.*, a phase with zero average spontaneous curvature of the surfactant film) by changing phase composition or temperature.

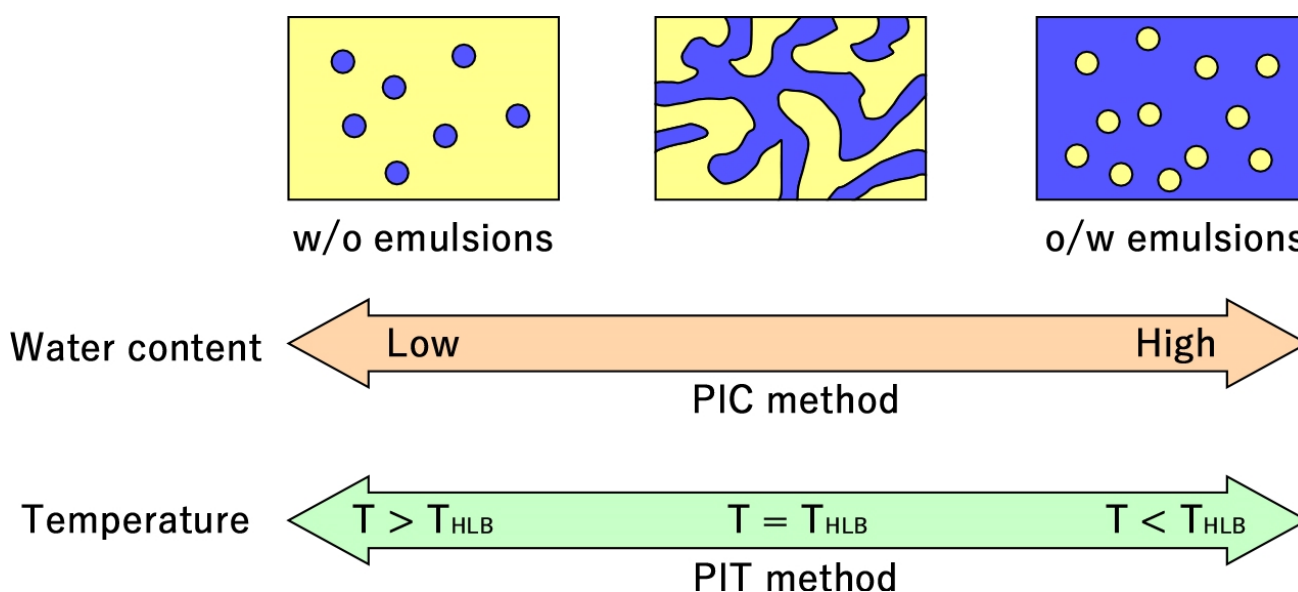


Fig. 3 Schematic illustration of the phase inversion process by PIC and PIT methods (T_{HLB} : temperature at which the average spontaneous curvature of surfactant membrane is zero).

2.1.1. PIT method

As mentioned above, PIT method is one of the most widely studied methods of low energy emulsification. However, most of the reports studied about spontaneous formation of “o/w” emulsions rather than w/o emulsions. Moreover, it is still difficult to cool the emulsions instantly when scaled up [36]. One of the few studies about “w/o” emulsions prepared by PIT methods was reported by Anton *et al.* The results demonstrated that, just as the oil-oil soluble surfactant ratio is important factor for o/w emulsions formation, the regulation of the water-water soluble surfactant ratio is also important for w/o emulsions formation via bi-continuous phase [37].

Spontaneous emulsion formation by PIT method can be modulated in terms of properties by mixing multiple surfactants. For example, the control of surface charge, transfer temperature, and size of emulsion droplets can be achieved by using a mixture of nonionic and cationic surfactants [38]. This is because the spontaneous curvature of surfactant films changes by changing the mixing ratio of hydrophilic and hydrophobic surfactants (Tween 80 and Span 80, respectively) [39,40].

2.1.2. PIC method

PIC method is a method of gradually adding the continuous phase to the surfactant-containing dispersed phase and spontaneously forming emulsion droplets once the composition of the system reaches a specific composition [41]. A detailed study by Pey *et al.* showed that by adjusting the surfactant-dispersion phase composition, a bi-continuous phase is formed in the process of adding the continuous phase and it was found to be necessary for spontaneous emulsion formation [42]. Recent examples of research aimed at the application of PIC method includes the medical field. Approximately 100 nm of poly(lactide-co-glycolide) (PLGA) particles are obtained by PIC method and subsequent solvent evaporation of o/w emulsions. The PLGA particles having various functions, such as passing through the blood brain barrier [43] and silencing a certain gene (Fig. 4) [44], were prepared by modifying the surface of the particles. On the other hand, only a few reports studied about preparing w/o emulsions by PIC method just as PIT method [45].

These phase invasion methods have been so much investigated as mentioned earlier. However, it should be noted that for polysaccharides and proteins, it is difficult to change the spontaneous curvature of the interfacial film due to the size of the molecular weight and surface charge of the polysaccharides and proteins, and no inversion emulsification using these high molecular weight materials has been reported [46].

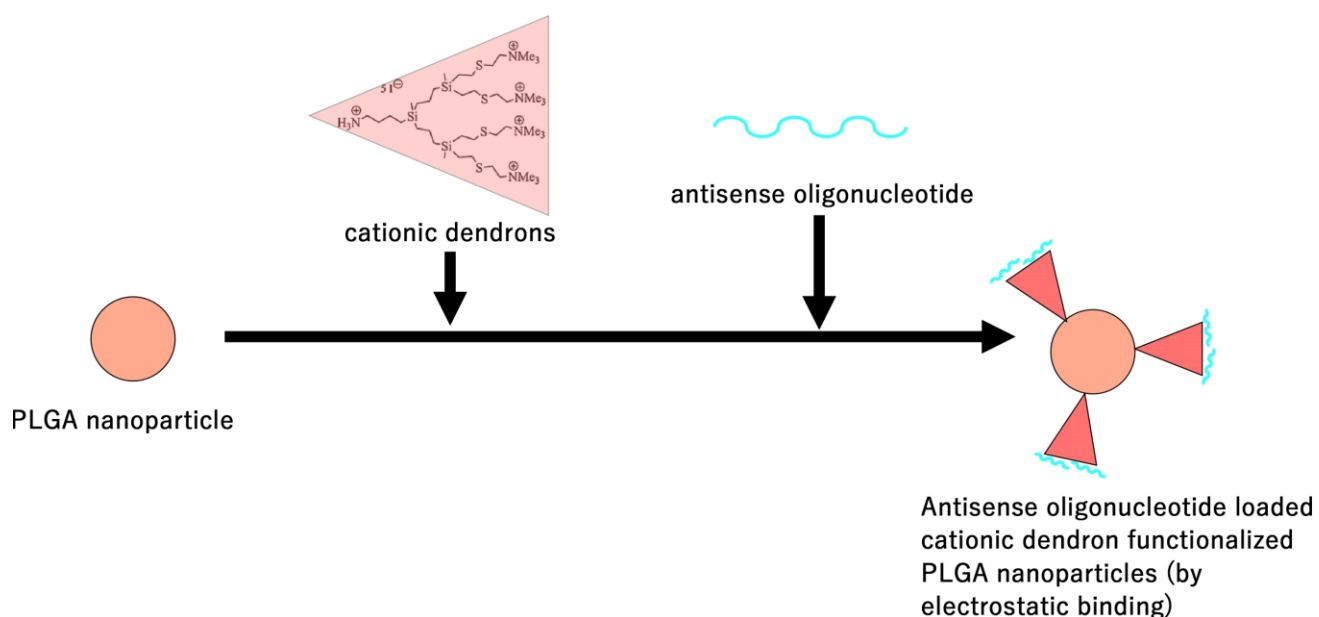


Fig. 4 Functionalized PLGA nanoparticles prepared through spontaneously formed o/w emulsions [44].

2.2. Spontaneous emulsification

The aforementioned inversion emulsification method is a phenomenon caused by a change in spontaneous curvature associated with a change in the hydration state of the hydrophilic group of the surfactant. In contrast, the phenomenon that does not involve a change in the spontaneous curvature of the surfactant is called spontaneous emulsification. Interfacial turbulence has been proposed as the main driving force of this phenomenon. The diffusion

of solute between the two phases or the non-uniformity of temperature in the system is presumed to cause turbulence at the interface. As a result of the increased turbulence, emulsion droplets might be formed [47]. This spontaneous diffusion increases the entropy and decreases the Gibbs free energy of the system. Non-uniformity of surfactant concentration near the interface of the two phases have also been proposed as a complementary driving force [48]. That is, local supersaturation of the surfactant causes the interface to spontaneously expand and induces nucleation of the droplets. The nuclei continuously grow and become emulsion droplets. Spontaneous emulsification by these mechanisms generally occurs in systems with extremely low (or negative) interfacial tensions containing surfactants. However, the systems containing co-solvents, which is miscible in both phases, instead of a surfactant can also cause spontaneous emulsification. A detailed explanation is described below.

2.2.1. Ouzo effect

The Ouzo effect, named by Vitale and Katz [49], is a self-emulsifying phenomenon in the ternary system of water, oil, and co-solvent, so to speak, "no surfactant required" process. Ouzo is an anise-flavored liquor produced in Greece and consists mainly of ethanol with a small amount of anethole dissolved in it. When water is added to this and the system reached the composition of anethole (0.1%), water (55%) and ethanol (45%), emulsions begin to be formed. In other words, the addition of water to the co-solvent with a very small amount of oil in it leads to the metastable regions, which exist in the narrow region between the binodal and spinodal curves, and the emulsions form spontaneously (Fig. 5).

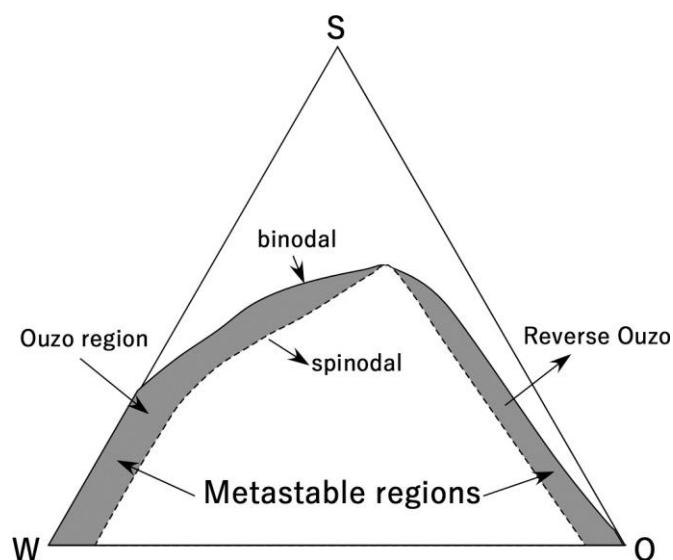


Fig. 5 Ternary phase diagram of water (W)/ co-solvent (S)/ oil (O) system at constant temperature.

The change in particle size and stability of emulsions formed by the Ouzo effect over time has been confirmed mainly by NMR spectroscopy [50,51]. Nordstierna *et al.* studied the toluene-ethanol-water ternary system in detail using light scattering and NMR diffusion simultaneously. The results showed a bimodal distribution of emulsion droplets about 100~400 nm and several μm in size [52]. This result suggests that the emulsions in the metastable state gradually separated into two phases through Ostwald ripening. Although Ouzo effect has an

advantage that spontaneous emulsification occurs with extremely low energy without surfactants, it also has a disadvantage that it often occurs in areas with a very low composition ratio of hydrophobic substances (or oil), resulting in greatly dilute o/w emulsions. Therefore, it is not an efficient method for manufacturing microparticles for drug carriers.

2.2.2. Spontaneous emulsification with polymers

Spontaneous emulsification caused by macromolecules have been reported, although the number of such report is small. Boury *et al.* reported that poly(ethylene glycol) (PEG), hydrophilic polymer, and a protein, hen egg-white lysozyme (HEWL), were dissolved in water and brought into contact with dichloromethane (DCM). As a result, o/w emulsions were spontaneously formed [53,54]. Boury's experiments showed that the amount of o/w emulsion droplets increased with increasing PEG molecular weight and that the oil phase must be a good solvent for PEG and a solvent that is not miscible or only partially miscible with water. Fig. 6 shows the images of spontaneous emulsification at various PEG and HEWL concentrations. The results revealed that the spontaneous formation of emulsions is induced by PEG and HEWL prevents the sedimentation and aggregation of the droplets. In other words, the adsorption of HEWL on the interface of the emulsion droplets increases the stability of the droplets. It was also found that the interfacial tension at the equilibrium state of the adsorption of PEG and HEWL is not negative, at least about 6.5 mN/m. Therefore, this study suggests that the main driving force for the spontaneous emulsification is the interfacial turbulence caused by the high mobility of the polymers rather than ultra-low interfacial tension.

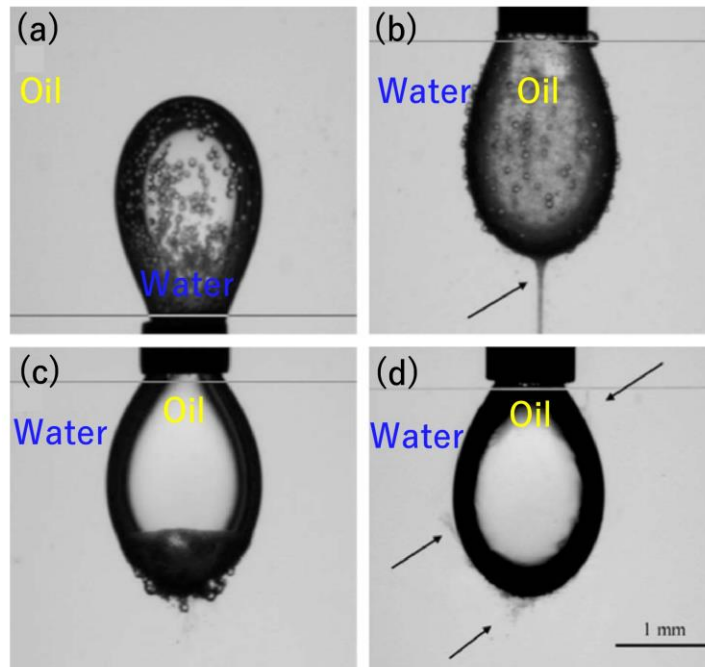


Fig. 6 Pictures of (a) a rising aqueous drop of HEWL (1 mg/mL) and PEG 2000 (10 mg/mL) immersed in DCM, (b) a pendant drop of DCM immersed in an aqueous phase of HEWL (1 mg/mL) and PEG 8000 (10 mg/mL), (c) a pendant drop of DCM immersed in an aqueous phase of PEG 2000 (10 mg/mL), and (d) a pendant drop of DCM immersed in an aqueous phase of PEG 2000 (50 mg/mL) [54].

2.3. Application of spontaneous emulsification for microparticle preparation

The low-energy emulsification method can easily prepare emulsions with the size of several hundred nanometers. In addition, a number of methods for the preparation of polymeric particles using these nano-emulsions as precursors have been proposed. Examples of these methods are presented here.

2.3.1. Spontaneous emulsification-solvent diffusion (SESD)

SESD method is based on the diffusion of polymer solutions into water [55]. A hydrophobic polymer is dissolved in a water-miscible organic solvent (or a mixture of water-soluble and water-immiscible solvent). The miscible organic solvent is diffused into the water by dropping the polymer solution into the water. In the process, the hydrophobic polymer (and the water-immiscible solvent) is immediately dispersed in the water as small droplets. This dispersion system is stirred to completely remove the organic solvent and form nano- or micro hydrophobic polymer particles. Although water miscible-water immiscible solvents such as acetone-dichloromethane mixtures have been used for a long time [56,57], recently, water miscible solvents such as acetone-alcohol mixtures have become the mainstream for the preparation of nanoparticles because of the difficulty in reducing the particle size to nanometer order due to aggregation of water immiscible solvents and the concern about the increase of residual solvent volume [58–61]. Kawashima *et al.* have successfully dissolved PLGA in acetone-alcohol and acetonitrile-alcohol mixtures for the preparation of nanoparticles. They found that both the affinity of these solvents with PLGA and with PVA in the aqueous phase contributed to the formation of nanoparticles [62] (Fig. 7).

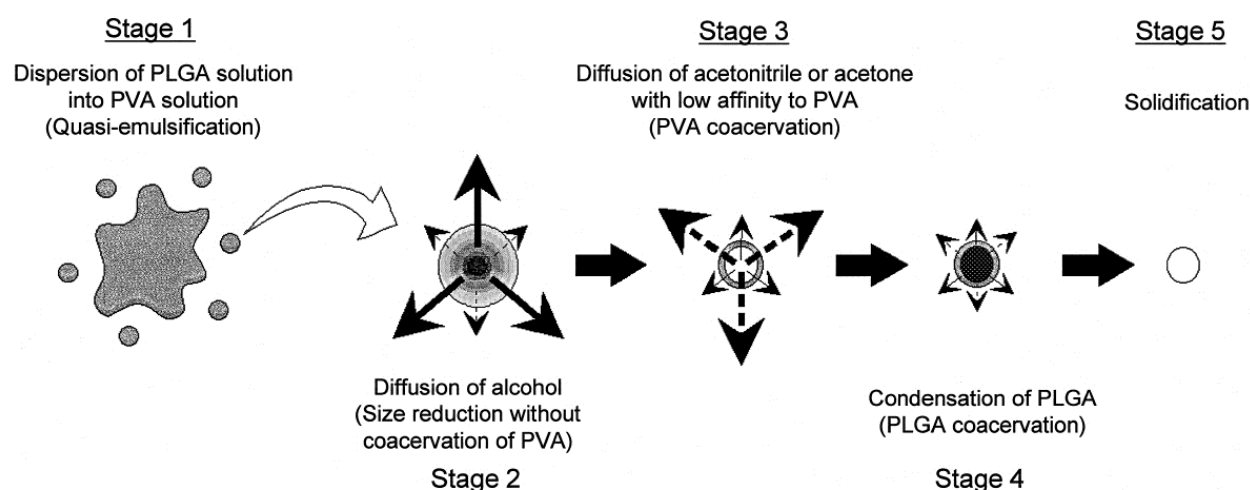


Fig. 7 The possible formation mechanism of PLGA nanoparticles through spontaneous emulsification-solvent diffusion method [62]

2.3.2. Porous particles

Most of the low-energy emulsification methods introduced so far have been used for the preparation of o/w-type nano-emulsions or nanoparticles. This is due to the fact that few studies have been done to prepare w/o-type nano-emulsions, PIT method has a limited preparation temperature, and PIC method requires excessive dilution and low yields. In such a situation, very few studies have been reported to apply w/o emulsions to the process of material preparation. Hayward *et al.* reported that an amphiphilic block copolymer, polystyrene-*block*-poly(*N*-isopropylacrylamide) (PS-PNIPAM) were synthesized [63]. The synthesized PS-PNIPAM was dissolved in chloroform and emulsified with pure water to prepare o/w emulsions. Then, due to the presence of organic salt species, which is the initiator of PS-PNIPAM synthesis, in the oil phase, w/o emulsions formed spontaneously inside the oil droplets because of osmotic pressure (Fig. 8 (a)). After solvent evaporation of this double emulsions, porous particles were obtained (Fig. 8 (b)). The mechanism of this method is different from those of the low-energy emulsification methods described so far. The preparation of w/o emulsion droplets with several hundreds of nanometers inherently requires high energy, such as ultrasound irradiation. However, this method is a cost-effective method because it eliminates the preparation of the porogens, the first step of emulsification.

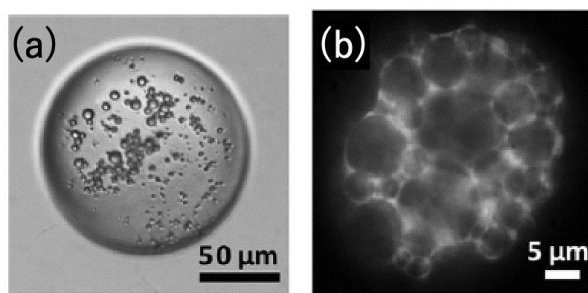


Fig. 8 The pictures of (a) an oil droplet containing spontaneously formed w/o emulsions and (b) resulting porous particle [63].

Lin *et al.* synthesized poly(4-vinylpyridine)-*block*-poly{6-[4-(4-butyloxyphenylazo)phenoxy]hexyl methacrylate} (P4VP-*b*-PAzoMA) as an amphiphilic block copolymer and they prepared o/w emulsions by using the synthesized polymer and sodium dodecyl sulfate (SDS) as co-surfactants [64]. o/w emulsions were observed to change over time and it was found that w/o emulsions spontaneously formed inside the oil droplets after the preparation of o/w emulsions, and eventually porous particles were formed (Fig. 9 (a, b)). Double emulsions and resulting porous microspheres were prepared through spontaneous emulsification under the various HLB values adjusted by using SDS and Span 60 as co-surfactants. As a result, porous microspheres, tremella-like aggregates, bowl-like aggregates, and wrinkled microspheres were formed in order of the HLB values (Fig. 9 (c-f)) [65]. This fact suggests that the stability of spontaneously formed w/o emulsions has a significant effect on the porosity of the particles. On the other hand, the formation mechanism of w/o emulsions has not been fully investigated.

Kim *et al.* used two amphiphiles, P4VP-PS and SDS, to prepare porous particles with the porogens of spontaneously formed emulsion droplets and found that the increase in the volume fraction of P4VP leads to a significant decrease in interfacial tension [66]. Although it may have been a key factor to use single-chain hydrophilic polymers because both Kim's team and Lin's team used P4VP as a hydrophilic block of the surfactant, the details of the mechanism are still unclear.

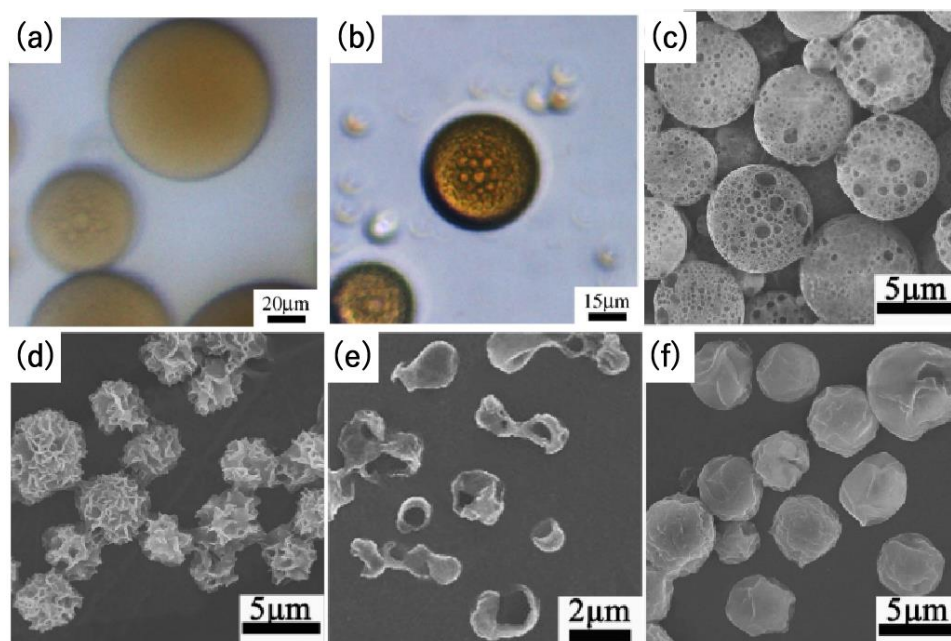


Fig. 9 Optical microscopy images (a, b) showed the spontaneous formation of water droplets in an organic droplet. The picture was taken emulsified after (a) 0.5 min and (c) 8 min [64]. SEM images (c-f) showed the shape-changing of the particles formed from emulsions with different HLB values at (c) 36, (d) 30, (e) 26, and (f) 20 [65].

An amphiphilic block copolymers consisting of hydrophilic poly(ethylene glycol) and hydrophobic poly(lactic acid) (PEG-PLA) was synthesized by Murakami and a technique to modify the biocompatible PEG chains on the surface of spherical nanoparticles was developed [67–69]. In the course of the investigation, it was unexpectedly discovered that decreasing the stirring speed by the homogenizer from about 20,000 rpm to around 10,000 rpm (from high-energy input to low-energy input) not only increased the size of the particles, but also formed particles with a porous structure in just one-step mechanical emulsification (Fig. 10 (b, d, f)) [70]. The observation of o/w emulsions after the mechanical emulsification suggested that w/o emulsions were formed inside the oil droplets, and these w/o emulsion droplets were working as porogen. In other words, the w/o emulsions were already spontaneously formed when the organic solution of PEG-PLA and the pure water contacted with each other (Fig. 10 (a, c, e)). This particle preparation method, which utilizes the spontaneously emulsifying property of amphiphilic polymers for the formation of surface and internal porous structures rather than the outline of microparticles, was first reported. w/o/w emulsions and the resulting porous particles have been used as a hydrophobic carrier which can contain hydrophilic substances. In conventional high-energy emulsification methods, w/o emulsions, which are primary emulsions, require higher energy input than o/w emulsions, which are secondary emulsions (*e.g.*, ultrasonic irradiation and high-speed emulsification at 20,000 rpm). In other words, the high energy method has a problem in terms of the possibility of destroying hydrophilic substances and the high energy cost. In contrast, the novel preparation method for porous particles based on spontaneous emulsification is expected to solve these problems.

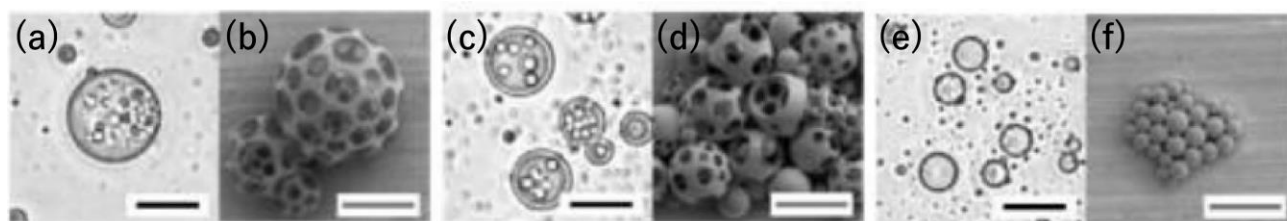


Fig. 10 Optical microscopy images of the (w/o) emulsions (a, c, e) and SEM images of the particles (b, d, f): scale bar shows 10 μm (black) and 5 μm (gray). Homogenization rate was (a, b) 8,000 rpm, (c, d) 12,000 rpm, and (e, f) 16,000 rpm [70].

3. Porous Materials used in the medical field

Recent studies have shown that it is possible to prepare porous particles by low-energy emulsification methods [63–66,70]. In particular, porous particles developed by Murakami are composed of polymers with low toxicity to living organisms and have a high potential for application as medical materials [70]. In this section, various forms of porous materials for medical applications are reviewed.

3.1. Porous particles

Porous particles are mainly used as drug carriers for drug delivery systems (DDS). In addition to their role as drug release carriers, their geometrically specific shapes have been utilized for various applications. The followings are examples of such applications.

3.1.1. Tissue regeneration scaffold

Many researchers have been trying to use porous particles as a scaffold for tissue regeneration, being common to two-dimensional porous materials. Whereas porous two-dimensional substrates are used by implanting pre-formed substrate into tissues, porous particles are injected by the tailored amount to fill the defect tissue (Fig. 11) [71]. If the defect site is too large, it is immobilized by in-situ gelation after injection, and the porous structure of the particles acts as a scaffold (Fig. 11 (c)). Porous particles used in this application can be broadly divided into two categories: solidified particles by sintering [72,73] and suspended particles in tissue solution [74–76].

As will be discussed in the section of two-dimensional porous materials, efficient cell growth and differentiation requires the transport of nutrients and oxygen into and out of the material. For this purpose, porous materials with high porosity and interconnected pores are required [77]. Compared to porous two-dimensional materials, porous particles are advantageous to provide interconnected structure in the system. This is because, in addition to the pores present on the surface of the particles, huge voids can be created between the particles [74,78].

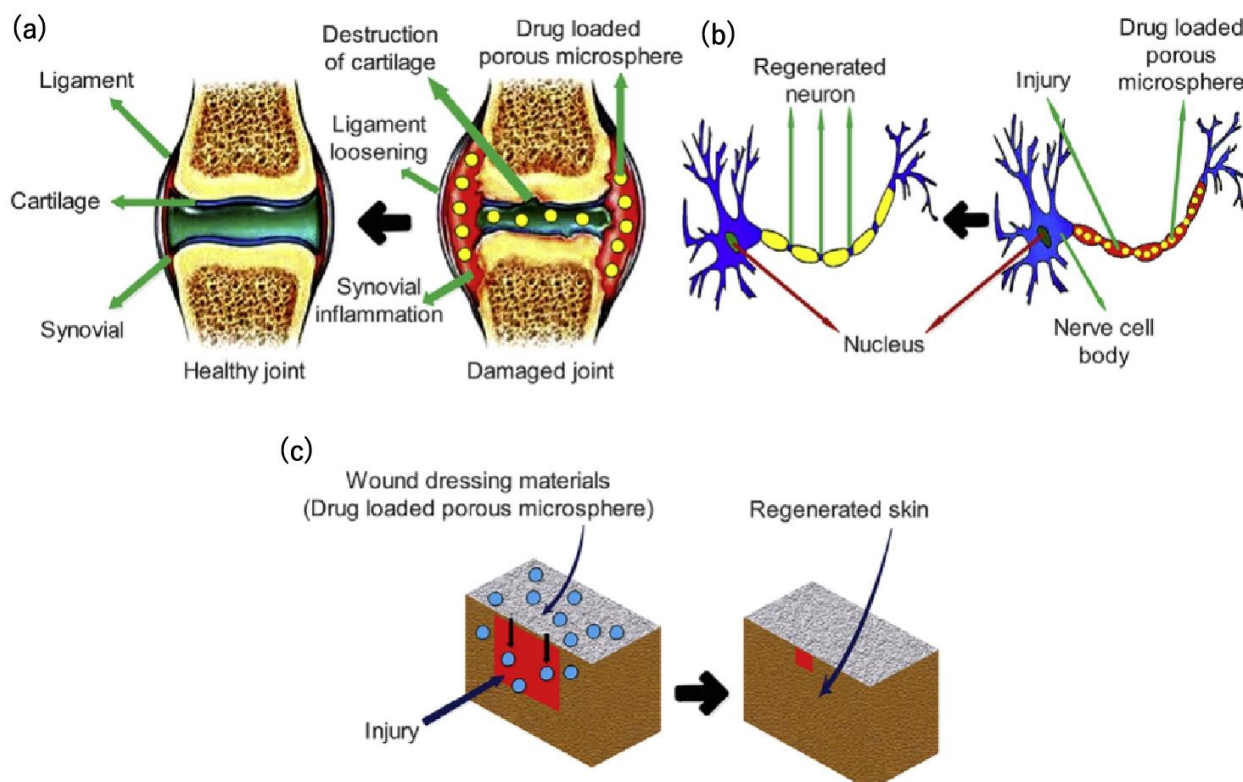


Fig. 11 Application of porous microparticles as tissue regeneration scaffold for (a) bone and cartilage, (b) nerve, and wound healing [71].

3.1.2. High speed chromatography

Due to their large specific surface area, porous microspheres are suitable for adsorption and desorption of substances. Therefore, they can be used in high speed chromatography where high separation efficiency of various substances such as proteins and phytochemicals from complex mixtures is required. The requirement for this application is that the porous particles should have narrow particle size distribution, excellent mechanical strength, and scientific stability over a wide range of pH. Solid silica particles, polystyrene, and poly(acrylic acid) are good examples to be used [79]. Using porous particles that meet these requirements, the huge voids between the particles packed into the solid phase reduce the flow resistance and facilitate the mobile phase to pass. Moreover, the porous structure of the particles provides a huge surface area and efficient binding of solutes [79]. For example, Zhiguo *et al.* evaluated the chromatographic performance of silica-based media and polystyrene porous particles with respect to icariin separation from crude extracts. The results showed that the porous particles purified icariin with a purity of up to 90% at the pressure of less than 0.05 MPa and achieved a recovery of 99.9% in a single analysis [80]. In other words, it enabled efficient separation of the objective compound at low pressure.

Liapis and McCoy developed a theoretical model to describe the adsorption-desorption process of a certain compound on porous particles when they are used in column chromatography [80,81]. To evaluate the dynamic behavior of the column, they used particle size, column length, fluid superficial velocities, intraparticle fluid velocities, the effective pore diffusion coefficient and the total number of active sites per volume of adsorbent. The

results showed that the size of the porous particles suitable for chromatography is 5-10 μm , the space between the porous particles is 600-800 nm, and the pore size of the particles is 80-150 nm as the optimum size. In addition, the depth of the pores was reduced to less than 1000 nm to achieve a high separation rate.

3.1.3. Drug carrier for pulmonary delivery

Many studies using porous particles as drug carriers have been reported since the 1990s [82]. Among the various medical applications, examples of studies of pulmonary administration have been focused on because the porous structure is considered to be most effectively utilized in this field. Pulmonary administration is an efficient method of delivering drugs to the deep sites of the lungs by inhalation. Lungs has a large surface area of more than 100 m^2 and the deeper the lung, the shorter the distance between epithelial cells and capillary blood vessels [82]. In addition, substances absorbed from the lungs can avoid initial hepatic metabolism [83]. These features provide numerous advantages over other drug delivery methods.

The requirements for drug carriers for pulmonary administration include (i) high delivery efficiency to the deep site of the lungs and (ii) avoidance of clearance. Particles with an aerodynamic diameter (Eq. 2), which is calculated as the diameter of a sphere having unit density, of 1-5 μm are considered to be appropriate for delivery to the deep lung [84].

$$d_a = d_g \sqrt{\frac{\rho_p}{\lambda \rho_s}} \quad (\text{Eq. 2})$$

Where d_a is the aerodynamic diameter, d_g is the geometric diameter, ρ_s is the unit particle density, ρ_p is the particle density, and λ is the shape factor of the particle. Particles with an aerodynamic diameter of less than 1 μm are likely to be re-exhaled by exhalation, particles of 5-10 μm are likely to be deposited in the pharynx and tracheobronchial tree, and particles larger than 10 μm are likely to be deposited in the oral cavity [85]. On the other hand, the two main clearances in the lung are phagocytosis by alveolar macrophages and mucus cilia in the airways [86]. Since the efficiency of drug absorption is highest in the deepest part of the lung, the alveoli, it is especially important to design particles to avoid phagocytosis. The uptake action of macrophages on particle properties has been evaluated in various ways (Table 1) [87][83,87].

Table 1 Strategy for enhancing or avoiding uptake from alveolar macrophages [83,87].

	Particle characteristics to enhance uptake	Particle characteristics to avoid uptake
Particle size	1.5-3 μm	Smaller than 1.5 μm and larger than 3 μm
Particle shape	<ul style="list-style-type: none"> • Spherical • Non-porous 	<ul style="list-style-type: none"> • Elongated, rod and filament shape • Porous
Surface charge	High positive or negative	Relatively neutral
Hardness	Hard	Soft

Many types of drug carriers have been proposed to establish pulmonary DDS. Nanoparticles are one of the representative type of carrier proposed from earlier. They are classified as such, including polymeric nanoparticles [88], micelles [89], liposomes [90], lipid nanoparticles [91], dendrimers [92], and polymer-drug complexes [93]. Clearance by alveolar macrophages has little effect on foreign particles smaller than 200 nm [94]. Therefore, the use of nanoparticles had been considered to be effective in avoiding phagocytosis and many studies have been conducted [88,89]. However, nanoparticles require enormous energy to adequately aerosolize, and current medical dry powder inhalers are difficult to disperse nano-sized dry powder particles. Therefore, it should be noted that aerosol preparations using nanoparticles alone are limited to the spraying of colloidal suspensions by nebulizers [90,95]. Therefore, in recent years, some studies have been conducted to increase the aerosol efficiency by compositing drug-encapsulated nanoparticles into microparticles [96–98]. PLGA nanoparticle-composite lactose particles developed by Ungaro *et al.* improved the flowability and delivering efficiency to the lung of dry powders *in vitro* (Fig. 12 (a)) [97].

Swellable microparticles are designed to acquire the ability to avoid phagocytosis after deposition in the deep lung [99–101]. Swellable microparticles are mainly composed of polysaccharides as particle-forming agents, and the preparation conditions are optimized to have a geometric diameter of 1-5 μm in the dry state [99–101]. Swellable particles swell to a particle size of more than 5 μm at the humid respiratory organs and can inhibit uptake by alveolar macrophages. Ni *et al.* showed that drug composite chitosan microparticle swelled in 5 minutes in a moist environment [99] (Fig. 12 (b)). However, the control of the swelling rate has not been investigated. Swellable particles need to swell rapidly just after deposition and the swollen particles should not block the bronchial tubes. Controlling the swelling rate is especially important for patients with cystic fibrosis, because their bronchial tubes are narrower than those of healthy peoples.

As well as swollen microparticles, the dominant design of drug carriers for pulmonary delivery in recent years has been “large” porous particles. Edwards *et al.* were the first to propose the use of porous particles larger than 5 μm [102]. They used “large” porous particles because particles with the geometric diameter of 1.5-3 μm are easily eliminated by phagocytosis [103]. Porous particles are likely to have a smaller particle density than non-porous particles of the same size due to the large number of voids on the surface and inside. The aerodynamic diameter of microparticles is inversely proportional to the particle density, as shown in Eq. 1. Therefore, it can be expected that porous particles with larger geometric diameters than 5 μm will exhibit smaller aerodynamic diameters. Their large porous particles achieved a high delivery efficiency to the lung that could not be achieved with conventional non-porous particles [102] and also inhibited uptake by alveolar macrophages. Subsequently, large porous particles have been proposed by many researchers [104–107].

To summarize this section, the pulmonary delivery system requires two things: achieving high delivery efficiency of drug carriers to the lung and avoiding phagocytosis by alveolar macrophages. The aerodynamic diameter suitable for pulmonary delivery and the geometric diameter of the particles which are preferentially eliminated by alveolar macrophages are really close to each other. Therefore, several forms of drug carriers and approaches have been proposed including nanoparticles, hydrophilic swellable particles, and porous particles (Table 2). Porous particles, especially, are expected to archive both requirements due to the low particle density. In other words, among various drug delivery systems, the geometric properties of porous particles may be most skillfully utilized in

pulmonary delivery.

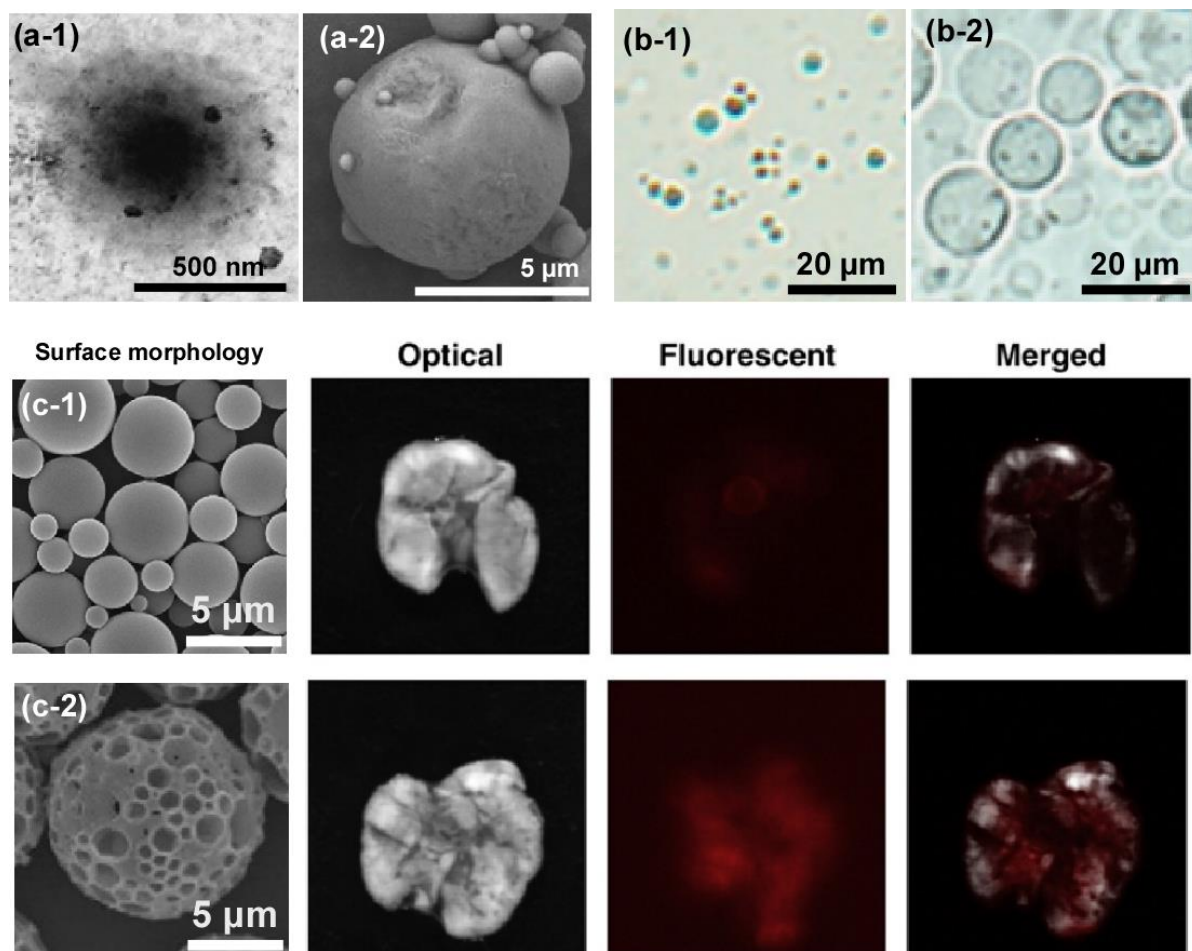


Fig. 12 Recently reported drug carriers for pulmonary delivery ((a) nanoparticle composited in microparticle [97], (b) swellable microparticle [99], and (c) large porous particles [104]). TEM image of (a-1) nanoparticle and SEM image of (a-2) microparticle containing nanoparticle. Photograph of chitosan microparticle (b-1) before and (b-2) after swelling. SEM image of microparticle and fluorescent image of the particle deposited in the murine lung ((c-1) nonporous microparticle and (c-2) porous microparticle).

Table 2 Designs of drug carrier for pulmonary delivery and their characteristics.

Type of drug carrier	Characteristics
Nanoparticle [88–90,92,93]	<ul style="list-style-type: none"> • Avoiding phagocytosis because of their small particle diameter. • Being afraid of particle aggregation. • Only few types of devices can be used. • Being afraid of re-exhaling from the lungs.
Nanoparticle composited in microparticle [91,96,97]	<ul style="list-style-type: none"> • Suitable size for deposition in the lungs. • Rapid breaking of microparticle is needed to avoid phagocytosis.
Swellable microparticle [99–101]	<ul style="list-style-type: none"> • Suitable size for deposition in the lungs. • Avoiding phagocytosis by swelling to larger than 5 μm • Rapid swelling is needed to avoid phagocytosis • Controlling the diameter of particle is needed to avoid blocking the airways.
Large porous microparticle [102,104–107]	<ul style="list-style-type: none"> • Suitable particle density for deposition in the lungs. • Hard to release a drug for a long time due to its large voids and phagocytosis.

3.2. Two-dimensional porous materials

While the porous particles are spherical in shape, this section describes two-dimensional porous materials such as substrates and films. The reason for noting “two-dimensional” is because it includes a porous thin “film”, a porous pattern on the surface of the cell culture “substrate”, and a tissue regeneration “scaffold” that forms a three-dimensional layered structure with interconnected vacancies even in the thickness direction.

3.2.1. Scaffold for tissue regeneration

Materials used as scaffolds for tissue regeneration are very effective in being porous. This is because it facilitates the establishment of mesenchymal stem cells by existing as a temporary replacement for the extracellular matrix of the defective area in the body [108]. The materials for this purpose mainly include hydroxyapatite, polysaccharides, and polylactic acid. Hydroxyapatite is proposed as a scaffolding material, especially for bone tissue, because it is the same as the main constituent of hard tissue in the body. There are many reported examples of hydroxyapatite and it has already been shown that one of the important aspects of porous materials made from hydroxyapatite for bone regeneration is the interconnection of pores [77]. Interconnected pores facilitate cell and vascular penetration and ensure the internal growth of bone in the pores. *In vitro*, the required minimum interconnection size is around 20 μm , but the most suitable size for cell permeation is said to be above 40 μm [77]. *In vivo*, similarly, the size of the interconnected pores around 20 μm have been found to be necessary. It has also been

suggested that robust calcification occurs when the interconnection size exceeds 50 μm [77,109].

Chitosan, a deacetylated compound of chitin, has been studied in a number of polysaccharide-based scaffold materials due to its high biocompatibility and high antimicrobial activity derived from its cationic nature. Porous structures of chitosan hydrogels, formed by freeze-drying and electrospinning methods, have excellent cell adhesion properties while they have poor mechanical strength [108]. Therefore, recent chitosan-based materials have been designed to include hard nanoparticles such as hydroxyapatite and ceramic in order to increase their mechanical strength [110–113].

PLA, which is highly biocompatible, is a synthetic polymer and is easy to obtain the desired mechanical strength and chemical modification. In fact, the modulus of elasticity of PLA is close to that of bone, making it an ideal material among synthetic polymers as a scaffold for bone tissue in terms of strength [114]. On the other hand, PLA is a hydrophobic polymer, and the property makes it difficult for water and living cells to penetrate the interior of PLA materials, leading to concerns about cell necrosis, bacterial adhesion, and biofilm formation [115,116]. Therefore, complexing PLA materials with hydrophilic polymers such as PEG have been proposed to improve the affinity between materials and cells [116,117]. Porous scaffold materials made from PLA have been more often reported in recent years because of advent of 3D printing method [116–119]. 3D printing method enables porous structure of PLA materials to be precisely controlled, whereas pores formed by the method are limited in size minimum to about 10 μm [120]. Mesopores are significantly important for tissue regeneration because the surface roughness promotes protein adsorption on the materials and cell adhesion to scaffolds [120]. Therefore, designing scaffolds that combine mesopores and macropores has been a challenge for this method.

3.2.2. Cell culture substrate

The scaffold material described in the previous section is an in-body implantable material that temporarily replaces the extracellular matrix of a defect in the body. In contrast, porous materials are also used as substrates for culturing cells *in vitro*. Traditionally, cells have been cultured on a flat substrate in a cell culture plate or flask. However, such cells cannot imitate *in vivo* natural tissue, resulting great deviation from *in vivo* experimental results. Therefore, a more *in vivo*-like environment cultured *in vitro* has been required to improve the accuracy of predicting the behavior of drug and help in understanding tissue morphogenesis [121,122]. For example, cells cultured *in vitro* can be used to assess various properties such as the mechanical strength of cells. Janshoff *et al.* cultured cells on a porous substrate with varying vacancies of 450-500 nm in diameter. They found that the mechanical strength of the cells was stiffer on the non-porous substrate and that the cell tissue flow was proportional to the porosity [123]. These findings could be important for improving the quality of artificially cultured cell structure closer to *in vivo*. One of the methods for the preparation of porous substrates is electrospinning, in which polymer solutions are spun into fibers [124,125]. Although this method is capable of creating interconnected pores in the gaps of the fibers, it has been suggested that the cells would grow in a linear pattern along the fibers and they do not fully mimic the biological environment [126,127]. The particulate leaching process, of which particles that serve as porogen templates are removed in the process, can produce a porous substrate without the presence of directionality like electrospinning. On the other hand, the interconnections between the pores may be limited, which may lead to the formation of isolated

cells [128,129]. One fabrication method by which spherical and interconnected pores can be formed is the emulsion-template method [130–132]. Emulsion-template method is a porous scaffold obtained by solvent evaporation from a polymer solution with extremely high volume fraction of the internal water phase. Due to the high volume fraction of the dispersed aqueous phase, the porosity is extremely high and the pores are easily interconnected with each other. The high porosity of these scaffolds allows cells to occupy and form tissue-like structures, which more closely mimic the *in vivo* conditions.

The porosity of the culture substrate is not necessarily only aimed at mimicking the shape of the extracellular matrix. Traditionally, cultured cells are detached by adding chelating agents after incubation in polystyrene dishes to partially disrupt ion channels and cell membrane proteins. Okano *et al.* developed a new technique of cell detachable substrate [121,122]. They successfully detached the cultured cell sheets by hydrophilize the substrate at low temperatures (20°C) owing to a temperature-responsive polymer, poly(*N*-isopropylacrylamide) (PIPAAm), grafted on a polystyrene substrate. They increased the rate of water infiltration by making the substrate porous, thus establishing a technique for rapid and high cell sheet preparation with high cell viability (Fig. 13) [121,122].

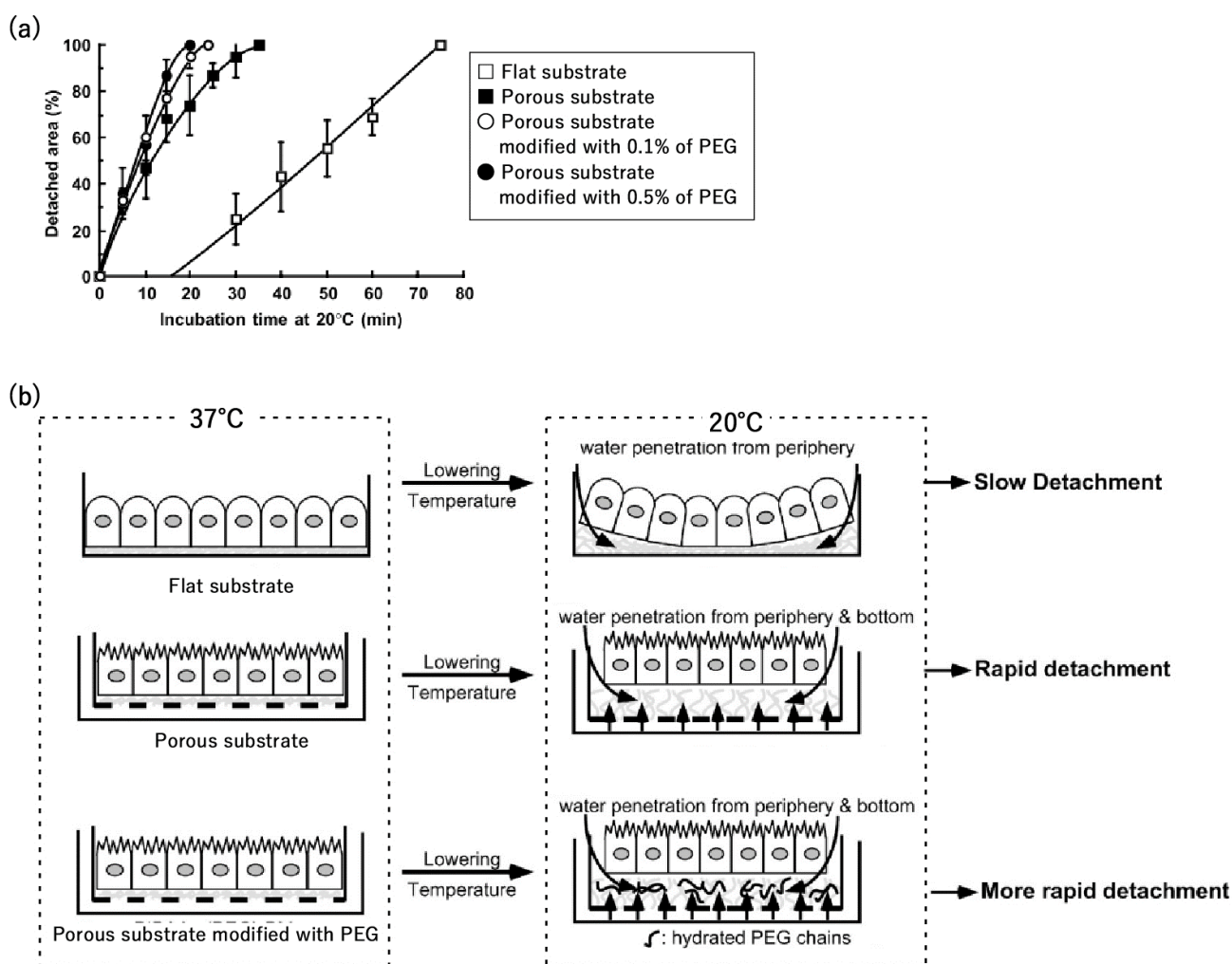


Fig. 13 (a) Average detached areas for cell sheets recovered from various substrates. (b) Illustration of cell sheet detachment through different types of substrates [122].

3.2.3. Drug delivery systems

Drug delivery systems based on porous two-dimensional materials have been studied mainly in applications related to tissue engineering. That is, porosity of the materials is thought to influence the amount of encapsulation of drug and release rate and it can be an advantage [133]. For example, porous fiber scaffolds prepared by electrospinning promoted osteogenic differentiation of human adipose-derived stem cells compared to non-porous fiber scaffolds [134,135]. This may be due to the accelerated rate of tricalcium phosphate release; the hydroxyapatite patches produced by Uchida *et al.* had both nano- and micro-sized pores. This patch achieved sustained release of antibiotics from the nano-sized pores and fast bone regeneration due to the micro-sized interconnected pores in the rabbit body [136]. These successful results were obtained due to the combination of two advantages: the reported importance of interconnected pores for efficient bone regeneration [137] and the reported effectiveness of pores for antibiotic adsorption [137,138].

It has also been studied in areas other than tissue regeneration [139–142]. Daban *et al.* prepared polyurethane films by the breath figure method, in which a porous structure is formed by phase separation of organic polymer solutions and condensed water droplets. They reported that this film with regular pores successfully controlled the release of atorvastatin calcium, a drug for hyperlipidemia, in proportion to the size of the pores (Fig. 14) [143]. Recently, they have also reported the design of smart materials that release drugs stored in the vacancies in response to stimuli such as glucose and temperature in the body [143,144].

3.2.4. Biosensors

A number of two-dimensional porous substrates have been investigated for the fabrication of biosensors to detect specific substances in living organisms. The predominant material in this field is silicon substrates [145–148]. Devices for detecting low molecular weight molecules such as water and oligopeptides, [145,147] and even devices for detecting proteins [149–151] and microorganisms [152,153] have been proposed. The development of multi-sensors for simultaneous detection of two substances, glucose and lactic acid, by immobilizing enzymes using the positive charge and porous structure of chitosan fibers, has also been reported in recent years [148]. Pore size is a greatly significant factor in the design of these porous substrates. In order to fix enough amounts of signal-generating molecules such as antibodies and enzymes on the substrate, the pore size should be fabricated above the size of [154,155]. In addition to that, porosity of the sensor must also be considered because efficient penetration of biological fluids containing target molecules into the substrate is needed [154,156]. The proposals of Segal *et al.* in this area are particularly remarkable. Initially, they succeeded in detecting microorganisms by immobilizing antibodies on porous SiO₂ substrates [152,153], and then immobilized a variety of detection molecules on these porous structures, including proteins [150,151,157], organophosphorous compounds [158], heavy metals [159], DNA [160], they have been successfully used to detect various biomolecules. Furthermore, this porous silicon substrate has a very wide range of applications in DDS [161–163] and bone regeneration [164].

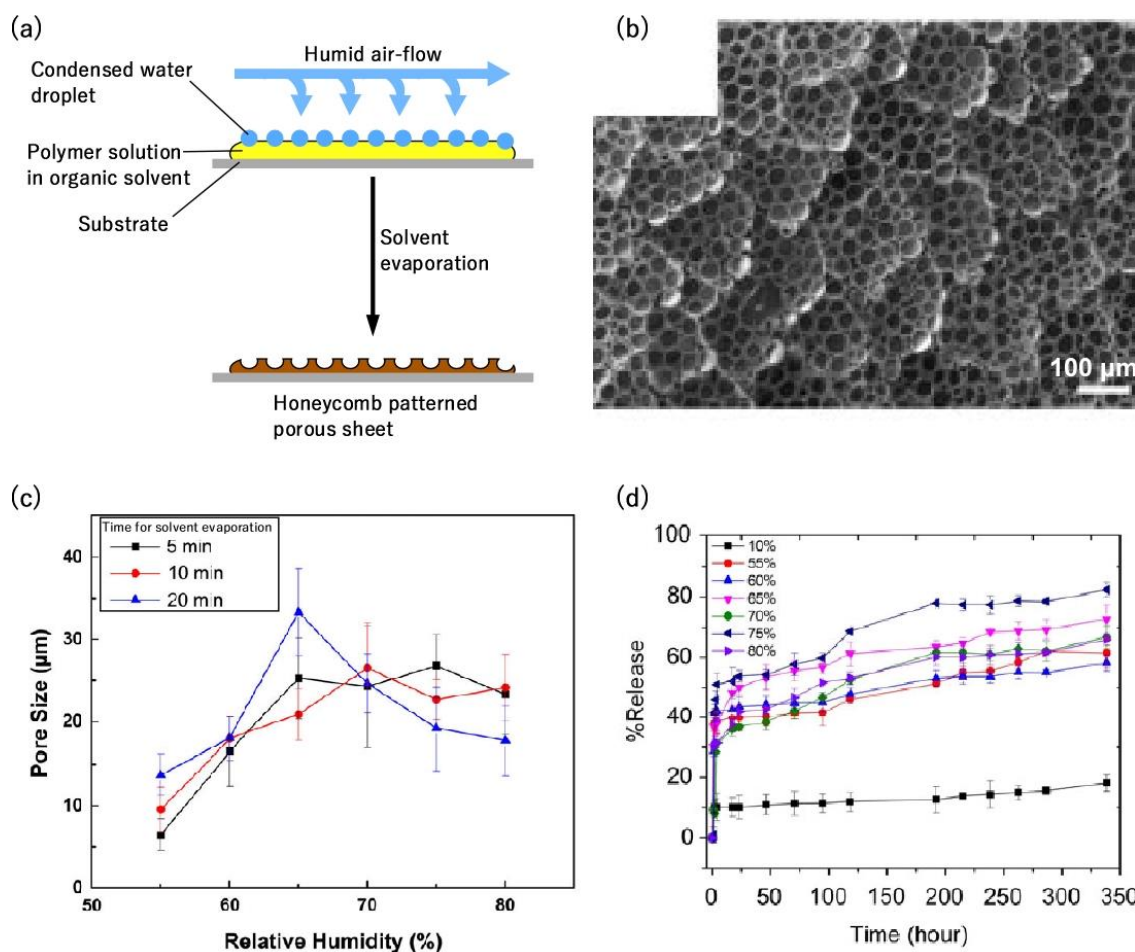


Fig.14 (a) Pore formation mechanism of breath figure method. (b) SEM image of porous polyurethane film prepared through 10 min of solvent evaporation at 70 % of relative humidity. (c) Effect of relative humidity on (c) pore size and (d) drug-release behavior of polyurethane film [143].

3.2.5. Membrane for material separation

Porous membranes can be used as a tool for separating specific substances based on the size of the pores and the strength of interaction with the components of membranes. The porous ceramic filter fabricated by Zhou *et al.* increased the efficiency of microbial separation by introducing hydroxyapatite [165]. Some silicon wafer porous membranes have been fabricated as membranes to separate specific components of blood rather than for diagnostic purposes; Lee *et al.* have successfully separated plasma from blood using silicon wafers with pores about 1 μm in diameter [166]. For the separation of substances using membrane size, the use of hydrophilic polymer membranes with pores of several hundred nm developed by Minko *et al.* has been proposed [167–169].

3.3. Porous microneedle

Transdermal administration is one of the major routes of drug administration, although subcutaneous injections are painful and require specialized skills [170]. There is also a risk of infection due to reuse of the needles

[171]. Microneedle can be a solution to these problems. Microneedle is a material consisting of a number of protrusions less than 1 mm in height fixed on a patch a few cm square [172]. This material makes only a very shallow depth of invasion when attached to the skin, which makes it less painful and easier to use [171]. Microneedle can be mainly used in two ways. They are materials for collecting biological fluids for diagnosis and materials for drug administration. They are introduced below.

3.3.1. Biological fluid collectors

Blood and interstitial fluids contain a variety of biomarkers such as metabolites, ions, proteins, and glucose. Therefore, a minimally invasive method of collecting these fluids would allow for efficient and easy diagnosis. Covering the microneedle surface with a porous layer allows the collection of biological fluids by capillary phenomenon depending on the shape of the pores and their hydrophilicity [172]. Verhoeven *et al.* showed that microneedles with pores can both deliver substances and extract compounds in the body at the same time [173]. In addition, Nishizawa *et al.* reported the first successful measurement of the components of biological fluids by connecting the needles to an external device [174,175]. However, these are still in the early stages of development, with fewer reported cases than the hollow microneedles, which were studied earlier [176–178].

3.3.2. Drug delivery

Porous microneedles for DDS have been studied earlier than microneedles for biological fluid collection, and their fabrication methods range from coating metal microneedles with a porous layer [179–183], sintering of ceramics [173], pressing polymeric particles or polymer solutions into molds [184,185], and plasma etching [186]. However, there is a concern about reducing mechanical strength and consequent difficulty to penetrate the skin by pore patterning on microneedles [173]. In fact, previous studies have suggested the possibility of bending needle tips by applying a mechanical load [180,184]. Humrez *et al.* fabricated porous microneedles by dissolving monomers in a mixed organic solvent and designing them to form pores by phase separation with the poor solvent as the polymerization progressed [186]. By this method, microneedles with irregular pores but high mechanical strength were successfully fabricated. Ullah *et al.* fabricated microneedles covered with a PLGA porous layer by immersing the metal microneedles in w/o emulsion and showed that the drug release could be controlled by tuning the porosity of the microneedles [182]. Furthermore, they designed a smart material that can release drugs only in response to glucose and acidic environment in the body (Fig. 15) [181,183].

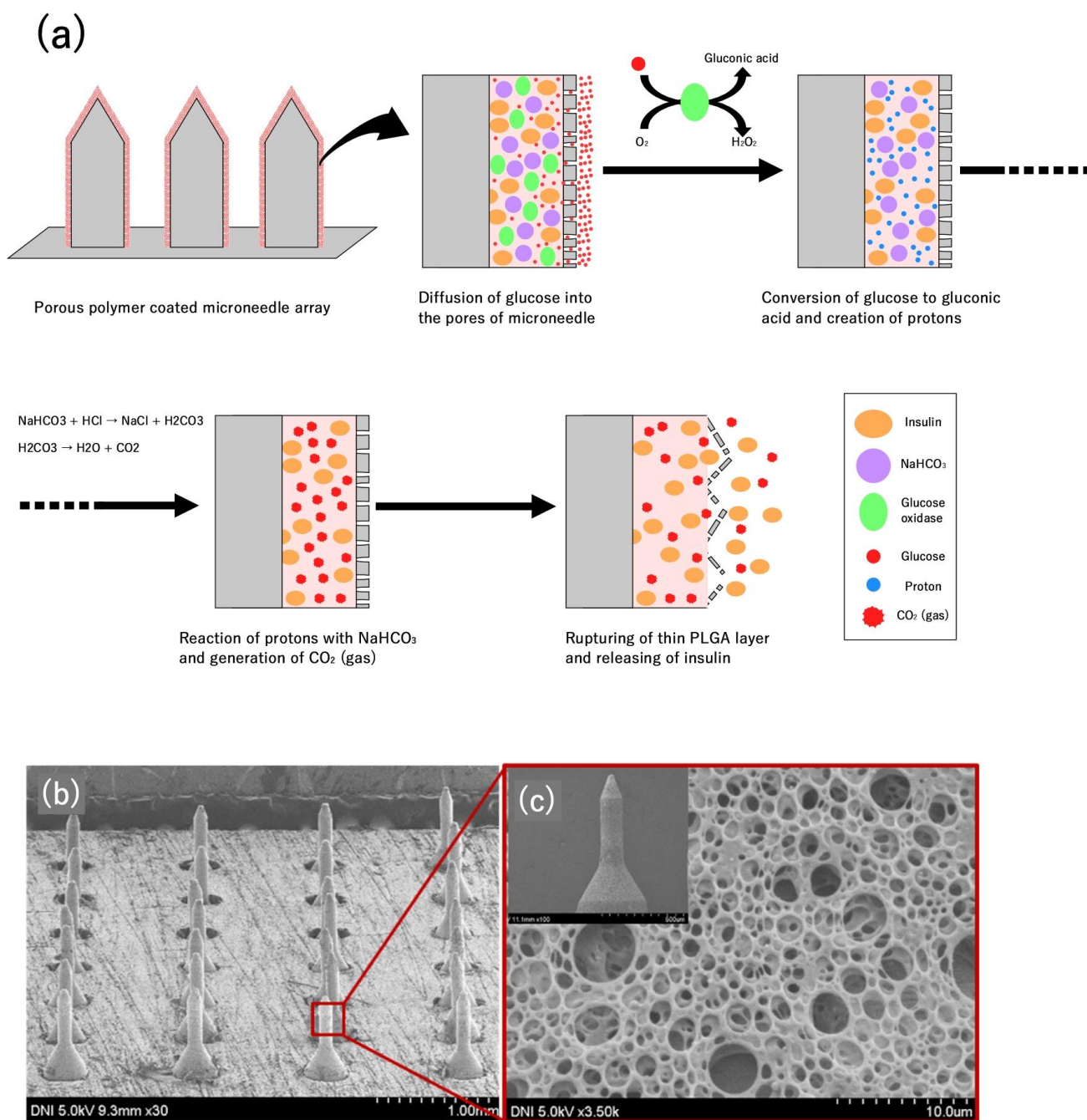


Fig. 15 Mechanism of glucose-responsive insulin release from the porous microneedle (a) and SEM images of the microneedle (b, c) [181].

4. The aim of this thesis

In this chapter, it was introduced that a variety of emulsions and emulsion-based microparticles have been proposed as substance-transport carriers. On the other hand, the preparation of tiny emulsion droplets of nanometer-order size requires extremely high energy, which is a challenge due to the high energy cost and the concern of destroying the substances. Therefore, spontaneous emulsification, which is one of the low energy emulsification

methods using the chemical energy inherent in the system, has been attracting attention. Although the mechanism of spontaneous emulsification is not completely clear, each report has been partially successful in controlling the particle size of particles by tuning preparation conditions. Most of these previous studies have been on the development of o/w emulsions or particles using o/w emulsions as precursors. In other words, spontaneous emulsification has been studied as a method to shape the outline of particles. On the other hand, a new technique for preparing porous particles by using spontaneously formed w/o emulsions as porogens was recently reported by Murakami [70]. The academic significance of this report is that it is the first example of cost-effective preparation of porous materials by using the spontaneous emulsification for the preparation of porous structures rather than the outline of spherical particles. In this doctoral thesis, the development of porous materials prepared via spontaneous emulsification is reported on. The preparation method of the porous materials proposed in this study is shown in Fig. 16.

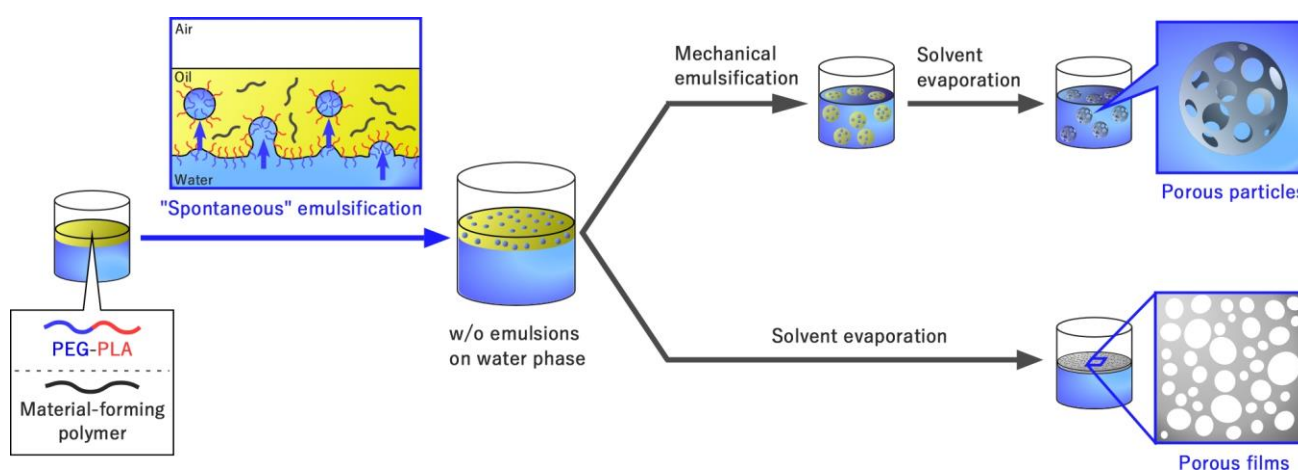


Fig. 16 Preparation method of porous materials through spontaneous emulsification induced by PEG-PLA.

Firstly, in chapter 2, the basic techniques of preparation of the porous particles are used to discuss the potential applications. As previously mentioned, the most effective use of the porous structure would be as a drug carrier for pulmonary delivery. It has been suggested that the porous particles have a large number of pores on the surface and inside [70] and are considered to have an extremely low density. In addition, the particle surface is modified by PEG, which is a hydrophilic non-ionic polymer, thereby having possible ability to avoid phagocytosis. Therefore, porous particles containing PEG-PLA are considered to be suitable for pulmonary delivery, combining high pulmonary delivery efficiency due to the low density and the ability to avoid phagocytosis of alveolar macrophages due to PEG modification.

In chapter 3, the precise morphological control of particles by factors different from those previously reported by Murakami [70] was examined. The results of chapter 2 suggest that independent control of particle surface modification and particle morphology is necessary to improve the delivery behavior to deep lung. The previous report showed that the size of pores on the surface of the porous particles containing PEG-PLA is inversely proportional to the molecular weight of PEG block [70]. In this conventional approach, the modification state of the particle surface, which is thought to be related to the adhesion of the particles, and the morphology of the particles, which is thought to affect their aerodynamic behavior, are simultaneously altered. In other words, it was difficult to evaluate the effect

of each physical property on the aerodynamic behavior of the porous particles. Therefore, a method to control the porous structure independent of the molecular weight of the PEG block was investigated. In this chapter, a detailed morphological evaluation of the internal structure of the porous particles was investigated in addition to the surface morphology.

In chapter 4, a method for fabricating the porous structure based on spontaneous emulsification is investigated for "film-type materials". The spontaneous emulsification process is a novel method for the fabrication of two-dimensional materials. The porous films prepared in this chapter were based on PLA, which has been used as a scaffold material for tissue regeneration due to its high biocompatibility. The potential of this novel material as a biomaterial was explored through fundamental studies on the formation of the porous structure.

Chapter 5 summarizes the investigations in chapters 2-4. Throughout this doctoral thesis, several forms of cost-effective porous materials based on spontaneous emulsification have been successfully fabricated.

5. References

- [1] D.J. McClements, Enhancing nutraceutical bioavailability through food matrix design, *Curr. Opin. Food Sci.* 4 (2015) 1–6. <https://doi.org/10.1016/j.cofs.2014.12.008>.
- [2] Q. Hu, H. Gerhard, I. Upadhyaya, K. Venkitanarayanan, Y. Luo, Antimicrobial eugenol nanoemulsion prepared by gum arabic and lecithin and evaluation of drying technologies, *Int. J. Biol. Macromol.* 87 (2016) 130–140. <https://doi.org/10.1016/j.ijbiomac.2016.02.051>.
- [3] L. Cornacchia, Y.H. Roos, Stability of β -carotene in protein-stabilized oil-in-water delivery systems, *J. Agric. Food Chem.* 59 (2011) 7013–7020. <https://doi.org/10.1021/jf200841k>.
- [4] Z. Wei, W. Yang, R. Fan, F. Yuan, Y. Gao, Evaluation of structural and functional properties of protein-EGCG complexes and their ability of stabilizing a model β -carotene emulsion, *Food Hydrocoll.* 45 (2015) 337–350. <https://doi.org/10.1016/j.foodhyd.2014.12.008>.
- [5] Z. Wei, Y. Gao, Physicochemical properties of β -carotene bilayer emulsions coated by milk proteins and chitosan-EGCG conjugates, *Food Hydrocoll.* 52 (2016) 590–599. <https://doi.org/10.1016/j.foodhyd.2015.08.002>.
- [6] Y. Mao, M. Dubot, H. Xiao, D.J. McClements, Interfacial engineering using mixed protein systems: Emulsion-based delivery systems for encapsulation and stabilization of β -carotene, *J. Agric. Food Chem.* 61 (2013) 5163–5169. <https://doi.org/10.1021/jf401350t>.
- [7] Q. Ma, P.M. Davidson, Q. Zhong, Antimicrobial properties of lauric arginate alone or in combination with essential oils in tryptic soy broth and 2% reduced fat milk, *Int. J. Food Microbiol.* 166 (2013) 77–84. <https://doi.org/10.1016/j.ijfoodmicro.2013.06.017>.
- [8] Y. Zhang, Q. Ma, F. Critzer, P.M. Davidson, Q. Zhong, Effect of alginate coatings with cinnamon bark oil and soybean oil on quality and microbiological safety of cantaloupe, *Int. J. Food Microbiol.* 215 (2015) 25–30. <https://doi.org/10.1016/j.ijfoodmicro.2015.08.014>.
- [9] Q. Ma, Y. Zhang, F. Critzer, P.M. Davidson, S. Zivanovic, Q. Zhong, Physical, mechanical, and antimicrobial properties of chitosan films with microemulsions of cinnamon bark oil and soybean oil, *Food Hydrocoll.* 52

- (2015) 533–542. <https://doi.org/10.1016/j.foodhyd.2015.07.036>.
- [10] Q. Ma, P.M. Davidson, Q. Zhong, Nanoemulsions of thymol and eugenol co-emulsified by lauric arginate and lecithin, *Food Chem.* 206 (2016) 167–173. <https://doi.org/10.1016/j.foodchem.2016.03.065>.
- [11] J. Xue, P. Michael Davidson, Q. Zhong, Antimicrobial activity of thyme oil co-nanoemulsified with sodium caseinate and lecithin, *Int. J. Food Microbiol.* 210 (2015) 1–8. <https://doi.org/10.1016/j.ijfoodmicro.2015.06.003>.
- [12] F. Niu, W. Pan, Y. Su, Y. Yang, Physical and antimicrobial properties of thyme oil emulsions stabilized by ovalbumin and gum Arabic, *Food Chem.* 212 (2016) 138–145. <https://doi.org/10.1016/j.foodchem.2016.05.172>.
- [13] T. Higuchi, H. Yabu, M. Shimomura, Simple preparation of hemispherical polystyrene particles, *Colloids Surfaces A Physicochem. Eng. Asp.* 284–285 (2006) 250–253. <https://doi.org/10.1016/j.colsurfa.2005.10.042>.
- [14] A. Potineni, D.M. Lynn, R. Langer, M.M. Amiji, Poly(ethylene oxide)-modified poly(β -amino ester) nanoparticles as a pH-sensitive biodegradable system for paclitaxel delivery, *J. Control. Release.* 86 (2003) 223–234. [https://doi.org/10.1016/S0168-3659\(02\)00374-7](https://doi.org/10.1016/S0168-3659(02)00374-7).
- [15] C.X. Song, V. Labhasetwar, H. Murphy, X. Qu, W.R. Humphrey, R.J. Shebuski, R.J. Levy, Formulation and characterization of biodegradable nanoparticles for intravascular local drug delivery, *J. Control. Release.* 43 (1997) 197–212. [https://doi.org/10.1016/S0168-3659\(96\)01484-8](https://doi.org/10.1016/S0168-3659(96)01484-8).
- [16] S. Izumikawa, S. Yoshioka, Y. Aso, Y. Takeda, Preparation of poly(l-lactide) microspheres of different crystalline morphology and effect of crystalline morphology on drug release rate, *J. Control. Release.* 15 (1991) 133–140. [https://doi.org/10.1016/0168-3659\(91\)90071-K](https://doi.org/10.1016/0168-3659(91)90071-K).
- [17] A. Bitar, N. Zafar, J.P. Valour, G. Agusti, H. Fessi, P. Humbert, S. Robin, C. Viennet, N. L  v  que, A. Elaissari, Elaboration of sponge-like particles for textile functionalization and skin penetration, *Colloid Polym. Sci.* 293 (2015) 2967–2977. <https://doi.org/10.1007/s00396-015-3704-7>.
- [18] P. Zakeri-Milani, B.D. Loveymi, M. Jelvehgari, H. Valizadeh, The characteristics and improved intestinal permeability of vancomycin PLGA-nanoparticles as colloidal drug delivery system, *Colloids Surfaces B Biointerfaces.* 103 (2013) 174–181. <https://doi.org/10.1016/j.colsurfb.2012.10.021>.
- [19] Y. Yang, Z. Fang, X. Chen, W. Zhang, Y. Xie, Y. Chen, Z. Liu, W. Yuan, An overview of pickering emulsions: Solid-particle materials, classification, morphology, and applications, *Front. Pharmacol.* 8 (2017) 1–20. <https://doi.org/10.3389/fphar.2017.00287>.
- [20] J. Marto, L. Gouveia, I.M. Jorge, A. Duarte, L.M. Gonalves, S.M.C. Silva, F. Antunes, A.A.C.C. Pais, E. Oliveira, A.J. Almeida, H.M. Ribeiro, Starch-based Pickering emulsions for topical drug delivery: A QbD approach, *Colloids Surfaces B Biointerfaces.* 135 (2015) 183–192. <https://doi.org/10.1016/j.colsurfb.2015.07.024>.
- [21] J. Frelichowska, M.A. Bolzinger, J.P. Valour, H. Mouaziz, J. Pelletier, Y. Chevalier, Pickering w/o emulsions: Drug release and topical delivery, *Int. J. Pharm.* 368 (2009) 7–15. <https://doi.org/10.1016/j.ijpharm.2008.09.057>.
- [22] Y. Hu, S. Zou, W. Chen, Z. Tong, C. Wang, Mineralization and drug release of hydroxyapatite/poly(l-lactic acid) nanocomposite scaffolds prepared by Pickering emulsion templating, *Colloids Surfaces B Biointerfaces.* 122 (2014) 559–565. <https://doi.org/10.1016/j.colsurfb.2014.07.032>.
- [23] M.F. Nsib, A. Maayoufi, N. Moussa, N. Tarhouni, A. Massouri, A. Houas, Y. Chevalier, TiO₂ modified by salicylic acid as a photocatalyst for the degradation of monochlorobenzene via Pickering emulsion way, *J.*

- Photochem. Photobiol. A Chem. 251 (2013) 10–17. <https://doi.org/10.1016/j.jphotochem.2012.10.007>.
- [24] L. Leclercq, R. Company, A. Mühlbauer, A. Mouret, J.M. Aubry, V. Nardello-Rataj, Versatile eco-friendly pickering emulsions based on substrate/native cyclodextrin complexes: A winning approach for solvent-free oxidations, *ChemSusChem*. 6 (2013) 1533–1540. <https://doi.org/10.1002/cssc.201300081>.
- [25] J.C. Garay-Jimenez, D. Gergeres, A. Young, D. V. Lim, E. Turos, Physical properties and biological activity of poly(butyl acrylate-styrene) nanoparticle emulsions prepared with conventional and polymerizable surfactants, *Nanomedicine Nanotechnology, Biol. Med.* 5 (2009) 443–451. <https://doi.org/10.1016/j.nano.2009.01.015>.
- [26] Y.H. Chang, Y. Der Lee, O.J. Karlsson, D.C. Sundberg, Particle nucleation mechanism for the emulsion polymerization of styrene with a novel polyester emulsifier, *J. Appl. Polym. Sci.* 82 (2001) 1061–1070. <https://doi.org/10.1002/app.1940>.
- [27] J. Bao, A. Zhang, Poly(methyl methacrylate) nanoparticles prepared through microwave emulsion polymerization, *J. Appl. Polym. Sci.* 93 (2004) 2815–2820. <https://doi.org/10.1002/app.20758>.
- [28] S.W. Pang, H.Y. Park, Y.S. Jang, W.S. Kim, J.H. Kim, Effects of charge density and particle size of poly(styrene/(dimethylamino)ethyl methacrylate) nanoparticle for gene delivery in 293 cells, *Colloids Surfaces B Biointerfaces*. 26 (2002) 213–222. [https://doi.org/10.1016/S0927-7765\(01\)00335-6](https://doi.org/10.1016/S0927-7765(01)00335-6).
- [29] G. Zhang, A. Niu, S. Peng, M. Jiang, Y. Tu, M. Li, C. Wu, Formation of novel polymeric nanoparticles, *Acc. Chem. Res.* 34 (2001) 249–256. <https://doi.org/10.1021/ar000011x>.
- [30] Z. Zhang, D.W. Grijpma, J. Feijen, Poly(trimethylene carbonate) and monomethoxy poly(ethylene glycol)-block-poly(trimethylene carbonate) nanoparticles for the controlled release of dexamethasone, *J. Control. Release*. 111 (2006) 263–270. <https://doi.org/10.1016/j.jconrel.2005.12.001>.
- [31] J. Leroux, F. De Jaeghere, E. Doelker, R. Gurny, Biodegradable nanoparticles- From sustained release formulations to improved site specific drug delivery, *J. Control. Release*. 39 (1996) 339–350.
- [32] X. Song, Y. Zhao, W. Wu, Y. Bi, Z. Cai, Q. Chen, Y. Li, S. Hou, PLGA nanoparticles simultaneously loaded with vincristine sulfate and verapamil hydrochloride: Systematic study of particle size and drug entrapment efficiency, *Int. J. Pharm.* 350 (2008) 320–329. <https://doi.org/10.1016/j.ijpharm.2007.08.034>.
- [33] C. Solans, I. Solé, Nano-emulsions: Formation by low-energy methods, *Curr. Opin. Colloid Interface Sci.* 17 (2012) 246–254. <https://doi.org/10.1016/j.cocis.2012.07.003>.
- [34] N. Anton, J.P. Benoit, P. Saulnier, Design and production of nanoparticles formulated from nano-emulsion templates-A review, *J. Control. Release*. 128 (2008) 185–199. <https://doi.org/10.1016/j.jconrel.2008.02.007>.
- [35] K. Shinoda, H. Saito, The effect of temperature on the phase equilibria and the types of dispersions of the ternary system composed of water, cyclohexane, and nonionic surfactant, *J. Colloid Interface Sci.* 26 (1968) 70–74. [https://doi.org/10.1016/0021-9797\(68\)90273-7](https://doi.org/10.1016/0021-9797(68)90273-7).
- [36] I. Solè, C.M. Pey, A. Maestro, C. González, M. Porras, C. Solans, J.M. Gutiérrez, Nano-emulsions prepared by the phase inversion composition method: Preparation variables and scale up, *J. Colloid Interface Sci.* 344 (2010) 417–423. <https://doi.org/10.1016/j.jcis.2009.11.046>.
- [37] N. Anton, P. Saulnier, Adhesive water-in-oil nano-emulsions generated by the phase inversion temperature method, *Soft Matter*. 9 (2013) 6465–6474. <https://doi.org/10.1039/c3sm51064f>.
- [38] Z. Mei, S. Liu, L. Wang, J. Jiang, J. Xu, D. Sun, Preparation of positively charged oil/water nano-emulsions with

- a sub-PIT method, *J. Colloid Interface Sci.* 361 (2011) 565–572. <https://doi.org/10.1016/j.jcis.2011.05.011>.
- [39] G. Lv, F. Wang, W. Cai, X. Zhang, Characterization of the emulsions formed by catastrophic phase inversion, *Colloids Surfaces A Physicochem. Eng. Asp.* 450 (2014) 141–147. <https://doi.org/10.1016/j.colsurfa.2014.03.023>.
- [40] M. Hesseien, C. Kim, E. Prouzet, N. Singh, Stability and tunability of O/W Nanoemulsions prepared by PIC, *Langmuir*. 27, 2299–2 (2011) 2299–2307.
- [41] G. Calderó, M.J. García-Celma, C. Solans, Formation of polymeric nano-emulsions by a low-energy method and their use for nanoparticle preparation, *J. Colloid Interface Sci.* 353 (2011) 406–411. <https://doi.org/10.1016/j.jcis.2010.09.073>.
- [42] C.M. Pey, A. Maestro, I. Solé, C. González, C. Solans, J.M. Gutiérrez, Optimization of nano-emulsions prepared by low-energy emulsification methods at constant temperature using a factorial design study, *Colloids Surfaces A Physicochem. Eng. Asp.* 288 (2006) 144–150. <https://doi.org/10.1016/j.colsurfa.2006.02.026>.
- [43] C. Fornaguera, A. Dols-Perez, G. Calderó, M.J. García-Celma, J. Camarasa, C. Solans, PLGA nanoparticles prepared by nano-emulsion templating using low-energy methods as efficient nanocarriers for drug delivery across the blood-brain barrier, *J. Control. Release.* 211 (2015) 134–143. <https://doi.org/10.1016/j.jconrel.2015.06.002>.
- [44] C. Fornaguera, S. Grijalvo, M. Galán, E. Fuentes-Paniagua, F.J. De La Mata, R. Gómez, R. Eritja, G. Calderó, C. Solans, Novel non-viral gene delivery systems composed of carbosilane dendron functionalized nanoparticles prepared from nano-emulsions as non-viral carriers for antisense oligonucleotides, *Int. J. Pharm.* 478 (2015) 113–123. <https://doi.org/10.1016/j.ijpharm.2014.11.031>.
- [45] N. Usón, M.J. Garcia, C. Solans, Formation of water-in-oil (W/O) nano-emulsions in a water/mixed non-ionic surfactant/oil systems prepared by a low-energy emulsification method, *Colloids Surfaces A Physicochem. Eng. Asp.* 250 (2004) 415–421. <https://doi.org/10.1016/j.colsurfa.2004.03.039>.
- [46] A. Maestro, I. Solè, C. González, C. Solans, J.M. Gutiérrez, Influence of the phase behavior on the properties of ionic nanoemulsions prepared by the phase inversion composition method, *J. Colloid Interface Sci.* 327 (2008) 433–439. <https://doi.org/10.1016/j.jcis.2008.07.059>.
- [47] C.A. Miller, Spontaneous Emulsification Produced by Diffusion - A Review, *Colloids and Surfaces.* 29 (1988) 89–102. [https://doi.org/10.1016/0166-6622\(88\)80173-2](https://doi.org/10.1016/0166-6622(88)80173-2).
- [48] M. V. Ostrovsky, R.J. Good, Mechanism of microemulsion formation in systems with low interfacial tension: Occurrence, properties, and behavior of microemulsions, *J. Colloid Interface Sci.* 102 (1984) 206–226. [https://doi.org/10.1016/0021-9797\(84\)90213-3](https://doi.org/10.1016/0021-9797(84)90213-3).
- [49] S.A. Vitale, J.L. Katz, Liquid droplet dispersions formed by homogeneous liquid-liquid nucleation: “The ouzo effect,” *Langmuir*. 19 (2003) 4105–4110. <https://doi.org/10.1021/la026842o>.
- [50] D. Carteau, I. Pianet, P. Brunerie, B. Guillemat, D.M. Bassani, Probing the initial events in the spontaneous emulsification of trans-anethole using dynamic NMR spectroscopy, *Langmuir*. 23 (2007) 3561–3565. <https://doi.org/10.1021/la062339q>.
- [51] D. Carteau, D. Bassani, I. Pianet, The “Ouzo effect”: Following the spontaneous emulsification of trans-anethole in water by NMR, *Comptes Rendus Chim.* 11 (2008) 493–498. <https://doi.org/10.1016/j.crci.2007.11.003>.

- [52] A.R. Tehrani-Bagha, A. Viladot, K. Holmberg, L. Nordstierna, An Ouzo emulsion of toluene in water characterized by NMR diffusometry and static multiple light scattering, *Colloids Surfaces A Physicochem. Eng. Asp.* 494 (2016) 81–86. <https://doi.org/10.1016/j.colsurfa.2016.01.008>.
- [53] A. Malzert-Fréon, J.P. Benoît, F. Boury, Interactions between poly(ethylene glycol) and protein in dichloromethane/water emulsions: A study of interfacial properties, *Eur. J. Pharm. Biopharm.* 69 (2008) 835–843. <https://doi.org/10.1016/j.ejpb.2008.01.021>.
- [54] A. Malzert-Fréon, K. Schönhammer, J.P. Benoît, F. Boury, Interactions between poly(ethylene glycol) and protein in dichloromethane/water emulsions. 2. Conditions required to obtain spontaneous emulsification allowing the formation of bioresorbable poly(D,L lactic acid) microparticles, *Eur. J. Pharm. Biopharm.* 73 (2009) 66–73. <https://doi.org/10.1016/j.ejpb.2009.04.011>.
- [55] Y. Kawashima, T. Niwa, T. Handa, H. Takeuchi, T. Iwamoto, K. Itoh, Preparation of controlled-release microspheres of ibuprofen with acrylic polymers by a novel quasi-emulsion solvent diffusion method, *J. Pharm. Sci.* 78 (1989) 68–72. <https://doi.org/10.1002/jps.2600780118>.
- [56] A. Schade, T. Niwa, H. Takeuchi, T. Hino, Y. Kawashima, Aqueous colloidal polymer dispersions of biodegradable DL-lactide/glycolide copolymer as basis for latex films: A new approach for the development of biodegradable depot systems, *Int. J. Pharm.* 117 (1995) 209–217. [https://doi.org/10.1016/0378-5173\(94\)00333-Z](https://doi.org/10.1016/0378-5173(94)00333-Z).
- [57] S.H. Jung, D.H. Lim, S.H. Jung, J.E. Lee, K.S. Jeong, H. Seong, B.C. Shin, Amphotericin B-entrapping lipid nanoparticles and their in vitro and in vivo characteristics, *Eur. J. Pharm. Sci.* 37 (2009) 313–320. <https://doi.org/10.1016/j.ejps.2009.02.021>.
- [58] H. Murakami, M. Kobayashi, H. Takeuchi, Y. Kawashima, Preparation of poly(DL-lactide-co-glycolide) nanoparticles by modified spontaneous emulsification solvent diffusion method, *Int. J. Pharm.* 187 (1999) 143–152. [https://doi.org/10.1016/S0378-5173\(99\)00187-8](https://doi.org/10.1016/S0378-5173(99)00187-8).
- [59] Z. Wang, W. Liu, H. Xu, X. Yang, Preparation and in vitro Studies of Stealth PEGylated PLGA Nanoparticles as Carriers for Arsenic Trioxide, *Chinese J. Chem. Eng.* 15 (2007) 795–801. [https://doi.org/10.1016/s1004-9541\(08\)60005-1](https://doi.org/10.1016/s1004-9541(08)60005-1).
- [60] Y. Baimark, M. Srisa-ard, J. Threeprom, N.A. Narkkong, Preparation of nanoparticle colloids of methoxy poly(ethylene glycol)-b-poly(D,L-lactide): Effects of surfactant and organic solvent, *Colloid Polym. Sci.* 285 (2007) 1521–1525. <https://doi.org/10.1007/s00396-007-1731-8>.
- [61] Y. Baimark, M. Srisa-Ard, J. Threeprom, P. Phinyocheep, S. Kittipoom, Preparation of surfactant-free nanoparticles of methoxy poly(ethylene glycol)-b-poly(D,L-lactide-co-glycolide-co-ε-caprolactone), *Colloid J.* 71 (2009) 18–21. <https://doi.org/10.1134/S1061933X09010025>.
- [62] H. Murakami, M. Kobayashi, H. Takeuchi, Y. Kawashima, Further application of a modified spontaneous emulsification solvent diffusion method to various types of PLGA and PLA polymers for preparation of nanoparticles, *Powder Technol.* 107 (2000) 137–143. [https://doi.org/10.1016/S0032-5910\(99\)00182-5](https://doi.org/10.1016/S0032-5910(99)00182-5).
- [63] J. Bae, T.P. Russell, R.C. Hayward, Osmotically driven formation of double emulsions stabilized by amphiphilic block copolymers, *Angew. Chemie - Int. Ed.* 53 (2014) 8240–8245. <https://doi.org/10.1002/anie.201405229>.
- [64] C. Li, W. Wang, X. Wang, H. Jiang, J. Zhu, S. Lin, Fabrication of porous polymer microspheres by tuning amphiphilicity of the polymer and emulsion-solvent evaporation processing, *Eur. Polym. J.* 68 (2015) 409–418.

- <https://doi.org/10.1016/j.eurpolymj.2015.05.011>.
- [65] X. Gao, F. Gao, L. Chen, Y. Yao, T. Chen, S. Lin, Tuning the morphology of amphiphilic copolymer aggregates by compound emulsifier via emulsion–solvent evaporation, *J. Saudi Chem. Soc.* 22 (2018) 297–305. <https://doi.org/10.1016/j.jscs.2016.05.007>.
- [66] K.H. Ku, J.M. Shin, D. Klinger, S.G. Jang, R.C. Hayward, C.J. Hawker, B.J. Kim, Particles with Tunable Porosity and Morphology by Controlling Interfacial Instability in Block Copolymer Emulsions, *ACS Nano.* 10 (2016) 5243–5251. <https://doi.org/10.1021/acsnano.6b00985>.
- [67] Y. Kanakubo, F. Ito, Y. Murakami, Novel one-pot facile technique for preparing nanoparticles modified with hydrophilic polymers on the surface via block polymer-assisted emulsification/evaporation process, *Colloids Surfaces B Biointerfaces.* 78 (2010) 85–91. <https://doi.org/10.1016/j.colsurfb.2010.02.017>.
- [68] T. Takami, Y. Murakami, Development of PEG-PLA/PLGA microparticles for pulmonary drug delivery prepared by a novel emulsification technique assisted with amphiphilic block copolymers, *Colloids Surfaces B Biointerfaces.* 87 (2011) 433–438. <https://doi.org/10.1016/j.colsurfb.2011.06.004>.
- [69] N. Yoneki, T. Takami, T. Ito, R. Anzai, K. Fukuda, K. Kinoshita, S. Sonotaki, Y. Murakami, One-pot facile preparation of PEG-modified PLGA nanoparticles: Effects of PEG and PLGA on release properties of the particles, *Colloids Surfaces A Physicochem. Eng. Asp.* 469 (2015) 66–72. <https://doi.org/10.1016/j.colsurfa.2015.01.011>.
- [70] T. Takami, Y. Murakami, Unexpected and successful “one-step” formation of porous polymeric particles only by mixing organic solvent and water under “low-energy-input” conditions, *Langmuir.* 30 (2014) 3329–3336. <https://doi.org/10.1021/la500324j>.
- [71] D. Ghosh Dastidar, S. Saha, M. Chowdhury, Porous microspheres: Synthesis, characterisation and applications in pharmaceutical & medical fields, *Int. J. Pharm.* 548 (2018) 34–48. <https://doi.org/10.1016/j.ijpharm.2018.06.015>.
- [72] Y. Wang, X. Shi, L. Ren, C. Wang, D.A. Wang, Porous poly (lactic-co-glycolide) microsphere sintered scaffolds for tissue repair applications, *Mater. Sci. Eng. C.* 29 (2009) 2502–2507. <https://doi.org/10.1016/j.msec.2009.07.018>.
- [73] J.L. Brown, L.S. Nair, C.T. Laurencin, Solvent/non-solvent sintering: A novel route to create porous microsphere scaffolds for tissue regeneration, *J. Biomed. Mater. Res. - Part B Appl. Biomater.* 86 (2008) 396–406. <https://doi.org/10.1002/jbm.b.31033>.
- [74] K.K. Taek, J.Y. Jun, S.L. Doo, T.G. Park, Gas foamed open porous biodegradable polymeric microspheres, *Biomaterials.* 27 (2006) 152–159. <https://doi.org/10.1016/j.biomaterials.2005.05.081>.
- [75] J. Fang, Y. Zhang, S. Yan, Z. Liu, S. He, L. Cui, J. Yin, Poly(L-glutamic acid)/chitosan polyelectrolyte complex porous microspheres as cell microcarriers for cartilage regeneration, *Acta Biomater.* 10 (2014) 276–288. <https://doi.org/10.1016/j.actbio.2013.09.002>.
- [76] C. Yu, A. Kornmuller, C. Brown, T. Hoare, L.E. Flynn, Decellularized adipose tissue microcarriers as a dynamic culture platform for human adipose-derived stem/stromal cell expansion, *Biomaterials.* 120 (2017) 66–80. <https://doi.org/10.1016/j.biomaterials.2016.12.017>.
- [77] J.X. Lu, B. Flautre, K. Anselme, P. Hardouini, A. Gallur, M. Descamps, B. Thierry, Role of interconnections in porous bioceramics on bone recolonization in vitro and in vivo, *J. Mater. Sci. Mater. Med.* 10 (1999) 111–120.

- [78] C. Zhang, T. Zhai, L.S. Turng, Aerogel microspheres based on cellulose nanofibrils as potential cell culture scaffolds, *Cellulose*. 24 (2017) 2791–2799. <https://doi.org/10.1007/s10570-017-1295-9>.
- [79] L. Wu, S. Bai, Y. Sun, Development of rigid bidisperse porous microspheres for high-speed protein chromatography, *Biotechnol. Prog.* 19 (2003) 1300–1306. <https://doi.org/10.1021/bp0201509>.
- [80] S. Haihong, L. Xiunan, M. Guanghui, S. Zhiguo, Polystyrene-type uniform porous microsphere enables high resolution and low-pressure chromatography of natural products - A case study with icariin purification, *Chromatographia*. 61 (2005) 9–15. <https://doi.org/10.1365/s10337-004-0466-7>.
- [81] A.I. Liapis, M.A. McCoy, Theory of perfusion chromatography, *J. Chromatogr. A*. 599 (1992) 87–104. [https://doi.org/10.1016/0021-9673\(92\)85461-2](https://doi.org/10.1016/0021-9673(92)85461-2).
- [82] Y. Cai, Y. Chen, X. Hong, Z. Liu, W. Yuan, Porous microsphere and its applications, *Int. J. Nanomedicine*. 8 (2013) 1111–1120. <https://doi.org/10.2147/IJN.S41271>.
- [83] Z. Liang, R. Ni, J. Zhou, S. Mao, Recent advances in controlled pulmonary drug delivery, *Drug Discov. Today*. 20 (2015) 380–389. <https://doi.org/10.1016/j.drudis.2014.09.020>.
- [84] S. Mangal, W. Gao, T. Li, Q.T. Zhou, Pulmonary delivery of nanoparticle chemotherapy for the treatment of lung cancers: Challenges and opportunities, *Acta Pharmacol. Sin.* 38 (2017) 782–797. <https://doi.org/10.1038/aps.2017.34>.
- [85] B.K. Rubin, R.W. Williams, Emerging aerosol drug delivery strategies: From bench to clinic, *Adv. Drug Deliv. Rev.* 75 (2014) 141–148. <https://doi.org/10.1016/j.addr.2014.06.008>.
- [86] C. Loira-Pastoriza, J. Todoroff, R. Vanbever, Delivery strategies for sustained drug release in the lungs, *Adv. Drug Deliv. Rev.* 75 (2014) 81–91. <https://doi.org/10.1016/j.addr.2014.05.017>.
- [87] B. Patel, N. Gupta, F. Ahsan, Particle engineering to enhance or lessen particle uptake by alveolar macrophages and to influence the therapeutic outcome, *Eur. J. Pharm. Biopharm.* 89 (2015) 163–174. <https://doi.org/10.1016/j.ejpb.2014.12.001>.
- [88] C. Lee, J.S. Choi, I. Kim, K.T. Oh, E.S. Lee, E.S. Park, K.C. Lee, Y.S. Youn, Long-acting inhalable chitosan-coated poly(lactic-co-glycolic acid) nanoparticles containing hydrophobically modified exendin-4 for treating type 2 diabetes, *Int. J. Nanomedicine*. 8 (2013) 2975–2983. <https://doi.org/10.2147/IJN.S48197>.
- [89] M.N. Sahib, Y. Darwis, K.K. Peh, S.A. Abdulameer, Y.T. Fung Tan, Incorporation of beclomethasone dipropionate into polyethylene glycol-diacyl lipid micelles as a pulmonary delivery system, *Drug Dev. Res.* 73 (2012) 90–105. <https://doi.org/10.1002/ddr.21000>.
- [90] M. Beck-Broichsitter, M. Rieger, R. Reul, T. Gessler, W. Seeger, T. Schmehl, Correlation of drug release with pulmonary drug absorption profiles for nebulizable liposomal formulations, *Eur. J. Pharm. Biopharm.* 84 (2013) 106–114. <https://doi.org/10.1016/j.ejpb.2012.12.003>.
- [91] Y.Z. Li, X. Sun, T. Gong, J. Liu, J. Zuo, Z.R. Zhang, Inhalable microparticles as carriers for pulmonary delivery of thymopentin-loaded solid lipid nanoparticles, *Pharm. Res.* 27 (2010) 1977–1986. <https://doi.org/10.1007/s11095-010-0201-z>.
- [92] R. Inapagolla, B.R. Guru, Y.E. Kurtoglu, X. Gao, M. Lieh-Lai, D.J.P. Bassett, R.M. Kannan, In vivo efficacy of dendrimer-methylprednisolone conjugate formulation for the treatment of lung inflammation, *Int. J. Pharm.* 399 (2010) 140–147. <https://doi.org/10.1016/j.ijpharm.2010.07.030>.

- [93] S.J. Koussoroplis, G. Paulissen, D. Tyteca, H. Goldansaz, J. Todoroff, C. Barilly, C. Uyttenhove, J. Van Snick, D. Cataldo, R. Vanbever, PEGylation of antibody fragments greatly increases their local residence time following delivery to the respiratory tract, *J. Control. Release.* 187 (2014) 91–100. <https://doi.org/10.1016/j.jconrel.2014.05.021>.
- [94] M. Semmler-Behnke, S. Takenaka, S. Fertsch, A. Wenk, J. Seitz, P. Mayer, G. Oberdörster, W.G. Kreyling, Efficient elimination of inhaled nanoparticles from the alveolar region: Evidence for interstitial uptake and subsequent reentrainment onto airways epithelium, *Environ. Health Perspect.* 115 (2007) 728–733. <https://doi.org/10.1289/ehp.9685>.
- [95] L.A. Dailey, T. Schmehl, T. Gessler, M. Wittmar, F. Grimminger, W. Seeger, T. Kissel, Nebulization of biodegradable nanoparticles: Impact of nebulizer technology and nanoparticle characteristics on aerosol features, *J. Control. Release.* 86 (2003) 131–144. [https://doi.org/10.1016/S0168-3659\(02\)00370-X](https://doi.org/10.1016/S0168-3659(02)00370-X).
- [96] N. Tsapis, D. Bennett, B. Jackson, D.A. Weitz, D.A. Edwards, Trojan particles: Large porous carriers of nanoparticles for drug delivery, *Proc. Natl. Acad. Sci. U. S. A.* 99 (2002) 12001–12005. <https://doi.org/10.1073/pnas.182233999>.
- [97] F. Ungaro, I. D’Angelo, C. Coletta, R. D’Emmanuele Di Villa Bianca, R. Sorrentino, B. Perfetto, M.A. Tufano, A. Miro, M.I. La Rotonda, F. Quaglia, Dry powders based on PLGA nanoparticles for pulmonary delivery of antibiotics: Modulation of encapsulation efficiency, release rate and lung deposition pattern by hydrophilic polymers, *J. Control. Release.* 157 (2012) 149–159. <https://doi.org/10.1016/j.jconrel.2011.08.010>.
- [98] P. Begat, D.A.V. Morton, J.N. Staniforth, R. Price, The cohesive-adhesive balances in dry powder inhaler formulations II: Influence on fine particle delivery characteristics, *Pharm. Res.* 21 (2004) 1826–1833. <https://doi.org/10.1023/B:PHAM.0000045236.60029.cb>.
- [99] R. Ni, J. Zhao, Q. Liu, Z. Liang, U. Muenster, S. Mao, Nanocrystals embedded in chitosan-based respirable swellable microparticles as dry powder for sustained pulmonary drug delivery, *Eur. J. Pharm. Sci.* 99 (2017) 137–146. <https://doi.org/10.1016/j.ejps.2016.12.013>.
- [100] I.M. El-Sherbiny, H.D.C. Smyth, Biodegradable nano-micro carrier systems for sustained pulmonary drug delivery: (I) Self-assembled nanoparticles encapsulated in respirable/swellable semi-IPN microspheres, *Int. J. Pharm.* 395 (2010) 132–141. <https://doi.org/10.1016/j.ijpharm.2010.05.032>.
- [101] K. Möbus, J. Siepmann, R. Bodmeier, Zinc-alginate microparticles for controlled pulmonary delivery of proteins prepared by spray-drying, *Eur. J. Pharm. Biopharm.* 81 (2012) 121–130. <https://doi.org/10.1016/j.ejpb.2012.01.018>.
- [102] D.A. Edwards, J. Hanes, G. Caponetti, J. Hrkach, A. Ben-Jebria, M. Lou Eskew, J. Mintzes, D. Deaver, N. Lotan, R. Langer, Large porous particles for pulmonary drug delivery, *Science* (80-.). 276 (1997) 1868–1871. <https://doi.org/10.1126/science.276.5320.1868>.
- [103] G. Oberdörster, Lung Clearance of Inhaled Insoluble and Soluble Particles, *J. AEROSOL Med.* 1 (1988) 289–330.
- [104] Y.J. Oh, J. Lee, J.Y. Seo, T. Rhim, S.H. Kim, H.J. Yoon, K.Y. Lee, Preparation of budesonide-loaded porous PLGA microparticles and their therapeutic efficacy in a murine asthma model, *J. Control. Release.* 150 (2011) 56–62. <https://doi.org/10.1016/j.jconrel.2010.11.001>.

- [105] D.S. Dhanda, P. Tyagi, S.S. Mirvish, U.B. Kompella, Supercritical fluid technology based large porous celecoxib-PLGA microparticles do not induce pulmonary fibrosis and sustain drug delivery and efficacy for several weeks following a single dose, *J. Control. Release.* 168 (2013) 239–250. <https://doi.org/10.1016/j.jconrel.2013.03.027>.
- [106] A. Rawat, Q.H. Majumder, F. Ahsan, Inhalable large porous microspheres of low molecular weight heparin: In vitro and in vivo evaluation, *J. Control. Release.* 128 (2008) 224–232. <https://doi.org/10.1016/j.jconrel.2008.03.013>.
- [107] B. Patel, V. Gupta, F. Ahsan, PEG-PLGA based large porous particles for pulmonary delivery of a highly soluble drug, low molecular weight heparin, *J. Control. Release.* 162 (2012) 310–320. <https://doi.org/10.1016/j.jconrel.2012.07.003>.
- [108] G. Tang, Z. Tan, W. Zeng, X. Wang, C. Shi, Y. Liu, H. He, R. Chen, X. Ye, Recent Advances of Chitosan-Based Injectable Hydrogels for Bone and Dental Tissue Regeneration, *Front. Bioeng. Biotechnol.* 8 (2020) 1–15. <https://doi.org/10.3389/fbioe.2020.587658>.
- [109] E. Chevalier, D. Chulia, C. Pouget, M. Viana, Fabrication of Porous Substrates: A Review of Processes Using Pore Forming Agents in the Biomaterial Field, *J. Pharm. Sci.* 97 (2008) 1135–1154. <https://doi.org/10.1002/jps>.
- [110] R.S. Leena, M. Vairamani, N. Selvamurugan, Alginate/Gelatin scaffolds incorporated with Silibinin-loaded Chitosan nanoparticles for bone formation in vitro, *Colloids Surfaces B Biointerfaces.* 158 (2017) 308–318. <https://doi.org/10.1016/j.colsurfb.2017.06.048>.
- [111] Y. Zhang, J.R. Venugopal, A. El-Turki, S. Ramakrishna, B. Su, C.T. Lim, Electrospun biomimetic nanocomposite nanofibers of hydroxyapatite/chitosan for bone tissue engineering, *Biomaterials.* 29 (2008) 4314–4322. <https://doi.org/10.1016/j.biomaterials.2008.07.038>.
- [112] K.C. Kavya, R. Jayakumar, S. Nair, K.P. Chennazhi, Fabrication and characterization of chitosan/gelatin/nSiO₂ composite scaffold for bone tissue engineering, *Int. J. Biol. Macromol.* 59 (2013) 255–263. <https://doi.org/10.1016/j.ijbiomac.2013.04.023>.
- [113] M. Peter, N.S. Binulal, S. V. Nair, N. Selvamurugan, H. Tamura, R. Jayakumar, Novel biodegradable chitosan-gelatin/nano-bioactive glass ceramic composite scaffolds for alveolar bone tissue engineering, *Chem. Eng. J.* 158 (2010) 353–361. <https://doi.org/10.1016/j.cej.2010.02.003>.
- [114] D. Mao, Q. Li, N. Bai, H. Dong, D. Li, Porous stable poly(lactic acid)/ethyl cellulose/hydroxyapatite composite scaffolds prepared by a combined method for bone regeneration, *Carbohydr. Polym.* 180 (2018) 104–111. <https://doi.org/10.1016/j.carbpol.2017.10.031>.
- [115] M. Gutiérrez-Sánchez, V.A. Escobar-Barrios, A. Pozos-Guillén, D.M. Escobar-García, RGD-functionalization of PLA/starch scaffolds obtained by electrospinning and evaluated in vitro for potential bone regeneration, *Mater. Sci. Eng. C.* 96 (2019) 798–806. <https://doi.org/10.1016/j.msec.2018.12.003>.
- [116] P. Kowalczyk, P. Trzaskowska, I. Łojarczyk, R. Podgórski, T. Ciach, Production of 3D printed polylactide scaffolds with surface grafted hydrogel coatings, *Colloids Surfaces B Biointerfaces.* 179 (2019) 136–142. <https://doi.org/10.1016/j.colsurfb.2019.03.069>.
- [117] J. Ju, X. Peng, K. Huang, L. Li, X. Liu, C. Chitrakar, L. Chang, Z. Gu, T. Kuang, High-performance porous PLLA-based scaffolds for bone tissue engineering: Preparation, characterization, and in vitro and in vivo

- evaluation, *Polymer (Guildf)*. 180 (2019) 121707. <https://doi.org/10.1016/j.polymer.2019.121707>.
- [118] B.I. Oladapo, S.A. Zahedi, A.O.M. Adeoye, 3D printing of bone scaffolds with hybrid biomaterials, *Compos. Part B Eng.* 158 (2019) 428–436. <https://doi.org/10.1016/j.compositesb.2018.09.065>.
- [119] L.R. Jaidev, K. Chatterjee, Surface functionalization of 3D printed polymer scaffolds to augment stem cell response, *Mater. Des.* 161 (2019) 44–54. <https://doi.org/10.1016/j.matdes.2018.11.018>.
- [120] P. Song, C. Zhou, H. Fan, B. Zhang, X. Pei, Y. Fan, Q. Jiang, R. Bao, Q. Yang, Z. Dong, X. Zhang, Novel 3D porous biocomposite scaffolds fabricated by fused deposition modeling and gas foaming combined technology, *Compos. Part B Eng.* 152 (2018) 151–159. <https://doi.org/10.1016/j.compositesb.2018.06.029>.
- [121] H.K. Oh, A. Kikuchi, M. Yamato, T. Okano, Accelerated cell sheet recovery by co-grafting of PEG with PIPAAm onto porous cell culture membranes, *Biomaterials*. 24 (2003) 1223–1232. [https://doi.org/10.1016/S0142-9612\(02\)00469-6](https://doi.org/10.1016/S0142-9612(02)00469-6).
- [122] O.H. Kwon, A. Kikuchi, M. Yamato, Y. Sakurai, T. Okano, Rapid cell sheet detachment from poly(N-isopropylacrylamide)-grafted porous cell culture membranes, *J. Biomed. Mater. Res.* 50 (2000) 82–89. [https://doi.org/10.1002/\(SICI\)1097-4636\(200004\)50:1<82::AID-JBM12>3.0.CO;2-7](https://doi.org/10.1002/(SICI)1097-4636(200004)50:1<82::AID-JBM12>3.0.CO;2-7).
- [123] J. Rother, M. Büchenschütz-Göbeler, H. Nöding, S. Steltenkamp, K. Samwer, A. Janshoff, Cytoskeleton remodelling of confluent epithelial cells cultured on porous substrates, *J. R. Soc. Interface*. 12 (2015). <https://doi.org/10.1098/rsif.2014.1057>.
- [124] A. Saraf, S.L. Baggett, R.M. Raphael, F.K. Kasper, A.G. Mikos, Regulated Non-Viral Gene Delivery from Coaxial Electrospun Fiber Mesh Scaffolds, *J. Control.* 143 (2010) 95–103. <https://doi.org/10.1038/jid.2014.371>.
- [125] K. Kim, Y.K. Luu, C. Chang, D. Fang, B.S. Hsiao, B. Chu, M. Hadjiargyrou, Incorporation and controlled release of a hydrophilic antibiotic using poly(lactide-co-glycolide)-based electrospun nanofibrous scaffolds, *J. Control. Release*. 98 (2004) 47–56. <https://doi.org/10.1016/j.jconrel.2004.04.009>.
- [126] B.M. Baker, R.L. Mauck, The effect of nanofiber alignment on the maturation of engineered meniscus constructs, *Biomaterials*. 28 (2007) 1967–1977. <https://doi.org/10.1016/j.biomaterials.2007.01.004>.
- [127] J.K. Wise, A.L. Yarin, C.M. Megaridis, M. Cho, Chondrogenic differentiation of human mesenchymal stem cells on oriented nanofibrous scaffolds: Engineering the superficial zone of articular cartilage, *Tissue Eng. - Part A*. 15 (2009) 913–921. <https://doi.org/10.1089/ten.tea.2008.0109>.
- [128] G. Wei, P. Ma X., Macroporous and nanofibrous polymer scaffolds and polymer/bone-like apatite composite scaffolds generated by sugar spheres, *J. Biomed. Mater. Res. Part A*. 78A (2006) 306–315. <https://doi.org/10.1002/jbm.a>.
- [129] Y.M. Elçin, B. Inanç, A.E. Elçin, Differentiation of human embryonic stem cells on periodontal ligament fibroblasts, *Methods Mol. Biol.* 1307 (2015) 223–236. https://doi.org/10.1007/7651_2014_130.
- [130] E. Knight, B. Murray, R. Carnachan, S. Przyborski, Alvetex® : Polystyrene Scaffold Technology for Routine Three Dimensional Cell Culture, *3D Cell Cult. Methods Protoc. Methods Mol. Biol.* 695 (2011) 323–340. <https://doi.org/10.1007/978-1-60761-984-0>.
- [131] M. Bokhari, R.J. Carnachan, S.A. Przyborski, N.R. Cameron, Emulsion-templated porous polymers as scaffolds for three dimensional cell culture: Effect of synthesis parameters on scaffold formation and homogeneity, *J. Mater. Chem.* 17 (2007) 4088–4094. <https://doi.org/10.1039/b707499a>.

- [132] R.J. Carnachan, M. Bokhari, S.A. Przyborski, N.R. Cameron, Tailoring the morphology of emulsion-templated porous polymers, *Soft Matter*. 2 (2006) 608–616. <https://doi.org/10.1039/b603211g>.
- [133] P. Sepulveda, F.S. Ortega, M.D.M. Innocentini, V.C. Pandolfelli, Properties of highly porous hydroxyapatite obtained by the gelcasting of foams, *J. Am. Ceram. Soc.* 83 (2000) 3021–3024. <https://doi.org/10.1111/j.1151-2916.2000.tb01677.x>.
- [134] M.M. Asli, B. Pourdeyhimi, E.G. Lobo, Release Profiles of Tricalcium Phosphate Nanoparticles from Poly(L-lactic acid) Electrospun Scaffolds with Single Component, Core-Sheath, or Porous Fiber Morphologies: Effects on hASC Viability and Osteogenic Differentiation, *Macromol. Biosci.* 12 (2012) 893–900. <https://doi.org/10.1002/mabi.201100470>.
- [135] S. Honarbakhsh, B. Pourdeyhimi, Scaffolds for drug delivery, part I: Electrospun porous poly(lactic acid) and poly(lactic acid)/poly(ethylene oxide) hybrid scaffolds, *J. Mater. Sci.* 46 (2011) 2874–2881. <https://doi.org/10.1007/s10853-010-5161-5>.
- [136] M. Hasegawa, A. Sudo, V.S. Komlev, S.M. Barinov, A. Uchida, High release of antibiotic from a novel hydroxyapatite with bimodal pore size distribution, *J. Biomed. Mater. Res. - Part B Appl. Biomater.* 70 (2004) 332–339. <https://doi.org/10.1002/jbm.b.30047>.
- [137] N. Tamai, A. Myoui, T. Tomita, T. Nakase, J. Tanaka, T. Ochi, H. Yoshikawa, Novel hydroxyapatite ceramics with an interconnective porous structure exhibit superior osteoconduction in vivo, *J. Biomed. Mater. Res.* 59 (2002) 110–117. <https://doi.org/10.1002/jbm.1222>.
- [138] V.S. Komlev, S.M. Barinov, Porous hydroxyapatite ceramics of bi-modal pore size distribution, *J. Mater. Sci. Mater. Med.* 13 (2002) 295–299. <https://doi.org/10.1023/A:1014015002331>.
- [139] T. Ponnusamy, L.B. Lawson, L.C. Freytag, D.A. Blake, R.S. Ayyala, V.T. John, In vitro degradation and release characteristics of spin coated thin films of PLGA with a “breath figure” morphology., *Biomater.* 2 (2012) 77–86. <https://doi.org/10.4161/biom.20390>.
- [140] M. Grabacka, P. Waligorski, A. Zapata, D.A. Blake, D. Wyczechowska, A. Wilk, M. Rutkowska, H. Vashistha, R. Ayyala, T. Ponnusamy, V.T. John, F. Culicchia, A. Wisniewska-Becker, K. Reiss, Fenofibrate subcellular distribution as a rationale for the intracranial delivery through biodegradable carrier, *J. Physiol. Pharmacol.* 66 (2015) 233–247.
- [141] E.D. Schoenberg, D.A. Blake, F.B. Swann, A.W. Parlin, D. Zurakowski, C.E. Margo, T. Ponnusamy, V.T. John, R.S. Ayyala, Effect of two novel sustained-release drug delivery systems on bleb fibrosis: An in vivo glaucoma drainage device study in a rabbit model, *Transl. Vis. Sci. Technol.* 4 (2015) 1–16. <https://doi.org/10.1167/tvst.4.3.4>.
- [142] Z. Dai, X. Yu, J. Hong, X. Liu, J. Sun, X. Sun, Development of a novel CsA-PLGA drug delivery system based on a glaucoma drainage device for the prevention of postoperative fibrosis, *Mater. Sci. Eng. C.* 66 (2016) 206–214. <https://doi.org/10.1016/j.msec.2016.04.077>.
- [143] G. Daban, C. Bayram, B. Bozdoğan, E.B. Denkbaş, Porous polyurethane film fabricated via the breath figure approach for sustained drug release, *J. Appl. Polym. Sci.* 136 (2019) 1–9. <https://doi.org/10.1002/app.47658>.
- [144] Y. Su, J. Dang, H. Zhang, Y. Zhang, W. Tian, Supramolecular Host-Guest Interaction-Enhanced Adjustable Drug Release Based on β -Cyclodextrin-Functionalized Thermoresponsive Porous Polymer Films, *Langmuir*. 33

- (2017) 7393–7402. <https://doi.org/10.1021/acs.langmuir.7b01502>.
- [145] J. Tian, H. Zhao, X. Quan, Y. Zhang, H. Yu, S. Chen, Fabrication of graphene quantum dots/silicon nanowires nanohybrids for photoelectrochemical detection of microcystin-LR, *Sensors Actuators, B Chem.* 196 (2014) 532–538. <https://doi.org/10.1016/j.snb.2014.02.046>.
- [146] R.P. Liang, Z.X. Wang, L. Zhang, J.D. Qiu, A label-free amperometric immunosensor for alpha-fetoprotein determination based on highly ordered porous multi-walled carbon nanotubes/silica nanoparticles array platform, *Sensors Actuators, B Chem.* 166–167 (2012) 569–575. <https://doi.org/10.1016/j.snb.2012.03.011>.
- [147] Y. Li, J. Zhang, L. Fang, T. Wang, S. Zhu, Y. Li, Z. Wang, L. Zhang, L. Cui, B. Yang, Fabrication of silicon/polymer composite nanopost arrays and their sensing applications, *Small.* 7 (2011) 2769–2774. <https://doi.org/10.1002/sml.201100313>.
- [148] X. Li, J. Zang, Y. Liu, Z. Lu, Q. Li, C.M. Li, Simultaneous detection of lactate and glucose by integrated printed circuit board based array sensing chip, *Anal. Chim. Acta.* 771 (2013) 102–107. <https://doi.org/10.1016/j.aca.2013.02.011>.
- [149] S.J. Bao, C.X. Guo, C.M. Li, Hydrophilic porous carbon with tailored nanostructure and its sensitive hydrogen peroxide biosensor, *RSC Adv.* 2 (2012) 1014–1020. <https://doi.org/10.1039/c1ra00319d>.
- [150] K. Urmann, P. Reich, J.G. Walter, D. Beckmann, E. Segal, T. Scheper, Rapid and label-free detection of protein a by aptamer-tethered porous silicon nanostructures, *J. Biotechnol.* 257 (2017) 171–177. <https://doi.org/10.1016/j.jbiotec.2017.01.005>.
- [151] N. Massad-Ivanir, S.K. Bhunia, N. Raz, E. Segal, R. Jelinek, Synthesis and characterization of a nanostructured porous silicon/carbon dot-hybrid for orthogonal molecular detection, *NPG Asia Mater.* 10 (2018) e463–e463. <https://doi.org/10.1038/am.2017.233>.
- [152] N. Massad-Ivanir, C. Shtenberg, T. Zeidman, E. Segal, Construction and characterization of porous SiO₂/hydrogel hybrids as optical biosensors for rapid detection of bacteria, *Adv. Funct. Mater.* 20 (2010) 2269–2277. <https://doi.org/10.1002/adfm.201000406>.
- [153] N. Massad-Ivanir, G. Shtenberg, N. Raz, C. Gazenbeek, D. Budding, M.P. Bos, E. Segal, Porous Silicon-Based Biosensors: Towards Real-Time Optical Detection of Target Bacteria in the Food Industry, *Sci. Rep.* 6 (2016) 1–12. <https://doi.org/10.1038/srep38099>.
- [154] R. Fopase, S. Paramasivam, P. Kale, B. Paramasivan, Strategies, challenges and opportunities of enzyme immobilization on porous silicon for biosensing applications, *J. Environ. Chem. Eng.* 8 (2020) 104266. <https://doi.org/10.1016/j.jece.2020.104266>.
- [155] K. Hisamatsu, T. Shiomi, S.I. Matsuura, T.Y. Nara, T. Tsunoda, F. Mizukami, K. Sakaguchi, α -Amylase immobilization capacities of mesoporous silicas with different morphologies and surface properties, *J. Porous Mater.* 19 (2012) 95–102. <https://doi.org/10.1007/s10934-011-9452-2>.
- [156] S.B. Sigurdardóttir, J. Lehmann, S. Ovtar, J.C. Grivel, M. Della Negra, A. Kaiser, M. Pinelo, Enzyme Immobilization on Inorganic Surfaces for Membrane Reactor Applications: Mass Transfer Challenges, Enzyme Leakage and Reuse of Materials, *Adv. Synth. Catal.* 360 (2018) 2578–2607. <https://doi.org/10.1002/adsc.201800307>.
- [157] S. Arshavsky-Graham, N. Massad-Ivanir, F. Paratore, T. Scheper, M. Bercovici, E. Segal, On Chip Protein Pre-

- Concentration for Enhancing the Sensitivity of Porous Silicon Biosensors, *ACS Sensors*. 2 (2017) 1767–1773. <https://doi.org/10.1021/acssensors.7b00692>.
- [158] M.A. Krepker, E. Segal, Dual-functionalized porous Si/hydrogel hybrid for label-free biosensing of organophosphorus compounds, *Anal. Chem.* 85 (2013) 7353–7360. <https://doi.org/10.1021/ac4011815>.
- [159] G. Shtenberg, N. Massad-Ivanir, E. Segal, Detection of trace heavy metal ions in water by nanostructured porous Si biosensors, *Analyst*. 140 (2015) 4507–4514. <https://doi.org/10.1039/c5an00248f>.
- [160] R. Vilensky, M. Bercovici, E. Segal, Oxidized Porous Silicon Nanostructures Enabling Electrokinetic Transport for Enhanced DNA Detection, *Adv. Funct. Mater.* 25 (2015) 6725–6732. <https://doi.org/10.1002/adfm.201502859>.
- [161] A. Tzur-Balter, A. Gilert, N. Massad-Ivanir, E. Segal, Engineering porous silicon nanostructures as tunable carriers for mitoxantrone dihydrochloride, *Acta Biomater.* 9 (2013) 6208–6217. <https://doi.org/10.1016/j.actbio.2012.12.010>.
- [162] N. Zilony-Hanin, M. Rosenberg, M. Richman, R. Yehuda, H. Schori, M. Motiei, S. Rahimipour, A. Groisman, E. Segal, O. Shefi, Neuroprotective Effect of Nerve Growth Factor Loaded in Porous Silicon Nanostructures in an Alzheimer’s Disease Model and Potential Delivery to the Brain, *Small*. 15 (2019) 1–13. <https://doi.org/10.1002/smll.201904203>.
- [163] N. Zilony, M. Rosenberg, L. Holtzman, H. Schori, O. Shefi, E. Segal, Prolonged controlled delivery of nerve growth factor using porous silicon nanostructures, *J. Control. Release*. 257 (2017) 51–59. <https://doi.org/10.1016/j.jconrel.2016.12.008>.
- [164] M. Rosenberg, D. Shilo, L. Galperin, T. Capucha, K. Tarabieh, A. Rachmiel, E. Segal, Bone morphogenic protein 2-loaded porous silicon carriers for osteoinductive implants, *Pharmaceutics*. 11 (2019) 4–6. <https://doi.org/10.3390/pharmaceutics11110602>.
- [165] L. Yang, X. Ning, K. Chen, H. Zhou, Preparation and properties of hydroxyapatite filters for microbial filtration, *Ceram. Int.* 33 (2007) 483–489. <https://doi.org/10.1016/j.ceramint.2005.10.014>.
- [166] D.S. Lee, Y.H. Choi, Y.D. Han, H.C. Yoon, S. Shoji, M.Y. Jung, Construction of membrane sieves using stoichiometric and stress-reduced Si₃N₄/SiO₂/Si₃N₄ multilayer films and their applications in blood plasma separation, *ETRI J.* 34 (2012) 226–234. <https://doi.org/10.4218/etrij.12.1711.0013>.
- [167] V. Gopishetty, I. Tokarev, S. Minko, Biocompatible stimuli-responsive hydrogel porous membranes via phase separation of a polyvinyl alcohol and Na-alginate intermolecular complex, *J. Mater. Chem.* 22 (2012) 19482–19487. <https://doi.org/10.1039/c2jm31778h>.
- [168] H. Kuroki, C. Islam, I. Tokarev, H. Hu, G. Liu, S. Minko, Tunable ultrathin membranes with nonvolatile pore shape memory, *ACS Appl. Mater. Interfaces*. 7 (2015) 10401–10406. <https://doi.org/10.1021/acsami.5b01416>.
- [169] I. Tokarev, M. Orlov, S. Minko, Responsive polyelectrolyte gel membranes, *Adv. Mater.* 18 (2006) 2458–2460. <https://doi.org/10.1002/adma.200601288>.
- [170] E.L. Giudice, J.D. Campbell, Needle-free vaccine delivery, *Adv. Drug Deliv. Rev.* 58 (2006) 68–89. <https://doi.org/10.1016/j.addr.2005.12.003>.
- [171] M.R. Prausnitz, R. Langer, Transdermal drug delivery, *Nat. Biotechnol.* 26 (2008) 1261–1268. <https://doi.org/10.1038/nbt.1504>.

- [172] K. Takeuchi, B. Kim, Functionalized microneedles for continuous glucose monitoring, *Nano Converg.* 5 (2018). <https://doi.org/10.1186/s40580-018-0161-2>.
- [173] M. Verhoeven, S. Bystrova, L. Winnubst, H. Qureshi, T.D. De Gruijl, R.J. Scheper, R. Luttge, Applying ceramic nanoporous microneedle arrays as a transport interface in egg plants and an ex-vivo human skin model, *Microelectron. Eng.* 98 (2012) 659–662. <https://doi.org/10.1016/j.mee.2012.07.022>.
- [174] L. Liu, H. Kai, K. Nagamine, Y. Ogawa, M. Nishizawa, Porous polymer microneedles with interconnecting microchannels for rapid fluid transport, *RSC Adv.* 6 (2016) 48630–48635. <https://doi.org/10.1039/c6ra07882f>.
- [175] K. Nagamine, J. Kubota, H. Kai, Y. Ono, M. Nishizawa, An array of porous microneedles for transdermal monitoring of intercellular swelling, *Biomed. Microdevices.* 19 (2017) 1–6. <https://doi.org/10.1007/s10544-017-0207-y>.
- [176] P.R. Miller, X. Xiao, I. Brener, D.B. Burckel, R. Narayan, R. Polsky, Microneedle-based transdermal sensor for on-chip potentiometric determination of K⁺, *Adv. Healthc. Mater.* 3 (2014) 876–881. <https://doi.org/10.1002/adhm.201300541>.
- [177] P. Miller, M. Moorman, R. Manginell, C. Ashlee, I. Brener, D. Wheeler, R. Narayan, R. Polsky, Towards an Integrated Microneedle Total Analysis Chip for Protein Detection, *Electroanalysis.* 28 (2016) 1305–1310. <https://doi.org/10.1002/elan.201600063>.
- [178] D. Nicholas, K.A. Logan, Y. Sheng, J. Gao, S. Farrell, D. Dixon, B. Callan, A.P. McHale, J.F. Callan, Rapid paper based colorimetric detection of glucose using a hollow microneedle device, *Int. J. Pharm.* 547 (2018) 244–249. <https://doi.org/10.1016/j.ijpharm.2018.06.002>.
- [179] M. Shirkhazadeh, Microneedles coated with porous calcium phosphate ceramics: Effective vehicles for transdermal delivery of solid trehalose, *J. Mater. Sci. Mater. Med.* 16 (2005) 37–45. <https://doi.org/10.1007/s10856-005-6444-2>.
- [180] W. Yu, G. Jiang, D. Liu, L. Li, H. Chen, Y. Liu, Q. Huang, Z. Tong, J. Yao, X. Kong, Fabrication of biodegradable composite microneedles based on calcium sulfate and gelatin for transdermal delivery of insulin, *Mater. Sci. Eng. C.* 71 (2017) 725–734. <https://doi.org/10.1016/j.msec.2016.10.063>.
- [181] A. Ullah, H.J. Choi, M. Jang, S. An, G.M. Kim, Smart microneedles with porous polymer layer for glucose-responsive insulin delivery, *Pharmaceutics.* 12 (2020) 1–15. <https://doi.org/10.3390/pharmaceutics12070606>.
- [182] A. Ullah, C.M. Kim, G.M. Kim, Porous polymer coatings on metal microneedles for enhanced drug delivery, *R. Soc. Open Sci.* 5 (2018). <https://doi.org/10.1098/rsos.171609>.
- [183] A. Ullah, H. Khan, H.J. Choi, G.M. Kim, Smart Microneedles with Porous Polymer Coatings for pH-Responsive Drug Delivery, *Polymers (Basel).* 11 (2019) 1834.
- [184] J.H. Park, S.O. Choi, R. Kamath, Y.K. Yoon, M.G. Allen, M.R. Prausnitz, Polymer particle-based micromolding to fabricate novel microstructures, *Biomed. Microdevices.* 9 (2007) 223–234. <https://doi.org/10.1007/s10544-006-9024-4>.
- [185] X. Zhao, S. Zhang, G. Yang, Z. Zhou, Y. Gao, Exploring trehalose on the release of levonorgestrel from implantable PLGA microneedles, *Polymers (Basel).* 12 (2020). <https://doi.org/10.3390/polym12010059>.
- [186] L. Humrez, M. Ramos, A. Al-Jumaily, M. Petchu, J. Ingram, Synthesis and characterisation of porous polymer microneedles, *J. Polym. Res.* 18 (2011) 1043–1052. <https://doi.org/10.1007/s10965-010-9505-2>.

Chapter 2

Preparation of the porous particles prepared via spontaneous emulsification and evaluation of the aerodynamic performance of the particles for pulmonary delivery

1. Introduction

The particles for pulmonary delivery are required to have the ability to be delivered to the deep site of the lungs and stay there. The particles having the aerodynamic diameter of 1-5 μm is proper for reaching the deep site of lungs [1,2]. Aerodynamic diameter can be controlled by tuning geometric diameter, density, and shape factor of the particle because it is a function of these parameters (Eq. 1).

$$d_a = d_g \sqrt{\frac{\rho_p}{\lambda \rho_s}} \quad (\text{Eq. 1})$$

In this equation, d_a is the aerodynamic diameter, d_g is the geometric diameter, ρ_p is the density of the particles, λ is the shape factor, and ρ_s is the value of 1.0 g/cm^3 . On the other hand, the most important ability for staying at the deep site of the lungs is to avoid the immune system in the lungs. There are numerous macrophages in alveoli, the deepest site of the lungs. alveolar macrophages phagocyte foreign substances and work on the substances of 1.5-3 μm preferentially [3,4]. Therefore, in terms of avoiding phagocytosis, it is desirable to use the particles as large as possible. However, these requirements are hard to archive at the same time because the values of the proper diameter of the particles for each required ability are far away from each other.

In order to archive these requirements, the feasibility of the porous particles prepared via “one-step emulsification” for pulmonary delivery was evaluated. This preparation method was unexpectedly discovered in a previous research by Murakami [5] by using the amphiphilic block copolymer, poly(ethylene glycol)-*b*-polylactide (PEG-PLA). The porous particles prepared by this method have many desirable characteristics (Fig. 1); (1) the surface of the particles are modified by PEG, one of the biocompatible polymers, (2) the particles are cost effectively prepared because of omitting the first step of mechanical emulsification, (3) the particles are expected to have the low density due to the pores on the surface and the inner structure. The third characteristic implies that the particles of greatly different d_g and d_a could be prepared (Eq. 1). Therefore, the requirements for pulmonary delivery could be archived

by developing the highly porous particles having large d_g (larger than 10 μm) and small d_a (1-5 μm).

In this chapter, the diameter and surface morphology of the porous particles were tried to control by tuning the emulsification rate and the composition of PEG-PLA. After preparing the porous particles having d_g of 5 or 10 μm , the density, the encapsulation ratio of rifampicin (RFP, a model drug for pulmonary tuberculosis), and aerodynamic performance of the particles were evaluated.

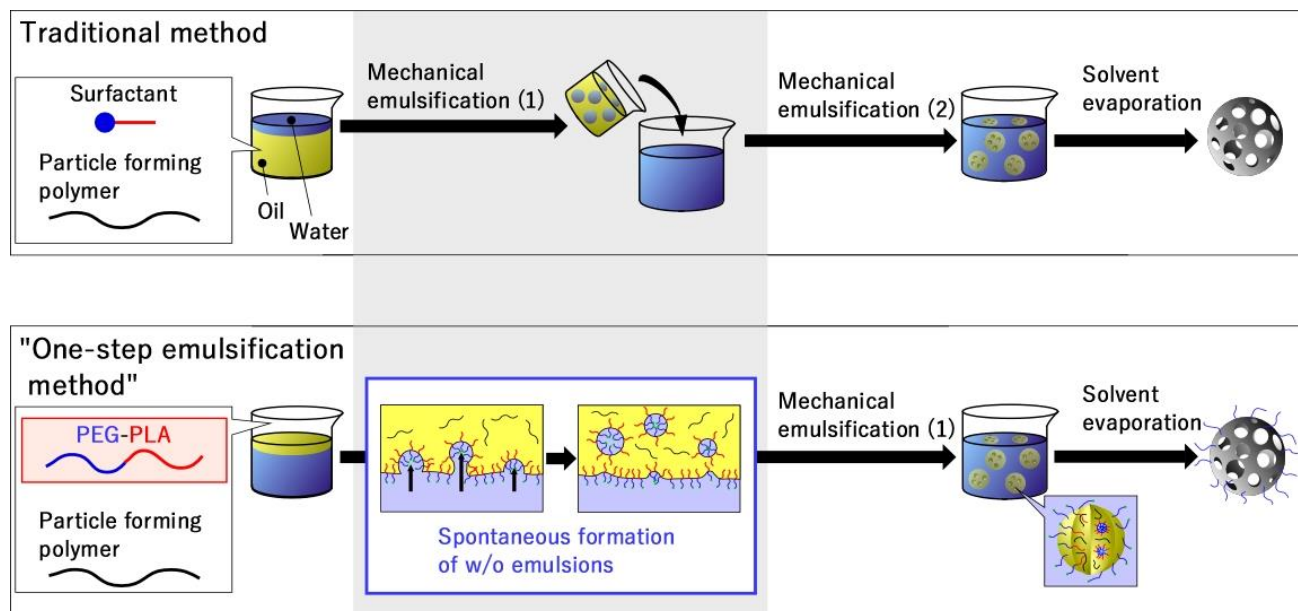


Fig. 1 Omitting the first step of emulsification to prepare the porous particles by using spontaneous emulsification.

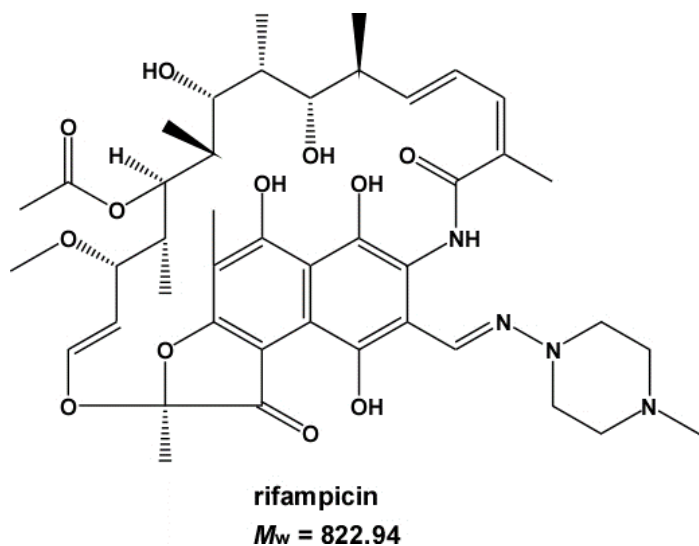


Fig. 2 The chemical structure of rifampicin.

2. Materials and Methods

2.1. Materials

Ethylene oxide (Sumitomo Seika Chemicals Co., Osaka, Japan) was purified by distillation in the presence of CaH₂. DL-Lactide (Tokyo Chemical Industry Co., Tokyo, Japan) was recrystallized twice from ethyl acetate. 2-methoxyethanol was distilled with sodium under reduced pressure. Potassium naphthalene was synthesized by mixing potassium and naphthalene in anhydrous tetrahydrofuran (THF) for 18 h. poly(lactic-co-glycolic acid (PLGA), monomer ratio of lactide/glycolide: 3, molecular weight: 10,000) was purchased from Wako Pure Chemical Industries (Osaka, Japan). Tween 85 was purchased from Tokyo Chemical Industry Co., Ltd. (Tokyo, Japan). Rifampicin was purchased from LKT laboratories, Inc. (Minnesota, USA). All the other reagents were of analytical grade and were used without further purification.

2.2. Synthesis of methoxy-terminated PEG-PLA

PEG-PLA was synthesized according to a slightly modified version of a previously reported method [6,7]. the ring-opening polymerization of both ethylene oxide and DL-lactide was used in THF. 2-Methoxyethanol (0.403–1.05 mmol) and potassium naphthalene (0.403–1.05 mmol) were mixed in THF for 1 h. The purified ethylene oxide (123–133 mmol) was added to the obtained potassium 2-methoxyethoxide solution (total volume: 50 mL). After stirring for 48 h, the THF solution of purified DL-lactide (12.8–23.8 mmol) was added to the solution. After the reaction, the resulting block copolymers were precipitated into cold 2-propanol, centrifuged at 10,500 rpm, and lyophilized in benzene. The average molecular weight of the obtained block copolymer was determined by the use of gel permeation chromatography (GPC) (column: TSK gel G3000HHR, TOSOH, Japan; eluent: *N,N'*-dimethylformamide in the presence of 10 mM LiBr; flow: 1 mL/min; column temperature: 40°C) and ¹H-NMR (AL-300, 300 MHz, JEOL Ltd., Tokyo; solvent: CDCl₃). In a notation of PEG_p-PLA_q, p and q represent the *M_n* of the PEG and PLA blocks, respectively.

2.3. Preparation of the porous and non-porous PLGA particles

The preparation of the porous PLGA particles proceeded according to the previously developed one-step emulsification method [5]. The solutions of PEG-PLA (5 mM) and PLGA (5 mM) were prepared in the mixed solvent of toluene and dichloromethane (*d* was adjusted to 1.0 g/cm³). Milli-Q water (53.76 mL) was added to the pre-mixed solution of PEG-PLA (1.12 mL) and PLGA (1.12 mL). The mixed solution was statistically placed for 3 min to spontaneously form w/o emulsions. Then, the solution was emulsified with a homogenizer (T-25 ULTRA-TURRAX Digital Homogenizer, IKA) for 10 seconds. The obtained w/o/w emulsions were added to Milli-Q water (144 mL) and stirred at 100 rpm for 12 h in order to evaporate the organic solvents and to form the particles. After 12 h, the purified particles were obtained by centrifuging and washing the suspension with Milli-Q water for three times (2000 rpm, 10 min). Then, the suspension was lyophilized and the resulting powder of the porous particles was obtained. Non-porous particles were prepared by using Tween 85 instead of PEG-PLA. The particles loading RFP were prepared by solving RFP in initial PLGA solution (32.5 mM).

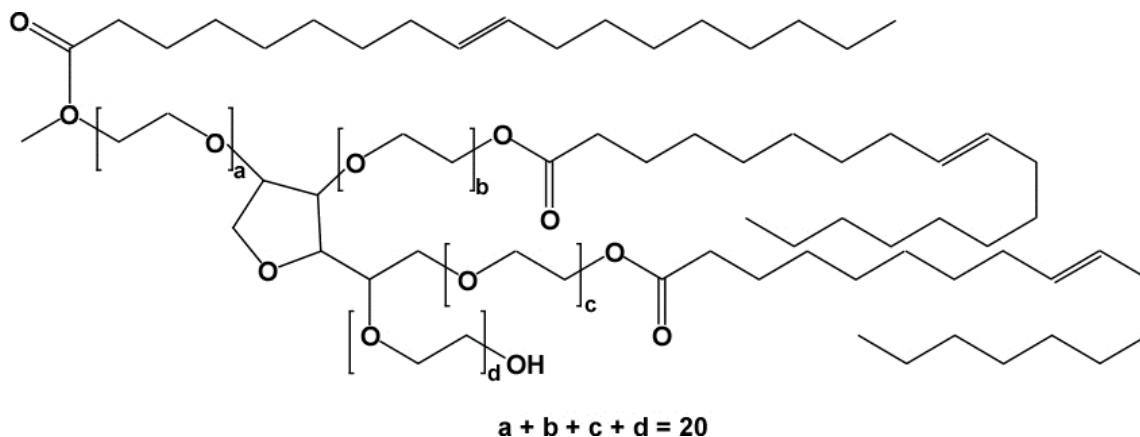


Fig. 3 The chemical structure of Tween 85.

2.4. Observation of the surface morphology of the porous and non-porous PLGA particles

The surface morphology of the porous particles was observed by using a scanning electron microscope (SEM, VE-9800, KEYENCE Co., Ltd., Japan, accelerating voltage: 1.0 kV). Suspension of the porous and non-porous particles was prepared by dispersing the dry powders of the particles in Milli-Q water. The suspension was dropped onto an aluminum plate and dried in desiccator for several hours. The obtained samples were coated by a thin platinum film (approximately 5 nm in thickness) under a reduced pressure with an MSP-1S ion-coater (Vacuum Device Inc., Ibaraki, Japan). The geometric diameter, pore diameter, and pore number were determined from SEM images ($n = 100$).

2.5. Determination the amount of the RFP loaded on the particles

The amount of RFP loaded on the particles was determined by using a UV-vis spectrophotometer (V-630BIO, JASCO Corporation, Japan). The powder of the RFP loading particles (3 mg) was dissolved in dichloromethane (2 mL). The absorbance of the solutions was measured by the UV-vis spectrophotometer (wavelength: 475 nm) and the concentration of RFP was calculated by using a calibration curve created with standard solutions of RFP. The drug loading (DL) and encapsulation efficiency (EE) were determined with Eqs. 2 and 3.

$$DL (\%) = \frac{\text{The concentration of RFP (mg/mL)}}{\text{The concentration of the particles (mg/mL)}} \times 100 \quad (\text{Eq. 2})$$

$$EE (\%) = \frac{\text{Mass of RFP loaded in the resulting particles (mg)}}{\text{Total mass of RFP added to the initial solution (mg)}} \times 100 \quad (\text{Eq. 3})$$

2.6. Determination of the tapped density of the porous and non-porous PLGA particles

The tapped density of the particles was determined according to previous reports (Fig. 4) [8,9]. A known weight of the particles (80–100 mg) was placed in a 5 mL-graduated cylinder. The cylinder was then mechanically tapped 1250 times (250 tappings/min). The tapped density of the particles was expressed as the ratio between the weight and the volume of the particles occupied after 1250 tappings.

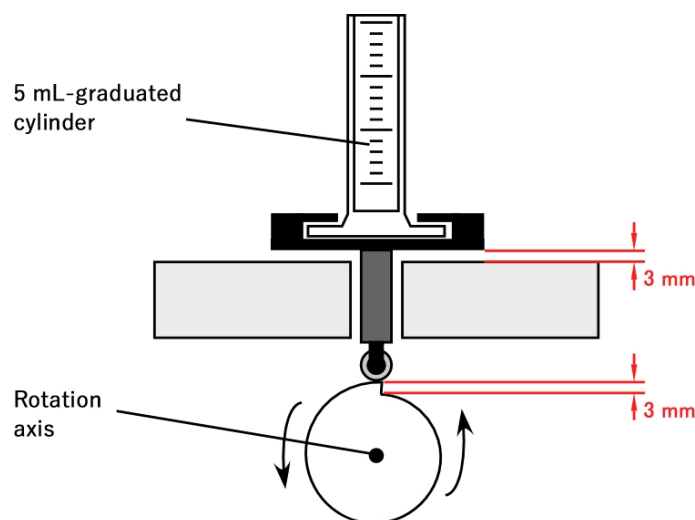


Fig. 4 Mechanism of tapping 5 mL-graduated cylinder.

2.7. Evaluation of in vitro aerosol-dispersion performance of the porous and non-porous PLGA particles

In vitro aerosol-dispersion performance of the porous and non-porous PLGA particles was evaluated according to previous reports [10,11]. Dry powder of the particles (10 mg) was placed in a capsule made of hydroxypropylcellulose. The capsule was set into an inhalation device (Jethaler dual chamber type, Hitachi Automotive Systems, Ltd., Ibaraki, Japan) (Fig. 5(a), (b)). Then the particles are inhaled into an Andersen cascade impactor (AN-200, Tokyo dylec Co., Ltd., Tokyo, Japan) (Fig. 5(c)) for 5 s at the airflow of 28.3 L/min. At this airflow rate, the each stage in the cascade impactor indicates the cutoff diameters and deposition sites of the lungs as follows: stage 1 (11 μm , nasal cavity); stage 2 (7.0 μm , pharynx); stage 3 (4.7 μm , trachea); stage 4 (3.3 μm , bronchi); stage 5 (2.1 μm , bronchi); stage 6 (1.1 μm , alveoli); stage 7 (0.65 μm , alveoli); and stage 8 (0.43 μm , alveoli). Mass of the particles deposited on each stage was determined by measuring the weight of the stage plates before and after inhalation. Then mass median aerodynamic diameter (MMAD), emitted dose (ED), and fine particle fraction (FPF) was calculated. MMAD, the diameter that corresponds to 50% cumulative volume, was determined by using the approximation curve, which was created from diameter-cumulative volume plots. ED and FPF were defined as the values calculated with Eqs. 4 and 5 [12].

$$\text{ED (\%)} = \frac{\text{Initial mass of partricles in a capsule} - \text{Final mass of particles in a capsule}}{\text{initial mass of particles in a capsule}} \times 100 \quad (\text{Eq. 4})$$

$$\text{FPF (\%)} = \frac{\text{Mass of particles of which } d_a \text{ is smaller than } 5 \mu\text{m}}{\text{Total mass of particles deposited on all stages}} \times 100 \quad (\text{Eq. 5})$$

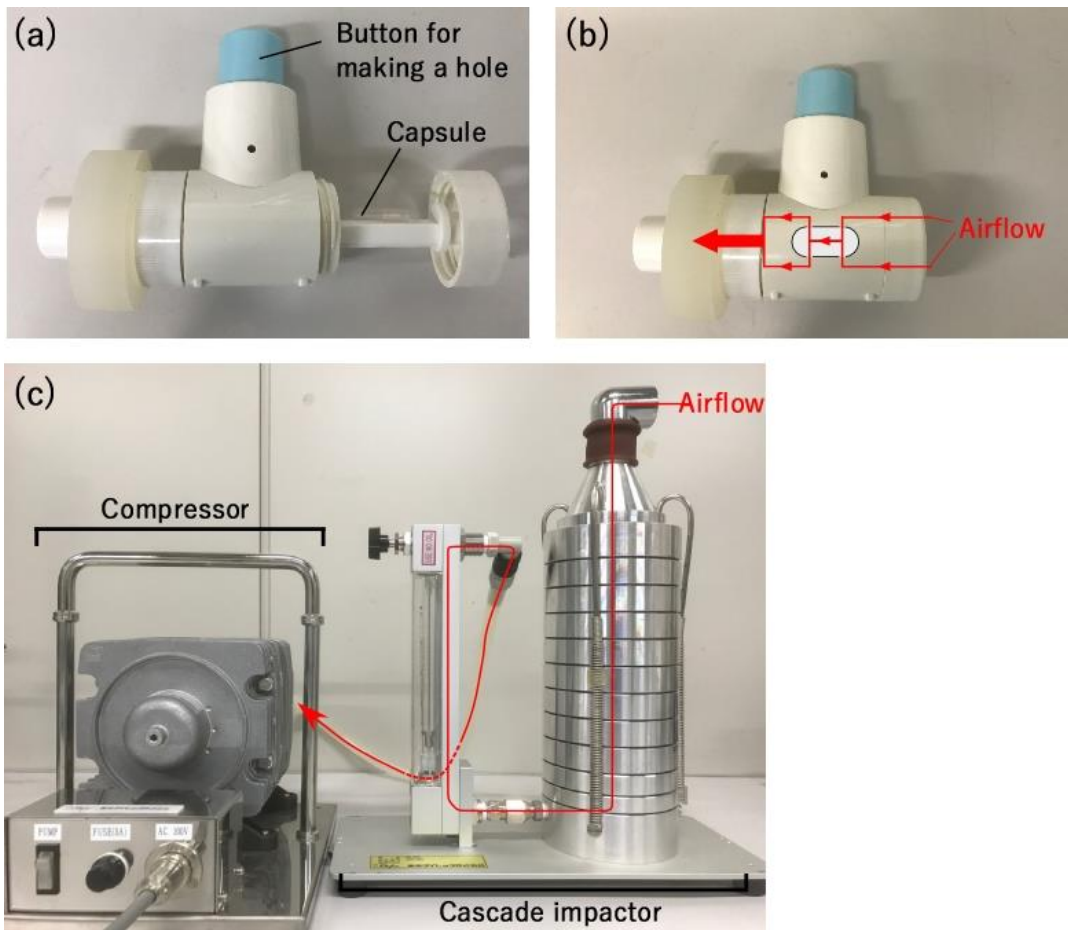


Fig. 5 Apparatus for evaluation of aerosol-dispersion performance: (a) (b) structure of Jethaler; (c) appearance of a cascade impactor.

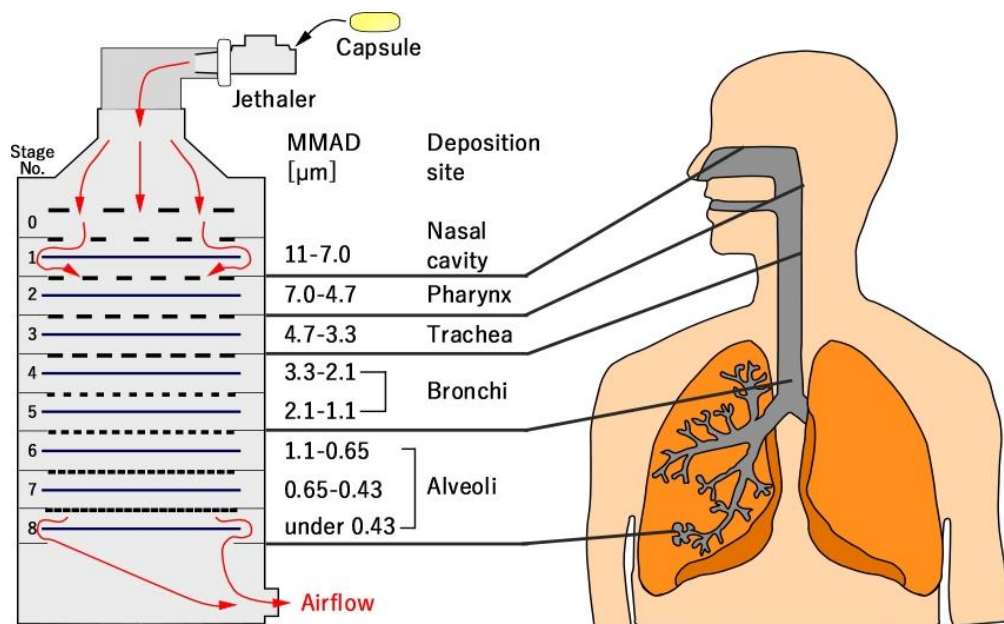


Fig. 6 Structure of a cascade impactor and deposition sites corresponding to each stage.

2.8. Observation of the morphology of the particles after inhalation

The morphology of the porous and non-porous PLGA particles was observed with SEM after inhalation. The powder depositing on each stage of the cascade impactor was collected with a fragment of the double-sided carbon tape. The obtained fragment was attached onto an aluminum plate and coated by a thin platinum film (approximately 2.5 nm in thickness). The samples were observed by means of SEM.

3. Results and Discussion

3.1. Characterization of synthesized methoxy-terminated PEG-PLA

In this thesis, the block copolymer of PEG (hydrophilic polymer) and PLA (hydrophobic polymer) was used as a polymeric surfactant because both the polymers are biocompatible [13,14]. The characterization of synthesized PEG-PLA was analyzed with GPC and $^1\text{H-NMR}$. The molecular weight of PEG was determined with GPC by analyzing an aliquot of PEG solution before lactide solution was added. The molecular weight of PLA was determined with $^1\text{H-NMR}$ spectrum of PEG-PLA (Fig. 7) by comparing the signal of PEG (peak b in Fig. 7) and PLA (peak d in Fig. 7). The characterization of methoxy-terminated PEG-PLA is shown in Table 1. The PEG-PLA with different compositions were obtained.

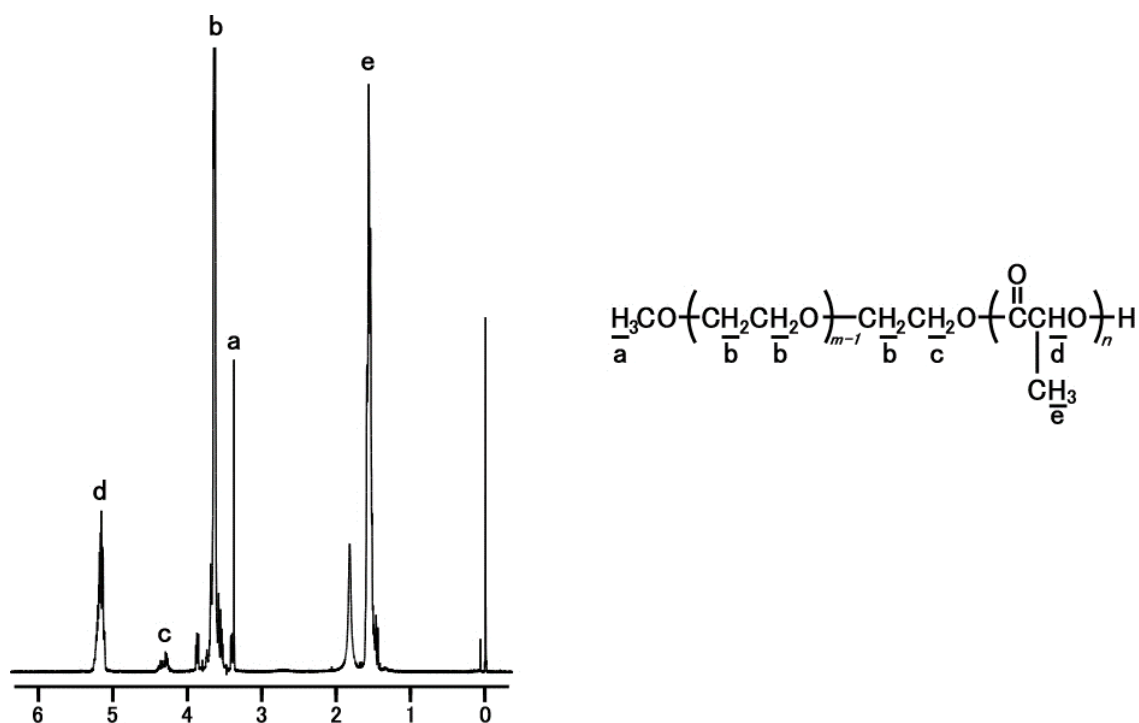


Fig. 7 $^1\text{H-NMR}$ spectrum of synthesized PEG-PLA.

Table 1 Characterization of synthesized PEG-PLA.

Code	PEG		PLA	PEG-PLA	
	M_n	M_w/M_n	M_n	M_n	M_w/M_n
PEG3900-PLA1600	3900	1.07	1600	5500	1.10
PEG6800-PLA1700	7800	1.06	3070	10870	1.07
PEG7800-PLA3100	6800	1.07	1700	8500	1.08

3.2. The morphology of the porous and non-porous particles

The porous and non-porous particles with d_g of 5 or 10 μm were tried to obtain to evaluate the aerodynamic performance. The particles in this chapter were prepared under the conditions shown at Table 2 and their surface morphology is shown in Fig. 8. Fig. 8 indicates that porous particles can be obtained via one-step emulsification in the presence of PEG-PLA. This phenomenon was reported in a previous research [5]. These results strongly suggest that spontaneous emulsification occurs in the organic phase and this is specific characteristic of PEG-PLA. Therefore, this particle-preparing-method is a cost-effective one to obtain particles of specific surface morphology.

Table 2 Preparation conditions of the porous and non-porous particles.

Code	Surfactants	Volume fraction of organic solvents [v/v%]	Homogenization rate [rpm]	Presence of RFP	d_g [μm]
Particle 1	Tween 85	4	3400	—	5.36±1.97
Particle 2	Tween 85	4	4400	○	5.08±1.38
Particle 3	PEG3900-PLA1600	4	7000	—	4.72±0.89
Particle 4	PEG3900-PLA1600	4	7200	○	5.17±0.76
Particle 5	PEG3900-PLA1600	4	4600	—	9.96±1.90
Particle 6	PEG6800-PLA1700	4	8000	—	5.19±0.98
Particle 7	PEG6800-PLA1700	4	10000	○	4.89±0.86
Particle 8	PEG6800-PLA1700	4	5000	—	10.15±2.26
Particle 9	PEG7800-PLA3100	4	8000	—	4.75±1.01
Particle 10	PEG7800-PLA3100	4	9400	○	5.33±1.03
Particle 11	PEG7800-PLA3100	4	6000	—	9.85±2.40

The pore diameter (d_p) and pore density of the porous particles are shown in Fig. 9. It was found out that d_g increased and d_p decreased as the molecular weight of PEG block increased when prepared under same homogenization rate. Increase of d_g occurred due to increasing the viscosity of the organic solution as the molecular weight of PEG block increased. The presence of RFP also affected the d_g of the particles. RFP could also increase the viscosity of the particles. The relation between the composition of PEG-PLA and d_p can be explained by changes in the diameter of the w/o emulsions. The amount of the block copolymer that adsorbed on the interface of the

emulsion increased as the molecular weight of PEG increased, thereby decreasing the surface tension of the system. One of the driving forces to induce spontaneous emulsification is the Brownian-motion based collision of water molecules on the interface of water and organic phase. Therefore, small water droplets, which have low kinetic energy, could be formed in the organic phase as the interfacial decreased.

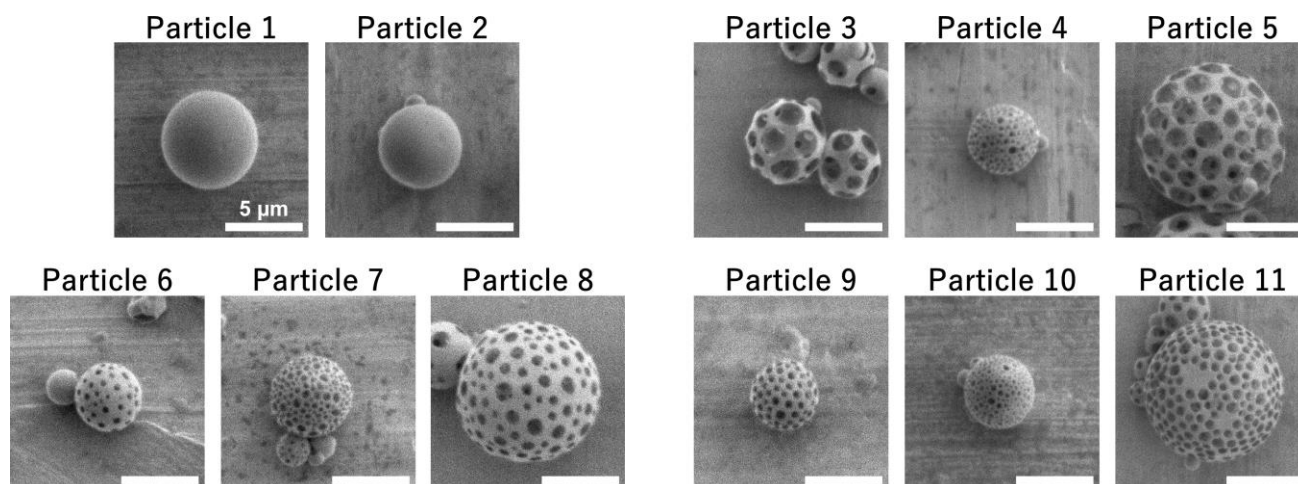


Fig. 8 The surface morphology of the particles used for evaluation of aerosol-dispersion performance.

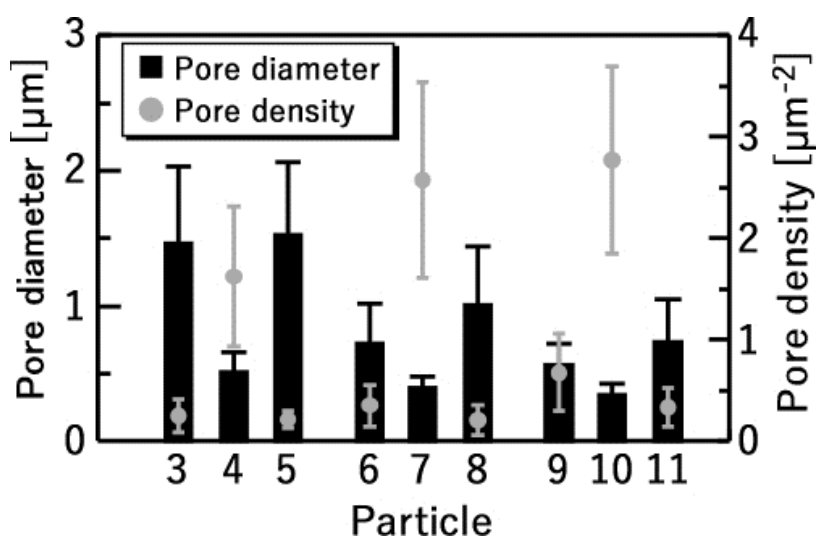


Fig. 9 The pore diameter and pore density of the porous PLGA particles.

3.3. Determination the quantity of RFP in the porous and non-porous particles

Fig. 10 shows DL and EE of the porous and non-porous PLGA particles. DL and EE were deferent only slightly between the non-porous and porous particles (i.e., the surfactant used was Tween 85 or PEG-PLA). The difference of these values among the porous particles (i.e., they are different in the composition of PEG-PLA) was also small. It is speculated that the little change and very low values of DL and EE was due to the characteristic of RFP. RFP can be partly solved in water because RFP has hydroxy groups. Therefore, RFP could be easily solubilized

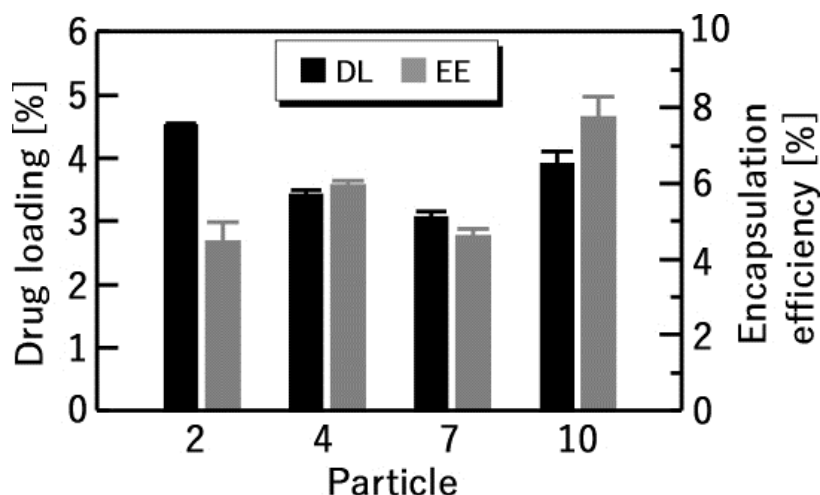


Fig. 10 The drug loading and encapsulation efficiency of RFP on the porous and non-porous particles.

in water phase and DL and EE decreased. This characteristic might also affect the morphology of the porous particles. Fig. 9 demonstrates that d_p of the particles decreased and the pore density increased when RFP coexisted in the initial organic solutions. It is speculated that transferring of RFP from organic to water phase during statically placing of water and organic phase promoted the collision of water molecules onto the water-organic solution interface and forming a large number of small water droplets in the organic phase. As the result, the particles of small d_p and large pore density with RFP were obtained.

3.4. Determination of the tapped density of the porous and non-porous particles

Fig. 11 shows the tapped density of the porous and non-porous particles. The tapped density of the non-porous particles was about 0.11-0.14 g/cm³ and the values are as large as that of the microparticles in many previous reports [9,15–18]. By contrast, the density of the porous particles showed extremely low values due to the highly porous structure. As shown in Eq. 1, d_a is proportional to square root of the density. Indeed, d_a of the microparticles

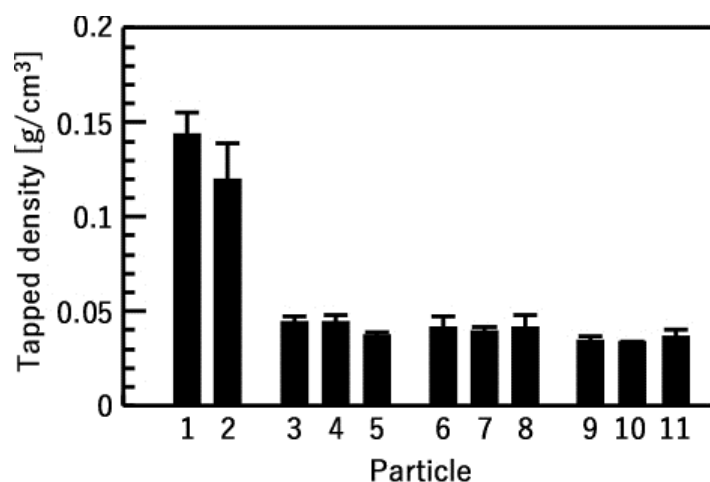


Fig. 11 The tapped density of the porous and non-porous particles.

was lower than d_g because of the low density (below 1.0 g/cm^3) [9,15–18]. Therefore, the porous particles are expected to demonstrate very low d_a than d_g and high efficiency to be delivered to the lungs due to the ultra-low density.

3.5. In vitro aerosol dispersion performance of the porous and non-porous particles

Fig. 12 shows MMAD of the porous and non-porous PLGA particles. Fig. 12 demonstrates that the porous particles had the greatly lower values of MMAD than non-porous particles. The non-porous particles (Particles 1 and 2) showed the larger MMAD (about 9 to 14 μm) than d_g (about 5 μm), whereas the large porous particles (Particles 5, 8, and 11) showed the smaller MMAD (about 5 μm) than d_g (about 10 μm). This great experimental performance of the porous particles for inhalation was consistent with an anticipation; that is due to extremely low density of the porous particles (shown in Fig. 11). Theoretically, MMAD is proportional to not only the density of the particles, but also the surface morphology of the particles, and consequently theoretical values of MMAD was anticipated by using Eq. 6 [19]:

$$\text{MMAD} \cong d_g \sqrt{\frac{\rho_p(1 - \varepsilon)}{\rho_s}} \quad (\text{Eq. 6})$$

where d_g is the geometric diameter, ρ_p is the density of the particles, ε is the porosity of the particles, and ρ_s is the value of 1.0 g/cm^3 . The value of ε can be calculated by using Eqs. 7 and 8:

$$\varepsilon = \frac{S_p}{S_0} \quad (\text{Eq. 7})$$

$$S_p = s_p \rho_{\text{pore}} S_0 \quad (\text{Eq. 8})$$

where S_0 is the surface area of the non-porous particles having the same d_g , S_p is the total area of the pores, s_p is the average area of pores, and ρ_{pore} is the density of the pores. Eq. 5 indicates that MMAD would decrease as the porosity of the particles increased (the largest value is 1) when particles having almost same d_g and ρ_p are used. Table 3 shows

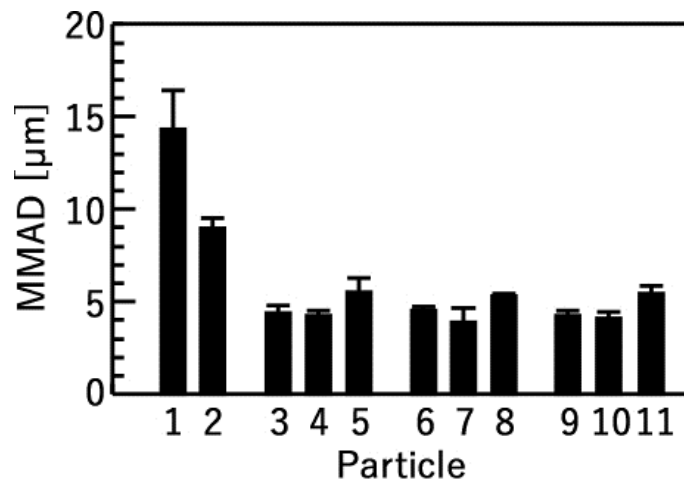


Fig. 12 MMAD of the porous and non-porous particles.

Table 3 The porosity of the porous and non-porous PLGA particles.

Code	ϵ [-]
Particle 1	0.00
Particle 2	0.00
Particle 3	0.42
Particle 4	0.33
Particle 5	0.38
Particle 6	0.14
Particle 7	0.30
Particle 8	0.16
Particle 9	0.17
Particle 10	0.26
Particle 11	0.14

the ϵ for all the particles used in this chapter and consequently the order of MMAD of the particles could be theoretically estimate, from least to greatest, as follows: Particle 3 < Particle 9 < Particle 7 < Particle 10 < Particle 4 < Particle 6 << Particle 2 < Particle 1 for the particles with d_g of approximately 5 μm ; Particle 5 < Particle 11 < Particle 8 for the particles with d_g of approximately 10 μm . On the other hand, the experimental order of MMAD of the particles did not correspond to the theoretical order (Particle 7 < Particle 10 < Particle 9 < Particle 4 < Particle 3 < Particle 6 << Particle 2 < Particle 1 for the particles with d_g of approximately 5 μm ; Particle 8 < Particle 11 < Particle 5 for the particles with d_g of approximately 10 μm). It is speculated that the inconsistency between the order of theoretical and experimental MMAD occurred due to the lack of consideration of shape factor (λ) in Eq. 6. In many reports, experimental MMADs were approximately 1.3-1.8 times as large as theoretical MMADs calculated under the assumption that λ is 1 [9,15–18], whereas the experimental MMADs were 4.7-5.8 times as large as theoretical MMADs for the particles with d_g of approximately 5 μm and the experimental MMADs were 2.8-3.7 times as large as theoretical MMADs for the particles with d_g of approximately 10 μm . The results strongly demonstrate that the porous particles showed the larger deference between theoretical and experimental MMADs than the microparticles in those reports and that λ should not be defined only from the outline of the particles. The porous particles could be considered to have the specific internal structures because they are obtained by means of a unique method, spontaneous emulsification-solvent evaporation-method. Therefore, the specific internal structures of the porous particles might be responsible for the specific MMAD values.

Fig. 13 shows the deposition ratio of the particles on the respiratory organs defined by the deposition ratio on each stage. The non-porous particles (Particles 1 and 2) mostly deposited on the nasal cavity, whereas the porous particles (Particles 3 to 11) deposited approximately 20-40% on the nasal cavity and mostly deposited on the bronchi. This result is presumably due to the deference in adhesive force of the particles. The force necessary to disperse an aggregation of non-porous particles is larger than that of porous particles [20]. Therefore, the cause of the great difference in the deposition ratio on the nasal cavity is presumed to be the difference in the amount of aggregation

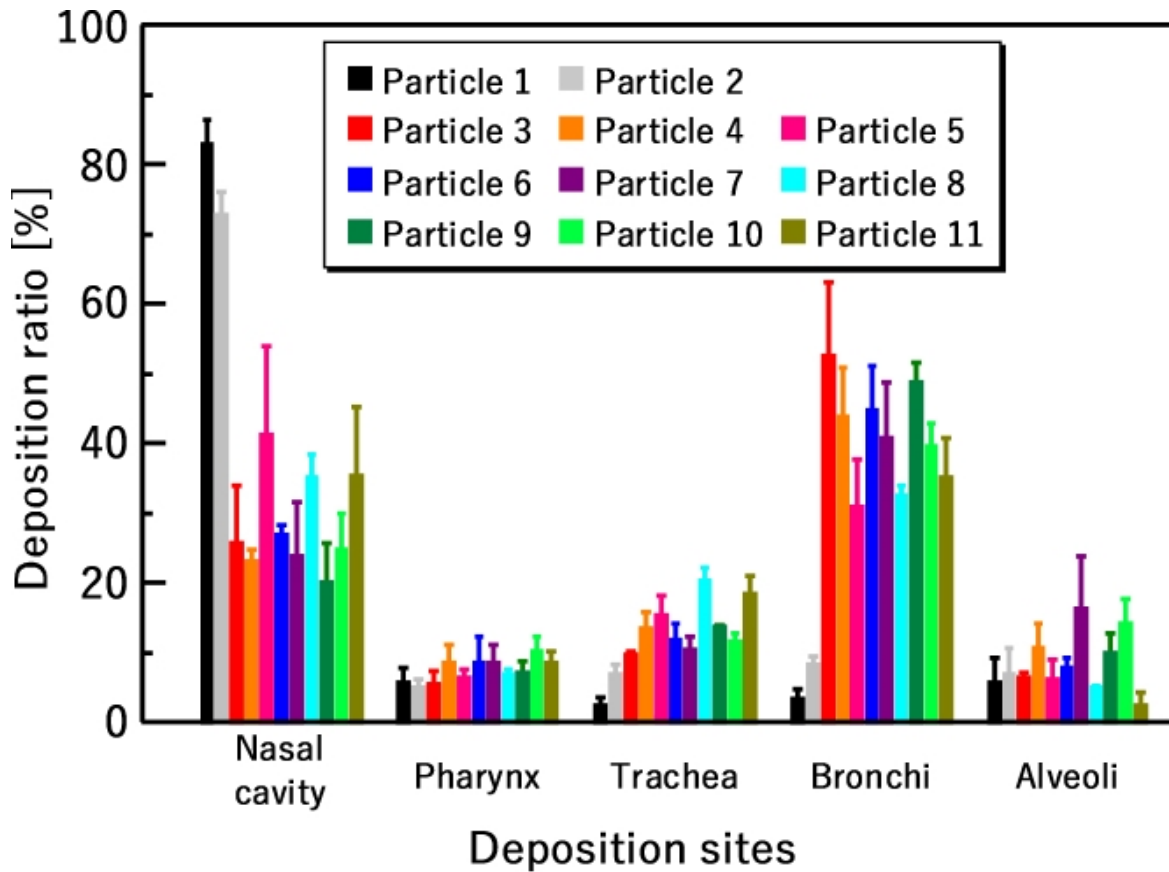


Fig. 13 The deposition ration of the porous and non-porous particles on the respiratory organs.

of the particles. When comparing the porous particles with d_g of 5 and 10 μm , the deposition ratio of the particles with d_g of 5 μm was higher on the trachea and alveoli and lower on the nasal cavity and bronchi than that of 10 μm . After passing the upper stage of a cascade impactor (i.e., removing the aggregations of the particles), the characteristic of a individual particle is considered to be reflected strongly on the aerosol-dispersion performance. Consequently, the difference in the deposition ratio among the porous particles was caused mainly by the difference in d_g because d_g is strongly related to the aerodynamic diameter (Eq. 1).

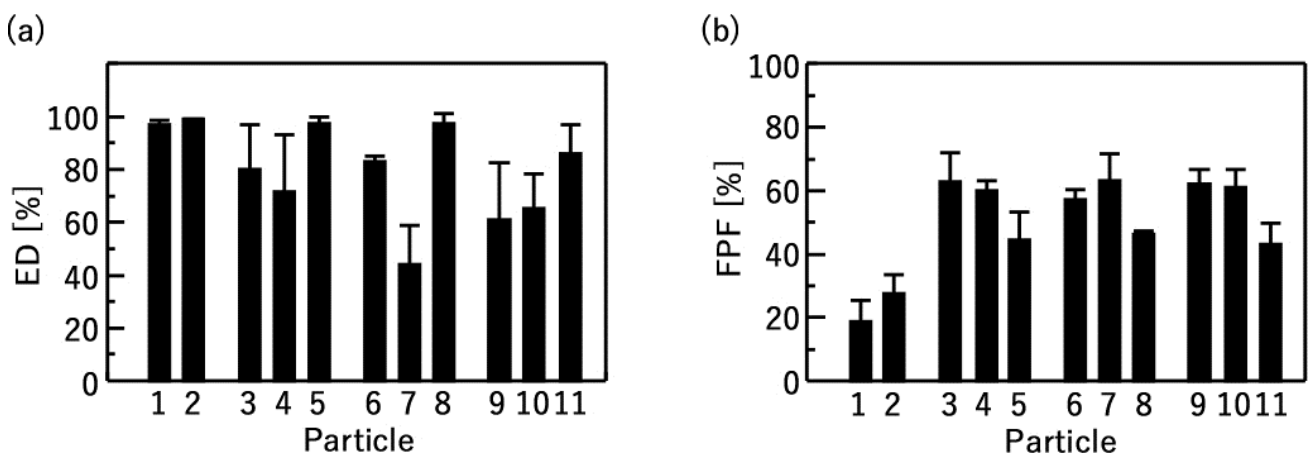


Fig. 14 (a) ED and (b) FPF of the porous and non-porous particles on the respiratory organs.

Fig. 14 shows ED and FPF of the non-porous and porous particles. As shown in Fig. 14 (a), the non-porous showed the higher ED than the porous particles by comparing the particles with d_g of approximately 5 μm . In addition, the residual porous particles in a capsule after inhalation was aggregated. These results indicate that the adhesive force between a capsule and the porous particles was larger than the force between a capsule and the non-porous particles and consequently releasing from a capsule was hard for the porous particles. When comparing ED of the porous particles made from the same compositions of PEG-PLA, the particles with d_g of approximately 10 μm (Particles 5, 8, and 11) showed the highest ED. This is because larger particles are considered to receive larger force from the airflow and leave from the wall of a capsule (Fig. 15).

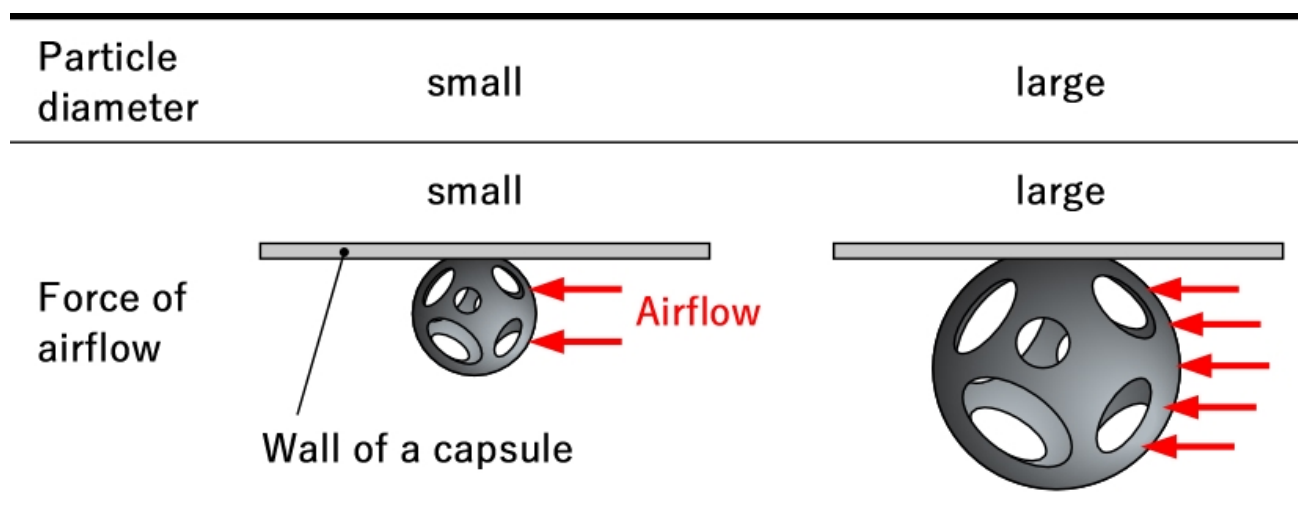


Fig 15 Effect of the geometric diameter of microparticles on the force of airflow.

FPF, fine particle fraction, express the delivery efficiency of microparticles to deep sites of the lungs (deeper than the trachea). Fig. 14 (b) demonstrates FPF of the porous and non-porous particles. The non-porous particles showed approximately only 20% of FPF, whereas the porous particles showed over 40% of FPF even the porous particles with d_g of approximately 10 μm (Particles 5, 8, and 11). The difference in FPF between the particles made from the same compositions of PEG-PLA (Particles 3 and 5; Particles 6 and 8; and Particles 9 and 11) was almost correspond to the difference in the deposition ratio on stage 1 for the same combination of the samples (Figs. 13 and 14 (b)). The results revealed that the porous particles exhibited the higher delivery efficiency to the deep site of the lungs than the non-porous particles and the difference in FPF occurred mainly due to the difference in aerodynamic behavior on the upper stages.

The specific aerodynamic performance of the porous particles Figs. 12-14 can be discussed more deeply in terms of the adhesive force of the materials in this experiment. Fig. 16 illustrates the relationship between the aerodynamic performance and the surface morphology of the particles. The experimental MMAD was not as small as the theoretical one, whereas the porous particles outperformed the non-porous particles. Generally the cause of aggregation of the microparticles are Van der Waals force [21], the capillary force of a liquid bridge [22], and electrostatic force [23]. Especially, Van der Waals force and the capillary force of a liquid bridge are predominant factors for cohesiveness of micro-scale particles [24]. Van der Waals force (F) is express as follows [21]:

$$F = \frac{Ad_g}{12H^2} + \frac{A}{6\pi H^3} \pi r^3 \quad (\text{Eq. 9})$$

where A is the Hamaker constant, H is the distance between the surface of two particles, and r is the radius of the contact area. In the present study, the surface of the porous particles was modified by PEG chains because PEG worked as the surfactant. Therefore, in the samples of the porous particles, H is presumed to be larger values than H in the samples of non-porous particles; that is smaller F values. On the other hand, PEG chains form the hydrogen-bond with water molecules. This characteristic might increase the adhesive force between the porous particles and the inner wall of the capsule through water molecules because the capsule is made from hydroxypropylcellulose, one of the hydrophilic polymers. Therefore, the porous particles are considered to be easy to disperse the powder of the particles owing to PEG chains on the surface and to be difficult to pull apart due to the hydrophilicity of the capsules.

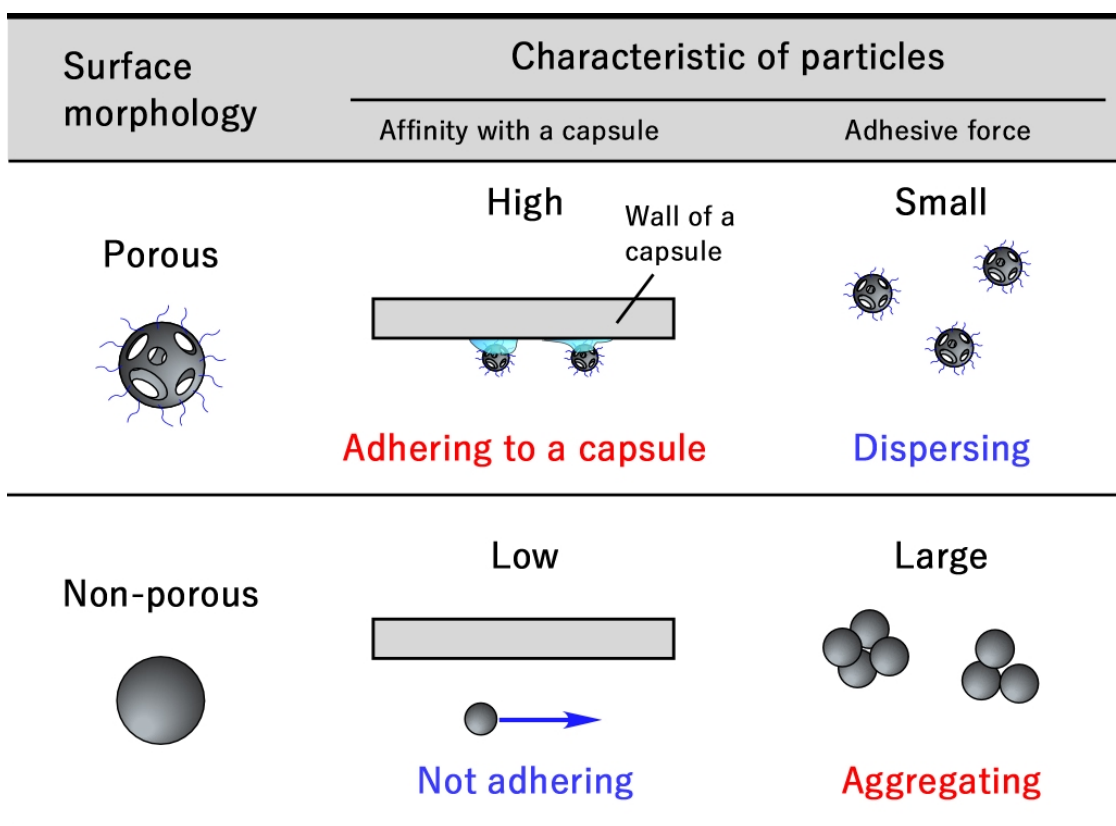


Fig. 16 Effect of the surface morphology of the PLGA particles on the cohesiveness of the particles.

3.6. Observation of the porous and non-porous particles after inhalation

the porous and non-porous particles deposited on the stages of the cascade impactor were collected to observe the morphology of the particles by means of SEM. The SEM images of the particles deposited on each stage are shown in Figs. 17-20. For Particles 5, 8, 11, a large number of the porous particles with d_g of approximately 10 μm were observed at the stages 1-3, whereas small number of the particles with d_g of approximately 10 μm were observed below the stage 4. That is presumably because the particles formed the aggregations by the capillary force

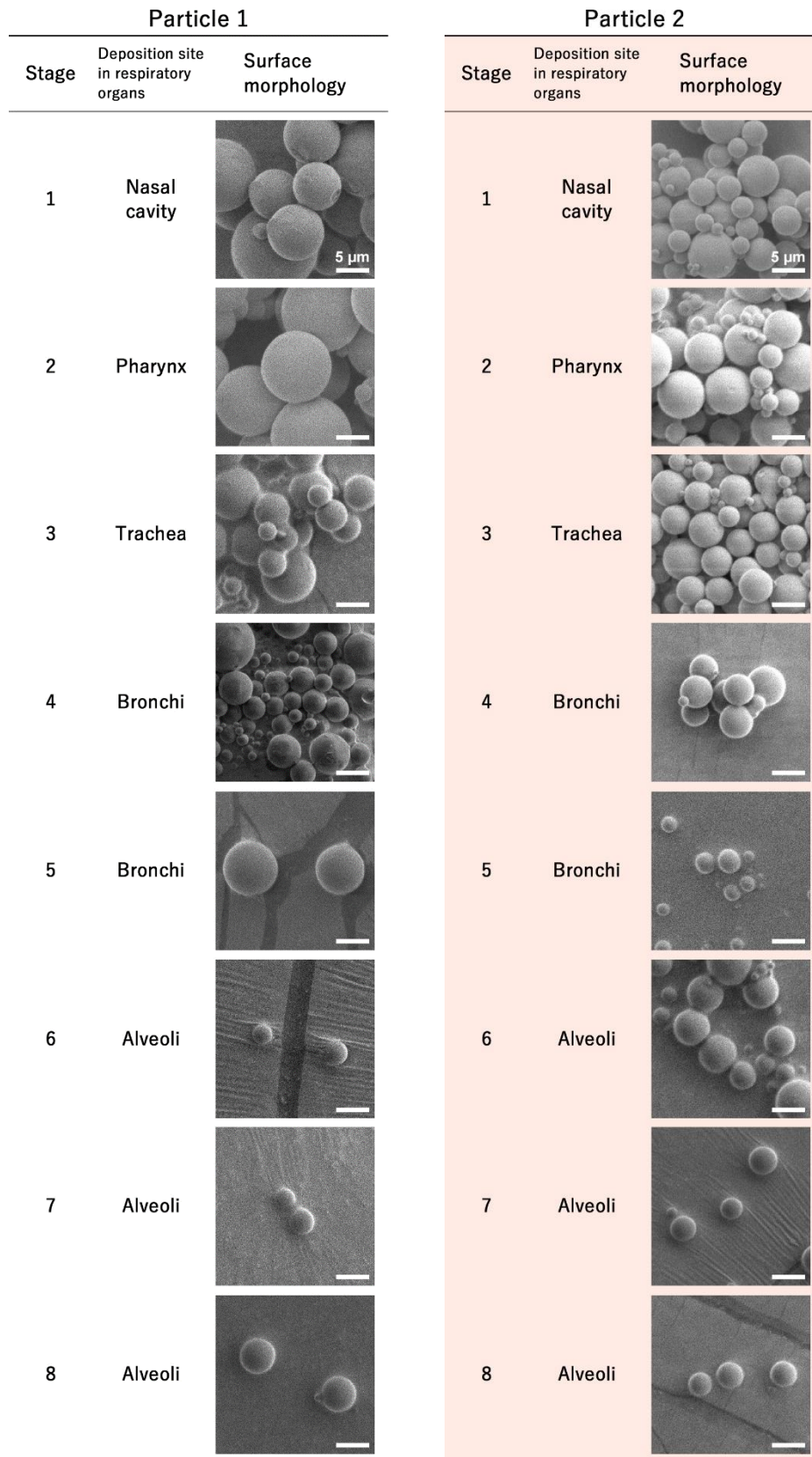


Fig. 17 The surface morphology of the PLGA particles after inhalation prepared with Tween 85.

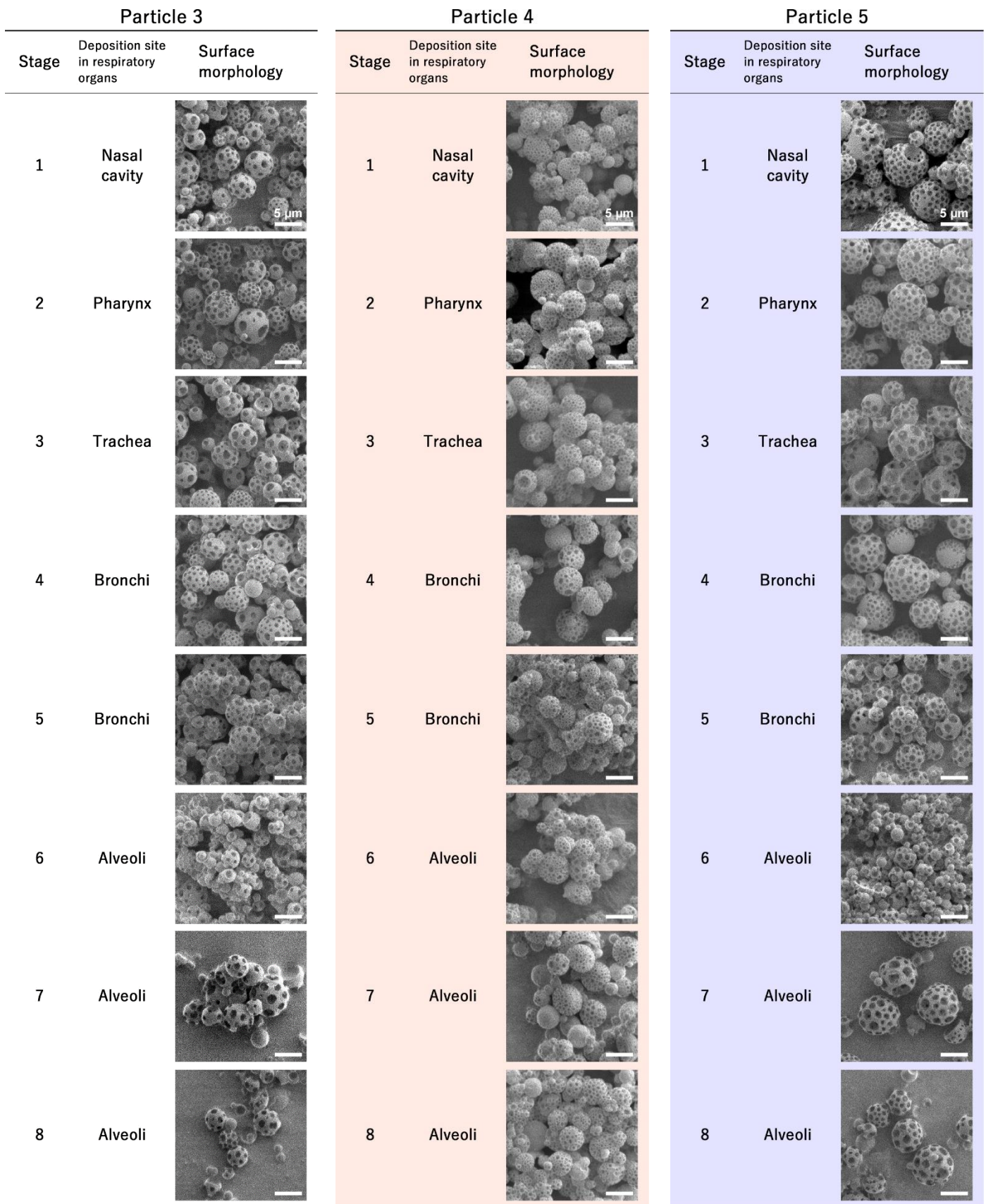


Fig. 18 The surface morphology of the PLGA particles after inhalation prepared with PEG3900-PLA1600.

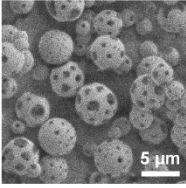
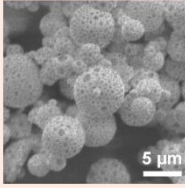
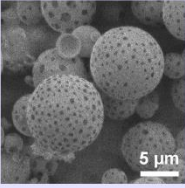
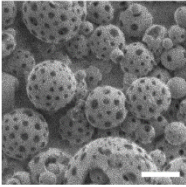
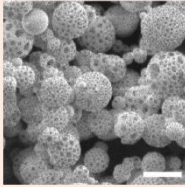
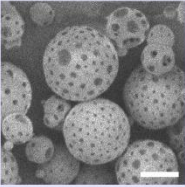
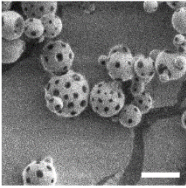
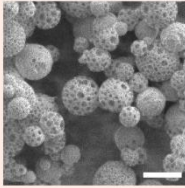
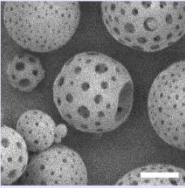
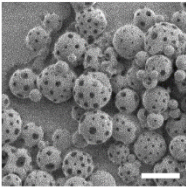
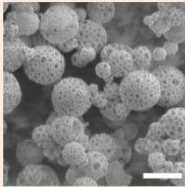
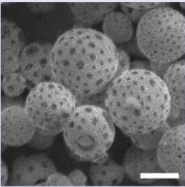
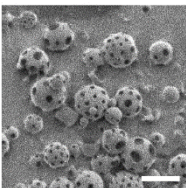
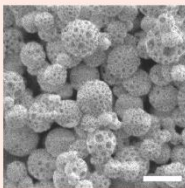
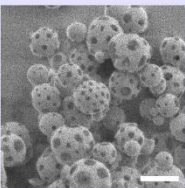
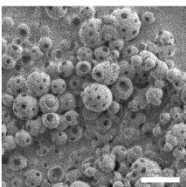
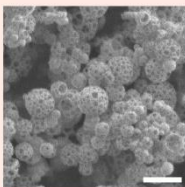
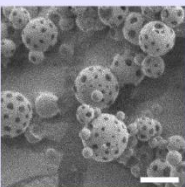
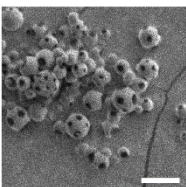
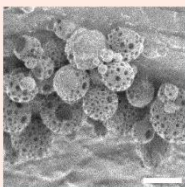
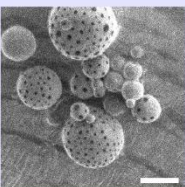
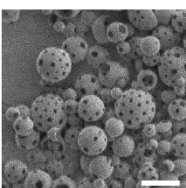
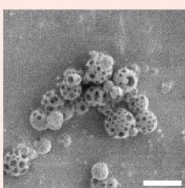
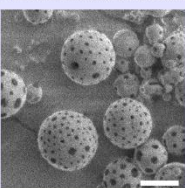
Particle 6			Particle 7			Particle 8		
Stage	Deposition site in respiratory organs	Surface morphology	Stage	Deposition site in respiratory organs	Surface morphology	Stage	Deposition site in respiratory organs	Surface morphology
1	Nasal cavity		1	Nasal cavity		1	Nasal cavity	
2	Pharynx		2	Pharynx		2	Pharynx	
3	Trachea		3	Trachea		3	Trachea	
4	Bronchi		4	Bronchi		4	Bronchi	
5	Bronchi		5	Bronchi		5	Bronchi	
6	Alveoli		6	Alveoli		6	Alveoli	
7	Alveoli		7	Alveoli		7	Alveoli	
8	Alveoli		8	Alveoli		8	Alveoli	

Fig. 19 The surface morphology of the PLGA particles after inhalation prepared with PEG6800-PLA1700.

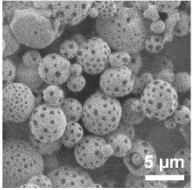
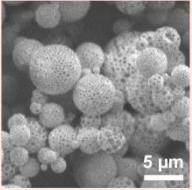
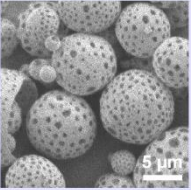
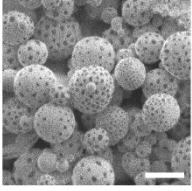
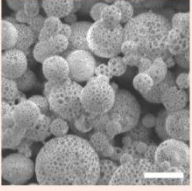
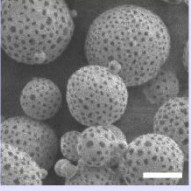
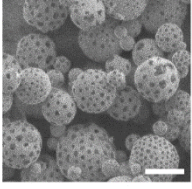
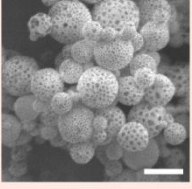
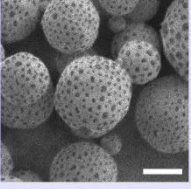
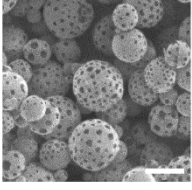
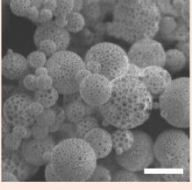
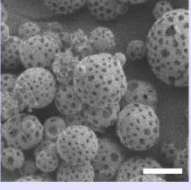
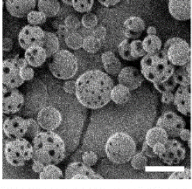
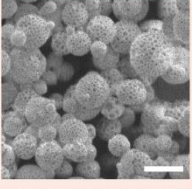
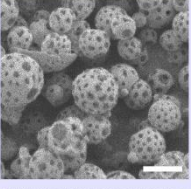
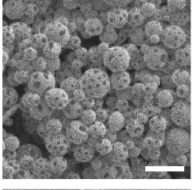
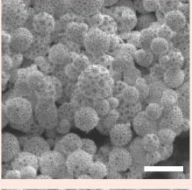
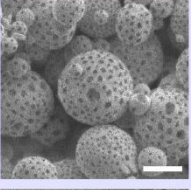
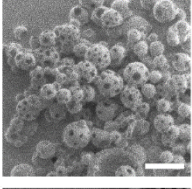
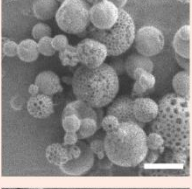
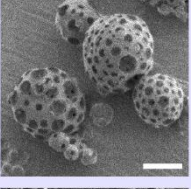
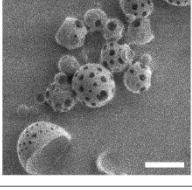
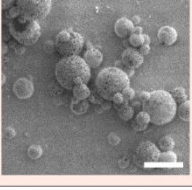
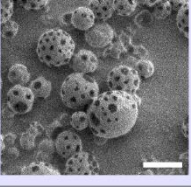
Particle 9			Particle 10			Particle 11		
Stage	Deposition site in respiratory organs	Surface morphology	Stage	Deposition site in respiratory organs	Surface morphology	Stage	Deposition site in respiratory organs	Surface morphology
1	Nasal cavity		1	Nasal cavity		1	Nasal cavity	
2	Pharynx		2	Pharynx		2	Pharynx	
3	Trachea		3	Trachea		3	Trachea	
4	Bronchi		4	Bronchi		4	Bronchi	
5	Bronchi		5	Bronchi		5	Bronchi	
6	Alveoli		6	Alveoli		6	Alveoli	
7	Alveoli		7	Alveoli		7	Alveoli	
8	Alveoli		8	Alveoli		8	Alveoli	

Fig. 20 The surface morphology of the PLGA particles after inhalation prepared with PEG7800-PLA3100.

of a liquid bridge and the characteristic of individual particles was not reflected on the aerosol dispersion performance. On the stages 6-8, the non-porous particles with d_g of less than 2 μm (likely derived from o/w emulsions) and the porous particles with d_g of more than 3 μm for Particles 3-11 were observed. Especially the non-porous ones were observed mainly on the stage 6. This is presumably because non-porous particles tend to form large aggregation due to the strong adhesive force. The SEM images shown in Fig. 17-20 demonstrate that the porous particles outperformed the non-porous particles in terms of pulmonary delivery and the deposited particles are expected to have the ability to stay in the deep sites of the lungs for a long time because the deposited porous particles have the enough d_g to avoid phagocytosis of the alveolar macrophages.

4. Conclusions

In this chapter, the surface morphology of the porous particles prepared via one-step emulsification-solvent evaporation-method was successfully controlled by tuning the compositions of PEG-PLA and the homogenization rates. The porous particles showed the extremely low tapped density and consequently they were expected to be used for the application of pulmonary drug delivery. Indeed, the porous particles outperformed the non-porous particles in terms of pulmonary delivery and SEM observation of the particles after inhalation revealed the porous particles might have the ability to avoid phagocytosis because the porous particles deposited on the lower stages (stages 6-8) had d_g of more than 3 μm . On the other hand, the difference in the aerodynamic performance between the porous particles could not be clarified regardless of the difference in the surface morphology of them. The reason why the difference was not unraveled was presumably because there were several factors which change at the same time when the porous particles were prepared; that is the length of PEG chains on the surface of the particles and the surface morphology (the pore diameter and the pore density) of them. In addition, the internal structure of the particles was not observed in detail in this chapter. Therefore, another factor should be found to control the surface morphology and the internal structure of the porous particles in order to unravel the correlation between the characteristic and the aerodynamic performance of the porous particles and improve the aerosol-dispersion performance.

5. References

- [1] C. Bosquillon, C. Lombry, V. Pr  at, R. Vanbever, Influence of formulation excipients and physical characteristics of inhalation dry powders on their aerosolization performance, *J. Control. Release.* 70 (2001) 329–339. [https://doi.org/10.1016/S0168-3659\(00\)00362-X](https://doi.org/10.1016/S0168-3659(00)00362-X).
- [2] A. Minne, H. Boireau, M.J. Horta, R. Vanbever, Optimization of the aerosolization properties of an inhalation dry powder based on selection of excipients, *Eur. J. Pharm. Biopharm.* 70 (2008) 839–844. <https://doi.org/10.1016/j.ejpb.2008.06.013>.
- [3] Z. Liang, R. Ni, J. Zhou, S. Mao, Recent advances in controlled pulmonary drug delivery, *Drug Discov. Today.* 20 (2015) 380–389. <https://doi.org/10.1016/j.drudis.2014.09.020>.

- [4] G. Oberdörster, Lung dosimetry: Pulmonary clearance of inhaled particles, *Aerosol Sci. Technol.* 18 (1993) 279–289. <https://doi.org/10.1080/02786829308959605>.
- [5] T. Takami, Y. Murakami, Unexpected and successful “one-step” formation of porous polymeric particles only by mixing organic solvent and water under “low-energy-input” conditions, *Langmuir*. 30 (2014) 3329–3336. <https://doi.org/10.1021/la500324j>.
- [6] M. Murata, Y. Uchida, T. Takami, T. Ito, R. Anzai, S. Sonotaki, Y. Murakami, Dual drug release from hydrogels covalently containing polymeric micelles that possess different drug release properties, *Colloids Surfaces B Biointerfaces*. 153 (2017) 19–26. <https://doi.org/10.1016/j.colsurfb.2017.02.008>.
- [7] H. Moroishi, C. Yoshida, Y. Murakami, A free-standing, sheet-shaped, “hydrophobic” biomaterial containing polymeric micelles formed from poly(ethylene glycol)-poly(lactic acid) block copolymer for possible incorporation/release of “hydrophilic” compounds, *Colloids Surfaces B Biointerfaces*. 102 (2013) 597–603. <https://doi.org/10.1016/j.colsurfb.2012.08.050>.
- [8] F. Ungaro, R. d’Emmanuele di Villa Bianca, C. Giovino, A. Miro, R. Sorrentino, F. Quaglia, M.I. La Rotonda, Insulin-loaded PLGA/cyclodextrin large porous particles with improved aerosolization properties: In vivo deposition and hypoglycaemic activity after delivery to rat lungs, *J. Control. Release*. 135 (2009) 25–34. <https://doi.org/10.1016/j.jconrel.2008.12.011>.
- [9] F. Ungaro, G. De Rosa, A. Miro, F. Quaglia, M.I. La Rotonda, Cyclodextrins in the production of large porous particles: Development of dry powders for the sustained release of insulin to the lungs, *Eur. J. Pharm. Sci.* 28 (2006) 423–432. <https://doi.org/10.1016/j.ejps.2006.05.005>.
- [10] H. Todo, H. Okamoto, K. Iida, K. Danjo, Improvement of stability and absorbability of dry insulin powder for inhalation by powder-combination technique, *Int. J. Pharm.* 271 (2004) 41–52. <https://doi.org/10.1016/j.ijpharm.2003.10.024>.
- [11] T. Mizoe, T. Ozeki, H. Okada, Preparation of drug nanoparticle-containing microparticles using a 4-fluid nozzle spray drier for oral, pulmonary, and injection dosage forms, *J. Control. Release*. 122 (2007) 10–15. <https://doi.org/10.1016/j.jconrel.2007.06.001>.
- [12] N. El-Gendy, S. Huang, P. Selvam, P. Soni, C. Berkland, Development of budesonide nanocluster dry powder aerosols: Formulation and stability, *J. Pharm. Sci.* 101 (2012) 3445–3455. <https://doi.org/10.1002/jps.23176>.
- [13] J. Milton Harris, N.E. Martin, M. Modi, Pegylation: A novel process for modifying pharmacokinetics, *Clin. Pharmacokinet.* 40 (2001) 539–551. <https://doi.org/10.2165/00003088-200140070-00005>.
- [14] S. Farah, D.G. Anderson, R. Langer, Physical and mechanical properties of PLA, and their functions in widespread applications — A comprehensive review, *Adv. Drug Deliv. Rev.* 107 (2016) 367–392. <https://doi.org/10.1016/j.addr.2016.06.012>.
- [15] S.A. Meenach, Y.J. Kim, K.J. Kauffman, N. Kanthamneni, E.M. Bachelder, K.M. Ainslie, Synthesis, optimization, and characterization of camptothecin-loaded acetalated dextran porous microparticles for pulmonary delivery, *Mol. Pharm.* 9 (2012) 290–298. <https://doi.org/10.1021/mp2003785>.
- [16] L.M. Nolan, L. Tajber, B.F. McDonald, A.S. Barham, O.I. Corrigan, A.M. Healy, Excipient-free nanoporous microparticles of budesonide for pulmonary delivery, *Eur. J. Pharm. Sci.* 37 (2009) 593–602. <https://doi.org/10.1016/j.ejps.2009.05.007>.

- [17] M.I. Amaro, F. Tewes, O. Gobbo, L. Tajber, O.I. Corrigan, C. Ehrhardt, A.M. Healy, Formulation, stability and pharmacokinetics of sugar-based salmon calcitonin-loaded nanoporous/nanoparticulate microparticles (NPMPs) for inhalation, *Int. J. Pharm.* 483 (2015) 6–18. <https://doi.org/10.1016/j.ijpharm.2015.02.003>.
- [18] A. Sharma, K. Vaghasiya, R.K. Verma, Inhalable microspheres with hierarchical pore size for tuning the release of biotherapeutics in lungs, *Microporous Mesoporous Mater.* 235 (2016) 195–203. <https://doi.org/10.1016/j.micromeso.2016.08.009>.
- [19] R. Vanbever, J.D. Mintzes, J. Wang, J. Nice, D. Chen, R. Batycky, R. Langer, D.A. Edwards, Formulation and physical characterization of large porous particles for inhalation, *Pharm. Res.* 16 (1999) 1735–1742. <https://doi.org/10.1023/A:1018910200420>.
- [20] A. Baldelli, R. Vehring, Analysis of cohesion forces between monodisperse microparticles with rough surfaces, *Colloids Surfaces A Physicochem. Eng. Asp.* 506 (2016) 179–189. <https://doi.org/10.1016/j.colsurfa.2016.06.009>.
- [21] M.S. Hassan, R.W.M. Lau, Effect of particle shape on dry particle inhalation: Study of flowability, aerosolization, and deposition properties, *AAPS PharmSciTech.* 10 (2009) 1252–1262. <https://doi.org/10.1208/s12249-009-9313-3>.
- [22] D. Megias-Alguacil, L.J. Gauckler, Capillary forces between two solid spheres linked by a concave liquid bridge: Regions of existence and forces mapping, *AIChE J.* 55 (2009) 1103–1109. <https://doi.org/10.1002/aic.11726>.
- [23] J. Peart, Powder electrostatics: Theory, techniques and applications, *KONA Powder Part. J.* 19 (2001) 34–45. <https://doi.org/10.14356/kona.2001009>.
- [24] H. SHINTO, Computational Fluid Dynamics Study of Wetting, Capillary Forces, and Pickering Emulsions, *Oleoscience.* 12 (2012) 63–70. <https://doi.org/10.5650/oleoscience.12.63>.

Chapter 3

Effect of the composition of organic solvent on pore formation for porous particles prepared with emulsification-solvent evaporation method

1 Introduction

the feasibility of the porous particles to be applied for pulmonary delivery has been shown in Chapter 2 and a paper [1] because of the higher delivery efficiency than the non-porous particles. However, the difference in aerodynamic performance among the porous particles was not revealed regardless of the difference in the surface morphology. This is presumably because many factors contribute to aerosol dispersion performance, such as surface morphology, surface modification, and internal structure. In this PEG-PLA containing system, spontaneous emulsification-solvent evaporation-method, the surface morphology of the porous particles (*i.e.*, the pore diameter and pore density) have been controlled by tuning the molecular weight of PEG. This means the multiple factors change at the same time related to aerosol dispersion performance. Hence, It is necessary to find out another factor for independent control of the surface morphology of the porous particles in order to establish the most suitable preparation conditions of the particles for pulmonary delivery.

Many researchers have been trying to control the morphology of the porous particles obtained from multiple emulsions and they discussed the effect of many factors such as the compositions of polymers, organic solvents, and solvent evaporation conditions on the morphology of the porous particles. However, only a few reports remark on both the surface morphology and the internal structure, and consequently the detail of pore forming mechanism has been remained unclear [2–6], whereas some reports partly achieved controlling the morphology of the porous particles by using osmotic pressure [7–9]. You can change the volume of water droplets in the o/w emulsion-droplets by arranging the difference in the concentration of salt between internal water droplets and external water phase. However, this method could not be applied to the system containing PEG-PLA because w/o emulsions are hard to form in the presence of salts because salts would prevent spontaneous emulsification. On the other hand, some researchers utilized the phase separation of good and poor solvents for particle forming polymers [10–12]. They achieved to form smaller pores on the surface and internal structure of the particles by decreasing poor solvent/good solvent ratio and consequent decrease of phase separation. The decrease of phase separation shortens the time to grow the poor solvent droplets (porogens in these systems) in an o/w emulsion droplet. These reports imply the rate of solvent evaporation is one of the key factors for the particle morphology. Mathematical or experimental investigation

of the solvent evaporation rate was conducted in some reports [13–18]. However, the effect of solvent evaporation rate on the morphology of the particles was not illustrated even by Deluca [16–18], who did both mathematical and experimental ways of evaluation.

In this chapter, both the surface morphology and internal structure of the porous particles were evaluated in detail. And then, another factor other than the molecular weight of PEG was tried to find out to control the morphology of the porous particles and clarify the pore forming mechanism.

2. Material and Methods

2.1. Materials

As a polymeric surfactant, methoxy-terminated PEG-PLAs with various compositions were used by the scheme written in Chapter 2. In a notation of PEG p -PLA q , p and q represent the M_n of the PEG and PLA blocks, respectively. As a particle forming polymer, PLGA (poly(lactide-co-glycolide), monomer unit ratio of lactide/glycolide: 3, molecular weight: 10,000) was used and it was purchased from FUJIFILM Wako Pure Chemical Corporation (Osaka, Japan). Guaranteed reagent of dichloromethane (DCM) and toluene were purchased from FUJIFILM Wako Pure Chemical Corporation (Osaka, Japan) and used without further purification.

2.2. Measurement of the interfacial tension between water and organic solutions

The interfacial tension between water and organic solution was measured with pendant drop method [19,20]. Toluene-DCM mixed organic solvent (TD-OS) was prepared in various mixing ratio with or without PEG3200-PLA7300 (0.1 mM). The solution was added into the glass tube (Fig 1). An organic droplet arose on the tip of the metal tube in the glass cell filled with Milli-Q water by opening the plug of the glass tube. a picture of an organic droplet was taken just before leaving the tip of the metal tube and calculated the value of interfacial tension with Eq. 1:

$$\gamma = \frac{g\Delta\rho(d_1)^2}{H} \quad (\text{Eq. 1})$$

where γ is the interfacial tension, g is the gravity acceleration, $\Delta\rho$ is the difference in the liquid density between organic and water phase, d_1 is the diameter at the equatorial plane of the droplet, and I/H is the correction value, which was calculated by Stauffer and Porter [19,20] where the value of S is given by using Eq. 2:

$$S = \frac{d_2}{d_1} \quad (\text{Eq. 2})$$

where d_2 is the diameter at the plane at a distance d_1 from the tip of the drop.

2.3. Preparation of the multiple emulsions and porous particles

The w/o/w emulsions and the porous particles were prepared with a slightly modified version of the method

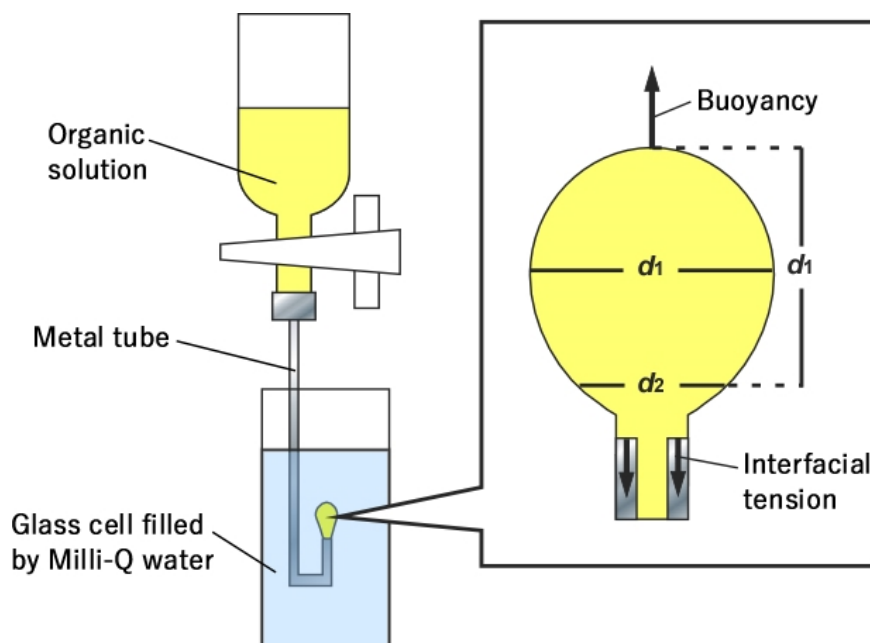


Fig. 1 The apparatus for measuring the interfacial tension.

written in Chapter 2. The organic solutions of PEG-PLA (5 mM) and of PLGA (5 mM) were prepared by solving them in TD-OS (toluene content was 50 to 80v/v%). 0.28 mL of each solution was mixed in a test tube and then water (13.44 mL) was added. The test tube was settled for 3 min in order to spontaneously obtain w/o emulsions. The obtained solution was emulsified (3 min, 8000 rpm) with a high-speed homogenizer (T-25 ULTRA-TURRAX Digital Homogenizer, IKA). The obtained w/o/w emulsions were poured into a beaker with water (36 mL) and the solution was then stirred at 100 rpm for 12 h to allow the organic solvent to diffuse into a continuous water phase and then evaporate into the air. The beakers with different liquid-gas interfacial areas from 13.3 cm² to 57.7 cm² were used and they were put on water bath to arrange the temperature from 10°C to 40°C for the purpose of evaluating the effect of the liquid-gas interfacial area and the temperature on the morphology of the porous particles. The purified particle suspension was obtained by centrifuging the porous particles-impurities mixed suspension at 2000 rpm for 10 min and washing them with Milli-Q water three times. The resulting suspension was lyophilized for 12 h and the powder of the particles was obtained.

2.4. Observation of the morphology of the obtained emulsions and particles

the sample of w/o/w emulsions was prepared by dropping the aliquot of w/o/w emulsions on a slide glass and covered by a thin glass plate. The obtained sample was observed by using a fluorescence microscope (BZ-9000, KEYENCE Co., Ltd., Japan) in bright field.

The surface morphology and internal structure of the porous particles were observed by using a scanning electron microscope (SEM) (VE-9800, KEYENCE Co., Ltd., Japan, accelerating voltage: 1.0 kV). For observing the surface morphology, the powder of the particles was attached onto a fragment of a double-sided carbon tape. The unused side of the obtained fragment was attached on an aluminum plate and coated with a thin platinum film

(approximately 10 nm in thickness) under a reduced pressure with an MSP-1S ion-coater (Vacuum Device Inc, Ibaraki, Japan). The internal structure of the particle was observed by breaking the particles into pieces. The powder of the particles was embedded in a block of agar gel. The block was frozen in liquid N₂ and smashed into pieces with a hammer. The broken small pieces were collected on a fragment of a carbon tape placed on an aluminum plate and the obtained sample were coated with a thin platinum film (approximately 10 nm in thickness).

2.5. Evaluation of the residual organic solvent

For the purpose of monitoring the amount of residual TD-OS in the process of solvent evaporation, a gas chromatography-mass spectrometry (GC-MS) was used. The w/o/w emulsions were prepared with PEG9400-PLA6000 and TD-OS with a toluene content of 50%. 0.3 mL of the emulsions was collected every 30 min in the process of solvent evaporation. These samples were diluted 2–10 times with water and analyzed by GC-MS (GC: 6890 series, Agilent Technologies, USA). A JMS-700 MS system (JEOL Ltd., Tokyo) was used with an InertCap 1 column (GL Sciences Inc., Tokyo, Japan) with a length of 30 m, internal diameter of 0.25 mm, and thickness of liquid phase of 0.25 μm, and He carrier gas. The heating rate was shifted from 10 °C/min (30 to 50°C) to 40 °C/min (50 to 240°C).

In addition, the change in the transmittance of w/o/w emulsions over time at a certain wavelength was also determined. 0.4 mL of the w/o/w emulsions was collected every 30 min into a glass cell and the transmittance was measured with UV-vis spectrophotometer (V-630BIO, JASCO Corporation, Tokyo, Japan; wavelength: 660 nm).

2.6. Determination of the composition of the porous particles

The composition ratio of each component in the porous particles was evaluated by analyzing the ¹H-NMR spectra of the particles and each component. The powder of the porous particles was solved in CDCl₃ and the ¹H-NMR spectrum was obtained. The obtained spectrum includes the specific signals of each component; that is 4.72ppm for methylene groups of PLGA and 3.64ppm for methylene groups of PEG in PEG-PLA. The molar ratio of PLGA and PEG-PLA was determined by comparing the integral ratios of them considering the number of ¹H and consequently, the composition ratio of each component (w/w) was determined.

3. Results and Discussion

3.1. Interfacial tension between water and organic phase

The effect of toluene content in TD-OS and PEG-PLA on the interfacial tension between water and organic phase and the density of the organic solvent is shown in Fig. 2. The interfacial tension in the system including PEG-PLA was lower than that without PEG-PLA in each composition of TD-OS. This result demonstrates that PEG-PLA, composed of hydrophilic PEG block and hydrophobic PLA block, worked as a polymeric surfactant in this system.

The interfacial tension decreased as the toluene content in TD-OS increased, which indicates that as a surfactant, PEG-PLA works better in toluene than in DCM. However, the interfacial tension increased when the toluene content rose from 80v/v% to 100v/v%. This specific behavior was triggered by the change of intermolecular interaction of organic solvents because the behavior appeared regardless of the presence of PEG-PLA. Experimental and theoretical values of interfacial tension in various ternary systems was compared by Wang [21]. Theoretical values of interfacial tension were calculated by using Eq. 3:

$$\sum_i (x_i^\alpha x_i^\beta)^{1/2} \exp \left\{ \gamma (v_i^{int})^{\frac{2}{3}} (N_A)^{\frac{1}{3}} / (RT) \right\} = 1 \quad (\text{Eq. 3})$$

where i expresses the component i , α and β mean organic or water phase, x_i^α is the molar ratio of i in the phase α , x_i^β is the molar ratio of i in the phase β , γ is the interfacial tension, v_i^{int} is the partial molar volume of i in the interfacial mixture, N_A is the Avogadro's number, R is the gas constant, T is the absolute temperature. Eq. 3 indicates that the γ values for water-mixed organic solvent (solvent₁ and solvent₂) systems should be between the values of water-solvent₁ and water-solvent₂ systems. However, when n -heptane and carbon tetrachloride were mixed, the γ was lower than that for each water-organic solvent system under a certain mixing ratio [21]. This indicates that the mixing of organic solvents with different molecular structures can increase the partial molar volume of i near the interface. A similar phenomenon occurred in this experiments, where the mixing of two organic solvents with different molecular structures, toluene and dichloromethane, affected γ . Consequently, γ showed a concave curve with increasing toluene fraction in the mixed organic solvent (Fig. 2).

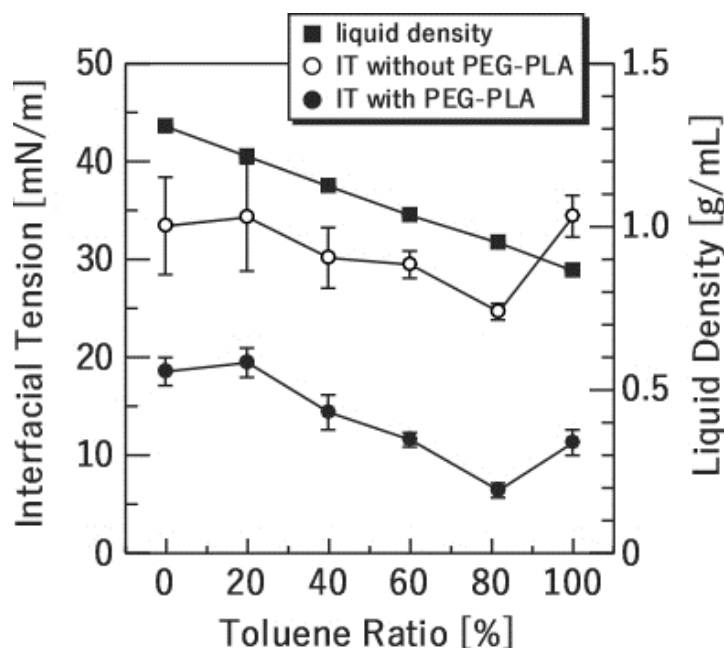


Fig. 2 Effect of the composition of TD-OS on the interfacial tension (IT) between water and organic phase.

3.2. Effect of the composition of TD-OS on the morphology of w/o/w emulsions

Interfacial tension strongly affects the stability of emulsions. Therefore, it was speculated that the

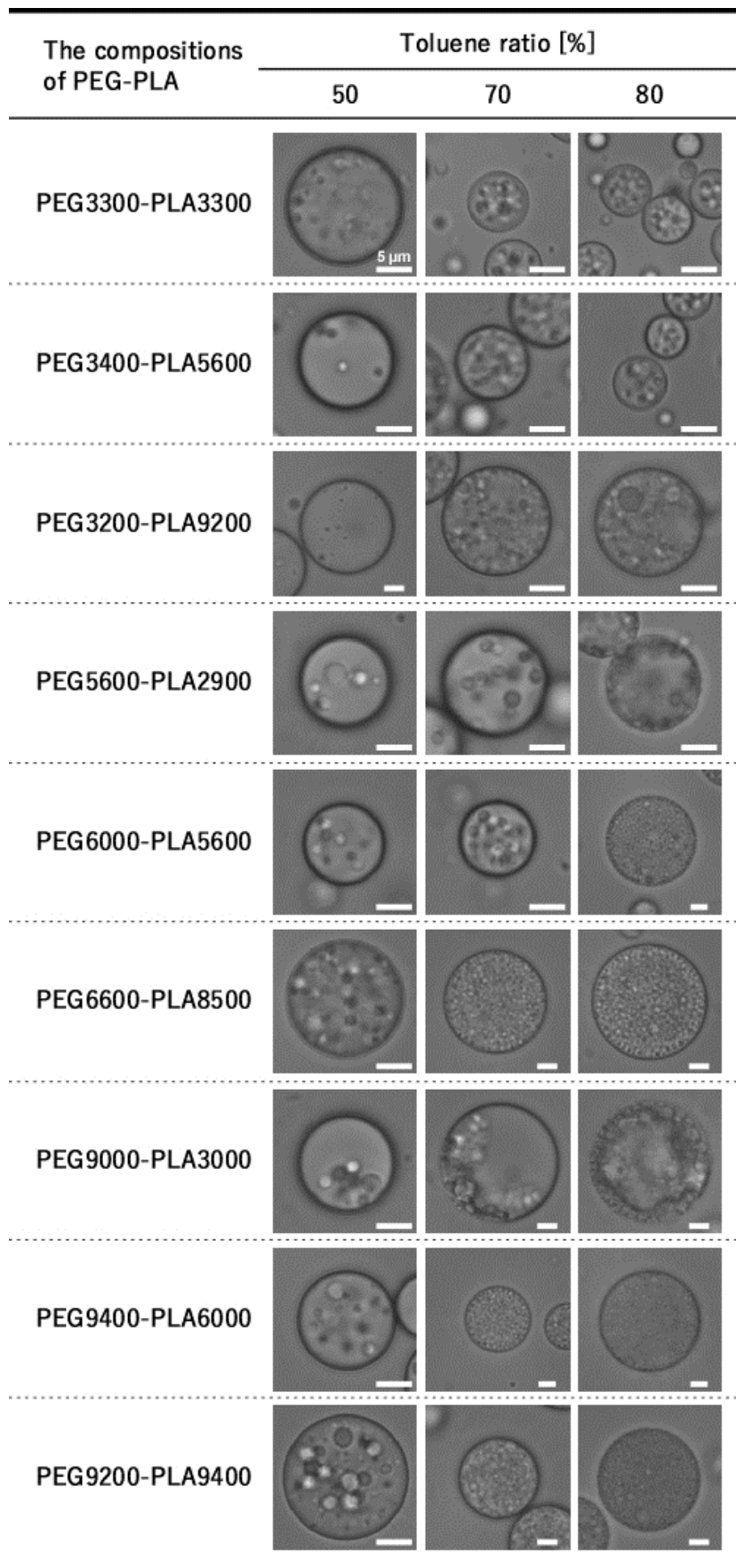


Fig. 3 Effect of the composition of TD-OS on the internal structure of w/o/w emulsions.

composition of TD-OS would strongly affect the morphology of w/o/w emulsions and subsequently obtained porous particles. W/o/w emulsions were observed with an optical microscope (OM). The OM images are shown in Fig. 3. The number of water droplets in an organic droplet increased as the toluene content in TD-OS increased due to decrease of the interfacial tension (shown in Fig. 2). The Brownian motion-based collision of water molecules on the water-oil interface is considered to be one of the driving forces for spontaneous emulsification [1]. In the system of low interfacial tension, small water droplets could be formed in an organic phase because small amount of water molecules would have enough kinetic energy to form w/o emulsion droplets. Fig. 3 also shows that the number of water droplets in an organic droplet increased and the diameter of them decreased as the molecular weight of PEG block increased. The same tendency appeared in the previous reports [1,22]. PEG-PLAs can easily absorb on the water-organic interface as the molecular weight of PEG block because the hydrophilicity of PEG-PLAs increase. Consequently, the interfacial tension would greatly decrease and a large number of smaller w/o emulsions would form.

3.3. Effect of the composition of TD-OS on the surface morphology and internal structure of the resulting particles

The morphology of the particles composed of PLGA and various compositions of PEG-PLA was observed by means of OM and SEM (Fig. 4). All of the particles shown in Fig. 4 were prepared under the same solvent evaporation conditions (temperature: 25°C; liquid-gas interfacial area: 19.9 cm²). SEM images in Fig. 4 have shown that there were dimples and/or pores on the surface of the particles because w/o emulsion droplets worked as porogen. On the other hand, OM images have suggested that several kinds of internal structures were obtained; a particle which has a dimpled surface layer and a large shadow at the center, a particle which has a honeycomb-like outer layer and one or more shadow(s), and a particle of uniformly honeycomb-like structure. It was speculated that the shadow(s) in a particle was a large hollow formed due to a large water droplet or a densely packed core composed of polymers. Then the cross section of the particles was observed (Fig. 5). The direct observation of the internal structure by means of SEM revealed that the shadow(s) observed in a particle was the densely packed core(s). From the results, the porous particles were classified into three kinds of the structures as follows (the graphical images of them are shown in Fig. 6):

- (1) *the particles with **d**imple surface and a totally **f**illed internal core (D-F)*
- (2) *the particles with **p**orous surface and topically **f**illed/**p**orous internal core (P-FP)*
- (3) *the particles with **p**orous surface and totally **p**orous internal core (P-P).*

By using this classification method, the particles in Fig. 4 could be described as shown in Table 1. This classification method suggests that the volume of the densely packed core decreases (and finally disappears) as the initial toluene content in TD-OS and/or the molecular weight of PEG increases. Both these factors induce decrease of interfacial tension, thereby improving the stability of emulsion droplets. Hence, it was expected that the morphology of the porous particles prepared thorough w/o/w emulsions can be precisely controlled by tuning the stability of w/o/w emulsions and that the composition of solvent might be a key factor to independently control the morphology of the particles from the molecular weight of PEG.

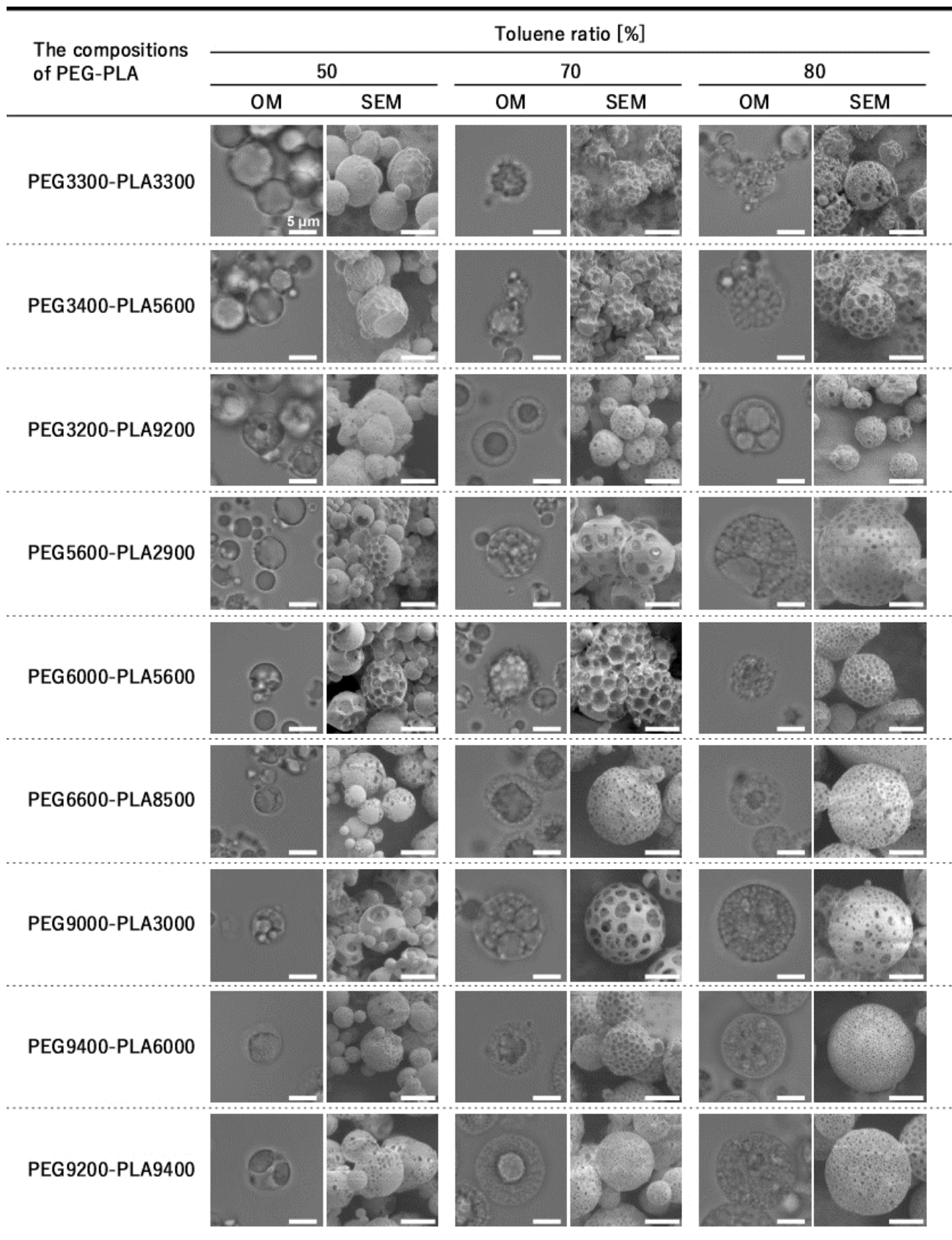


Fig. 4 OM and SEM images of the particles prepared under different conditions in the compositions of TD-OS and/or PEG-PLA.

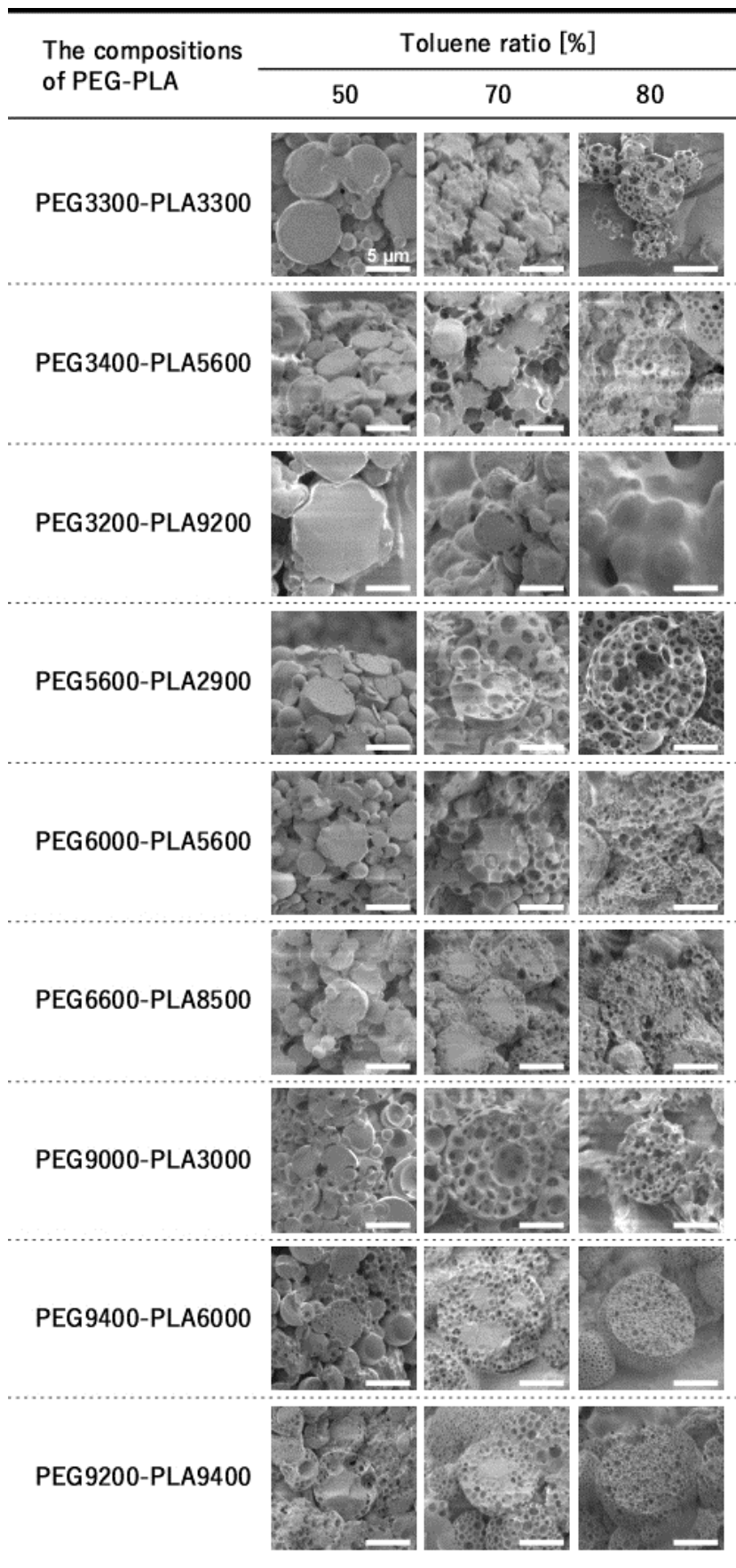


Fig. 5 Effect of the compositions of TD-OS and/or PEG-PLA on the internal structure of the porous particles.

Table 1 The classification of the particles with the types of the internal structures.

The compositions of PEG-PLA	Initial toluene content in TD-OS [%]		
	50%	70%	80%
3300-3300	D-F	D-F	P-P
3400-5600	D-F	D-F	P-P
3200-9200	D-F	P-FP	P-FP
5600-2900	D-F	P-P	P-P
6000-5600	D-F	P-FP	P-FP
6600-8500	D-F	P-FP	P-FP
9000-3000	P-FP	P-P	P-P
9400-6000	P-FP	P-FP	P-P
9200-9400	P-FP	P-FP	P-P

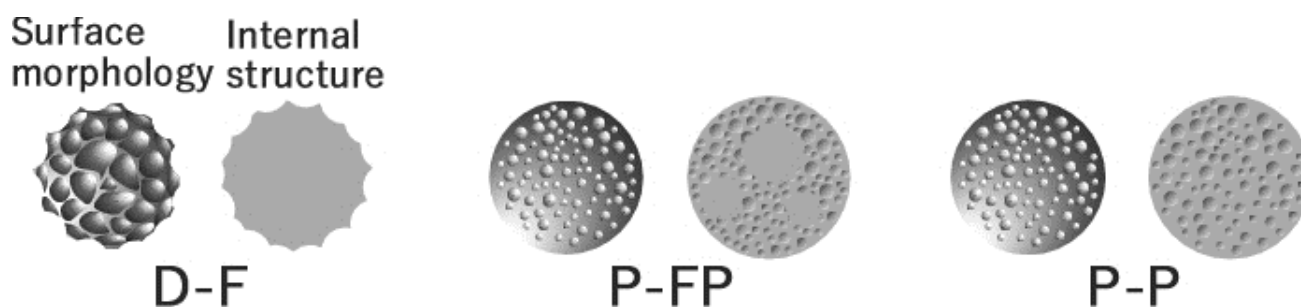


Fig. 6 Graphical images of the surface and internal structure of the porous particles.

3.4. Effect of solvent evaporation rate on the morphology of the particles

The results shown in the previous section indicate that the stability of the w/o/w emulsions greatly affected the morphology of the final porous particles, where the spontaneous emulsification was controlled by the composition of the PEG-PLA and mixed organic solvents. It is difficult to apply these results to other systems because PEG-PLA is a key factor in the spontaneous emulsification process. Therefore, to demonstrate the general applicability of this method, the morphology of the particles was attempted to control by tuning the evaporation of the organic solvents, which is a common factor in all methods for preparing porous particles via emulsion-solvent evaporation. There are two possible factors affecting the evaporation of organic solvents: the liquid-gas interfacial area and temperature.

3.4.1. Liquid-gas interfacial area

Organic solvents are gradually removed from w/o/w emulsions through two steps: (1) molecules of the organic solvents diffuse into water phase from the water-oil interface; (2) Suspending organic molecules vaporize into air from the water-air interface. The rate of the second step increases as the liquid-gas interfacial area increases.

The solubility in water and vapor pressure of each organic solvent at 25°C are described as follows; toluene: 0.52 g/L and 3.5 kPa; DCM: 17.2 g/L and 56.0 kPa [23–25]. From these physical properties, it was hypothesized that both the toluene fraction in the mixed organic solvent and the stability of the w/o emulsion droplets would increase rapidly during solvent evaporation with a high gas-liquid interfacial area (*i.e.*, using a large beaker), because of the high volatility of DCM. Accordingly, it was expected that P-P particle with a honeycomb-like inner structure would preferentially form instead of D-F and P-FP particles with a totally or partially filled core as the cross-sectional area of the beaker increases.

The effect of liquid-gas interfacial area on the morphology of the particles prepared with PEG-PLAs of which the molecular weight of PLA block was around 6,000 is shown in Fig. 7 (prepared at 25°C). From the results of Figs. 4 and 7, the types of the particles can be described as Table 2. In the systems of 50v/v% initial toluene content, the morphology of the particles was hardly affected by interfacial area because an organic droplet in these systems had smaller number of w/o emulsion droplets than the systems of other toluene contents; that is, there were only few porogens in w/o/w emulsions. The images of the particles prepared with TD-OS of 50v/v% toluene also exhibited that most of the pores were concentrated in only a part of the particle surface. The reason why this specific structure

The compositions of PEG-PLA	Liquid-gas interfacial area [cm ²]	Toluene ratio [%]					
		50		70		80	
		OM	SEM	OM	SEM	OM	SEM
PEG3400-PLA5600	13.3						
	57.7						
PEG6000-PLA5600	13.3						
	57.7						
PEG9400-PLA6000	13.3						
	57.7						

Fig. 7 Effect of the liquid-gas interfacial area in the process of solvent evaporation on the morphology of the porous particles.

Table 2 Summary of the effect of the liquid-gas interfacial area on the types of particle structure.

The compositions of PEG-PLA	Initial toluene content [%]	Liquid-gas interfacial area [cm ²]		
		13.3	19.9	57.7
3400-5600	50	D-F	D-F	D-F
	70	D-F	D-F	P-P
	80	D-F	P-P	P-P
6000-5600	50	D-F	D-F	D-F
	70	D-F	P-FP	P-FP
	80	P-FP	P-FP	P-FP
9400-6000	50	D-F	P-FP	D-F
	70	P-FP	P-FP	P-P
	80	P-FP	P-P	P-P

*All of the samples were prepared at 25°C

formed is illustrated with the Stokes equation [26]:

$$u = \frac{2r^2\Delta\rho g}{9\eta} \quad (\text{Eq. 4})$$

where u is the sedimentation velocity, η is the viscosity of continuous phase, r is the radius of emulsion droplets, $\Delta\rho$ is the difference in the density of dispersed and continuous phase, and g is the gravity acceleration. Eq. 4 suggests that a large difference in the density of dispersed and continuous phase accelerate the emulsion droplets move and concentrate to the upper or lower side of continuous phase. As shown in Fig. 2, the system of water ($\rho = 1.0 \text{ g/cm}^3$) and TD-OS of 50v/v% toluene has the largest difference in density in the range investigated in Figs. 4 and 7. Thus, the w/o emulsion droplets, in such a system, tend to gather on a certain side of an organic droplet and shaped the particles which had inclined dimples on the surface. By contrast, the morphology of the particles was greatly affected by change of the liquid-gas interface in the systems of 70 or 80% initial toluene content. In these systems, the volume of internal core(s) decreased (and finally disappeared) as the liquid-gas interfacial area increased; in other words, D-F tended to disappear whereas P-FP and P-P were likely to be obtained. The effect of liquid-gas interfacial area shown in Figs. 4 and 7 correspond to a tendency predicted at the beginning of this section. Therefore, the hypothesis that the stability of w/o emulsions has predominant effect on the morphology of the particles was further confirmed in the next section.

3.4.2. Temperature

It was hypothesized that increasing the temperature would result in fast removal of DCM (*i.e.*, a fast increase in the toluene fraction in TD-OS) due to the high volatility and low boiling point of DCM. The effect of temperature on the morphology of the particles prepared with PEG-PLAs of which the molecular weight of PLA block was around 6,000 is shown in Fig. 8 (prepared with the liquid-gas interfacial area of 19.9 cm²). From the results

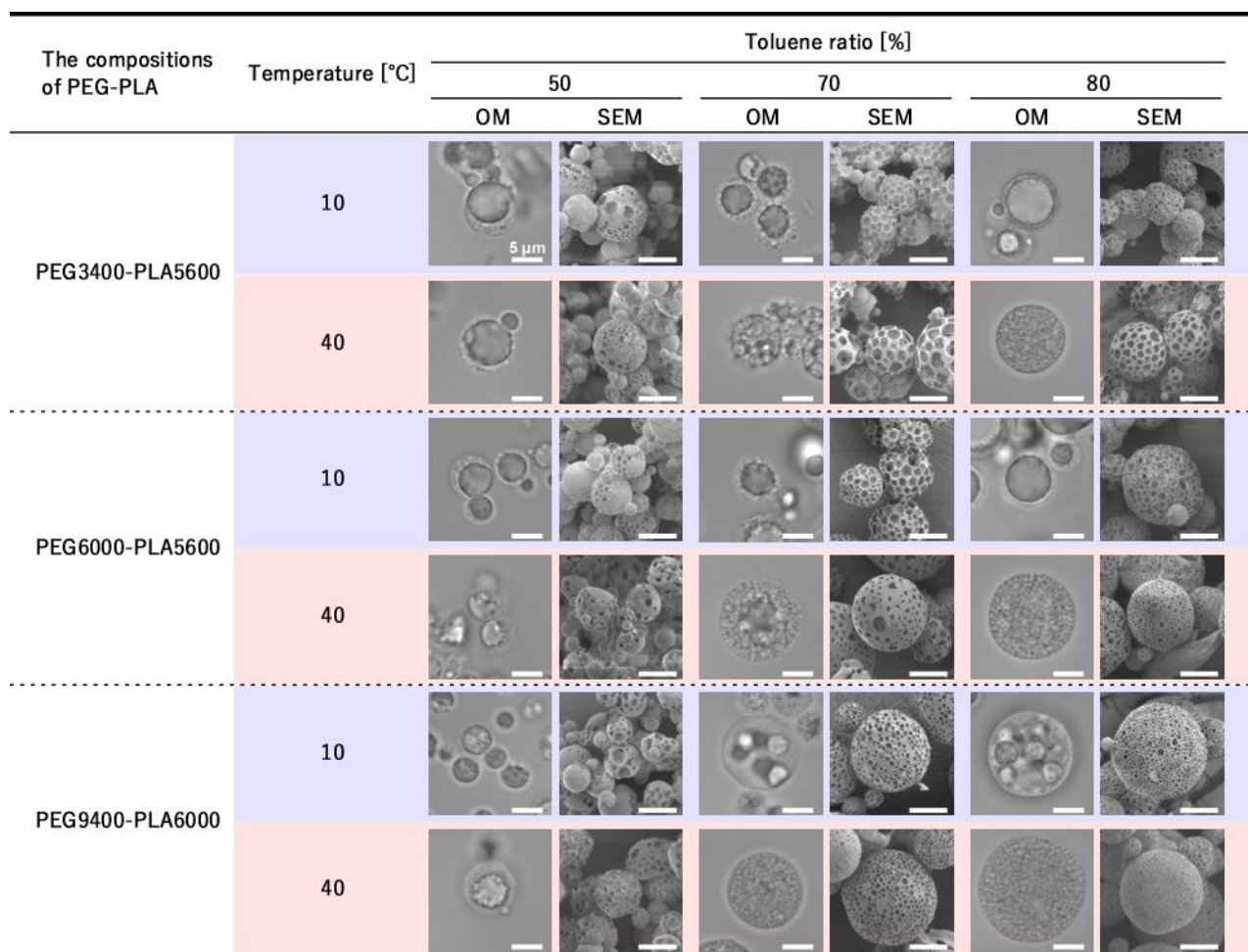


Fig. 8 Effect of the temperature in the process of solvent evaporation on the morphology of the particles.

Table 3 Summary of the effect of the temperature on the types of particle structure.

The compositions of PEG-PLA	Initial toluene content [%]	Temperature [°C]		
		10	25	40
3400-5600	50	D-F	D-F	D-F
	70	D-F	D-F	P-P
	80	D-F	P-P	P-P
6000-5600	50	D-F	D-F	D-F
	70	P-FP	P-FP	P-FP
	80	D-F	P-FP	P-P
9400-6000	50	D-F	P-FP	P-FP
	70	P-FP	P-FP	P-P
	80	P-FP	P-P	P-P

*All of the samples were prepared with the liquid-gas interfacial area of 19.9 cm²

of Figs. 4 and 8, the types of the particles can be described as Table 3. The results shown in Figs 4 and 8 demonstrate that temperature in the process of solvent evaporation affects the morphology of the particles as well as interfacial area; that is, the volume of internal core(s) decreased (and finally disappeared) as the temperature increased in the process of solvent evaporation. When PEG aqueous solutions are placed at high temperature, PEG chains tend to dehydrate [27,28]. In other words, the affinity of PEG chains of PEG-PLA with water decreases as it is placed at high temperature. Furthermore, the viscosity of liquids is inversely proportional to temperature [29], which means that high temperature causes decreasing the viscosity of organic solvents and makes it easier for w/o emulsion droplets to unite each other according to Eq. 4. These general theories imply that the stability of w/o emulsions would decrease and consequently D-F would easily form as the temperature increases. However, the series of results indicate the opposite tendency from the prediction described above (*i.e.*, a decrease in the volume of inner core with increasing temperature). This contradiction strongly suggests that the change in the composition of the mixed organic solvents affects both the emulsification and evaporation (*i.e.*, particle formation) processes, and has a greater effects on the morphology of the porous particles than the change in the surface activity of the surfactants and/or the viscosity of the liquids.

The effect of temperature on the particle morphology was also considered with respect to the molecular weight of PEG-PLA. For example, when the initial toluene fraction was 80v/v%, the morphology of the particle drastically changed from D-F to P-P in the presence of PEG3400-PLA5600, whereas it changed only slightly from P-FP to P-P in the presence of PEG9400-PLA6000. This was probably due to the difference in the stability of the spontaneous w/o emulsions. As the PEG chains contribute to the stabilization of spontaneous w/o emulsions, it can be assumed that the ability of the block copolymers to stabilize w/o emulsions increases as follows: PEG3400-PLA5600 < PEG6000-PLA5600 < PEG9400-PLA6000. Therefore, the change in the solvent evaporation condition affects the stability of w/o emulsions as follows: PEG3400-PLA5600 > PEG6000-PLA5600 > PEG9400-PLA6000. PEG6000-PLA5600 had only a moderate effect on the stability of the w/o emulsions. When PEG6000-PLA5600 was used and the initial toluene proportion was 80v/v%, the change in the particle morphology was as follows: P-FP → P-FP → P-FP (13.3 → 19.9 → 57.7 cm², respectively) and D-F → P-FP → P-P (10 → 25 → 40°C, respectively). This implies that the temperature has a greater effect on (1) the rate of solvent evaporation and/or (2) the change in the composition of TD-OS than the interfacial area. To clarify which factors was dominant, the time dependence of the residual ratio of the organic solvent (*i.e.*, evaporation behavior of each organic solvent from the mixed organic solvent) is discussed in the next section.

3.5. Evaluation of solvent evaporation rate

3.5.1. Monitoring the amount of the residual organic solvent with GC-MS

The time dependence of the total amount of residual organic solvent and the toluene content in TD-OS is shown in Fig. 9. Fig. 9 (a) shows that the solvent evaporation rate increased as the interfacial area or temperature increased. Moreover, Fig. 9 (b) shows that toluene fraction in TD-OS increased as the interfacial area or temperature increased as the DCM evaporates faster than toluene from the mixed organic solvents due to its high volatility. This

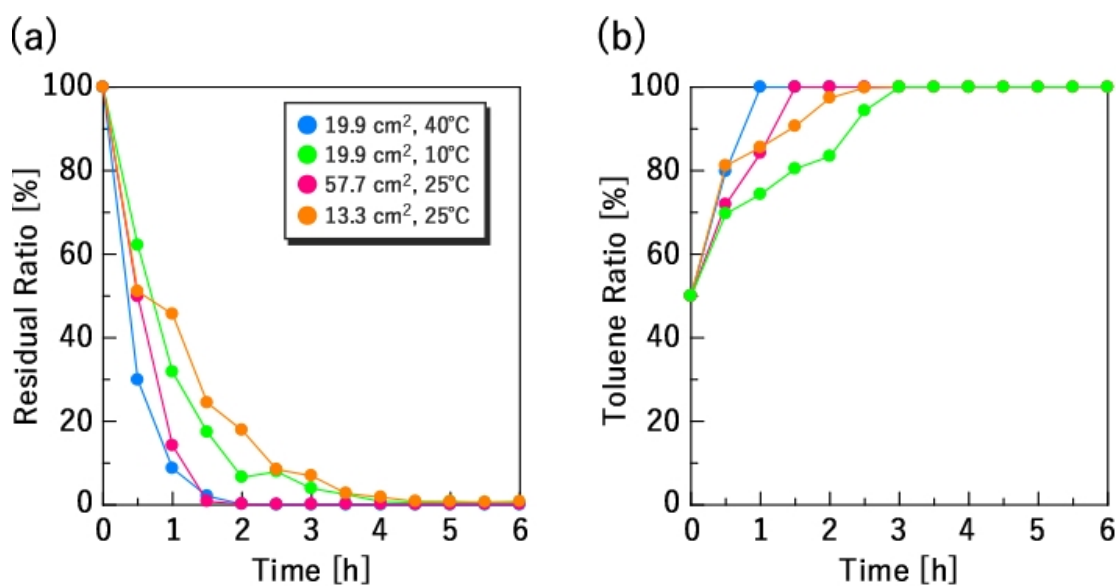


Fig. 9 Effect of the interfacial area or temperature on the time-dependent change in (a) the residual ratio of TD-OS and (b) the toluene fraction in TD-OS.

is because DCM was eliminated more quickly than toluene due to its high volatility. Fig. 9 (b) also shows that the increase in the toluene fraction was greater for a change in temperature from 10 to 40°C than for a change in the interfacial area from 13.3 to 57.7 cm². This suggests that, under the experimental conditions used here, temperature had a greater effect on the increase in the toluene fraction in the mixed organic solvent than the interfacial area. These results, and those shown in Figs. 7 and 8 (*i.e.*, the temperature had a greater effect on the morphology of the porous particles than the interfacial area) strongly suggest that the changes in the morphology of the porous particles was mainly dependent on changes in the composition of the mixed organic solvent rather than the rate of solvent evaporation.

3.5.2. Comparison of solvent evaporation rate with UV-vis spectrophotometer

Although the w/o/w emulsion solution is a milky white color immediately after its formation, the transparency of the solution increases as the solvent evaporation proceeds. Therefore, the change in transmittance of the solution over time was used as a measure of solvent evaporation. Fig. 10 (a) shows the effect of solvent evaporation conditions on the change in transmittance over time. Compared to the conditions used for the results in Section 3.3 (25°C, 19.9 cm², black circles), the time when the transmittance significantly changed became shorter as the interfacial area (pink circles) or temperature (blue circles) increased, whereas it became longer as the interfacial area (orange circles) or temperature (green circles) increased. As these experimental factors affect the solvent evaporation rate, the times required to observe a change in the transmittance should reflect changes in the solvent evaporation rate. Fig. 10 (b) shows the effect of the PEG-PLA composition on the change in transmittance of w/o/w emulsions. The saturation values of transmittance after a complete elimination of the organic solvents differed for each PEG-PLA composition because the physical properties (such as the diameter and morphology) of the resulting

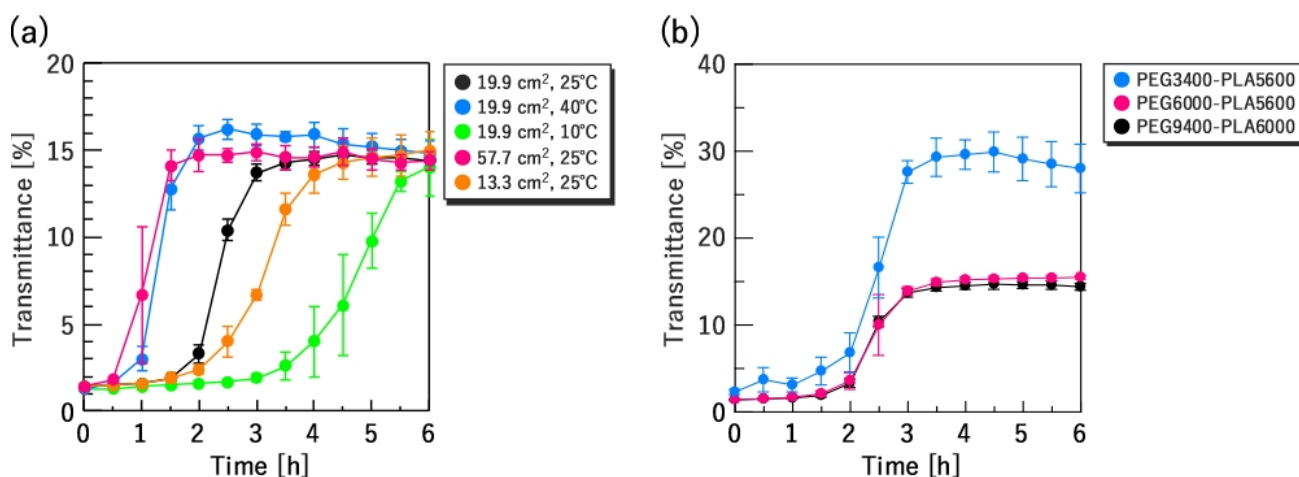


Fig. 10 The effect of the (a) solvent evaporation conditions and (b) composition of the block polymers on the change in transmittance over time.

particles are different. In contrast, the time when the transmittance significantly changed was similar for the three types of PEG-PLA. This indicates that the solvent evaporation conditions greatly affect the solvent evaporation rate, irrespective of the composition of PEG-PLA.

Fig. 11 shows the weight percentage of PEG-PLA in the porous particles prepared under various solvent evaporation conditions. Fig. 12 shows the effect of the molecular weight of the PLA block on the weight percentage of PEG-PLA in the particles. These results revealed that the dominant factor determining the polymeric composition of the porous particles was the molecular weight of the PLA block, while the solvent evaporation conditions had only a minor effect. Therefore, when the solvent evaporation conditions were changed, the corresponding changes in the particle morphology were not a result of compositional changes, but rather due to changes in the stability of the spontaneous emulsions.

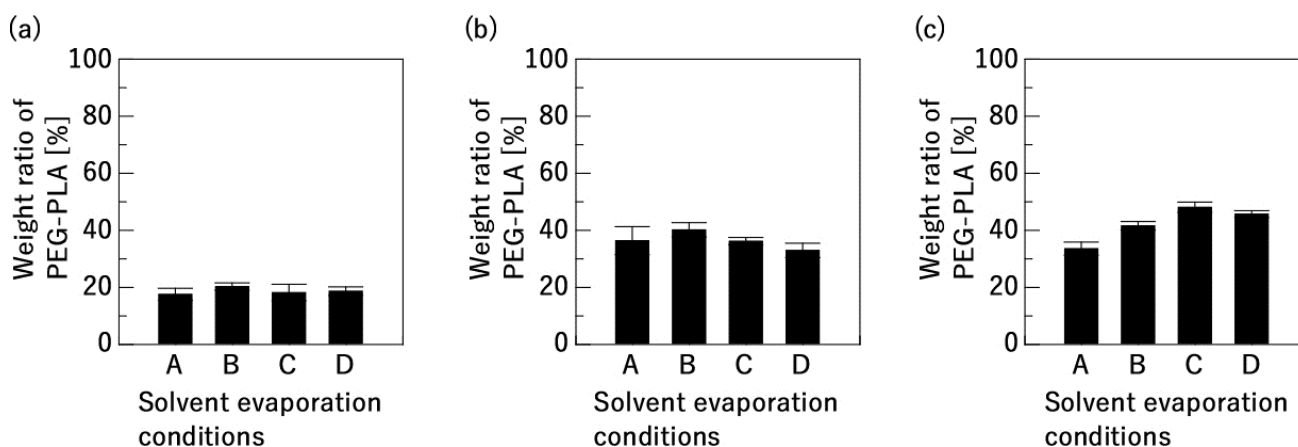


Fig. 11 Effect of the solvent evaporation conditions on weight ratio of PEG-PLA in the porous particles. Toluene content in TD-OS was (a) 50v/v%, (b) 70v/v%, and (c) 80v/v%. Solvent evaporation conditions were A: 10°C-19.9 cm², B: 40°C-19.9 cm², C: 25°C-13.3 cm², and D: 25°C-57.7 cm², respectively.

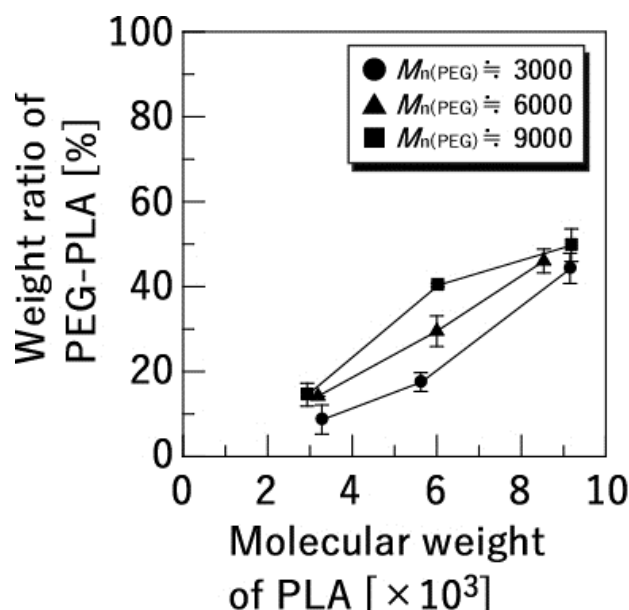


Fig. 12 Effect of the molecular weight of PLA on the weight ratio of PEG-PLA in the porous particles. The samples were prepared under the condition of 25°C and 19.9 cm².

3.6. Strategy to control the surface and internal morphology of porous particles

The results described above indicate that the surface morphology and internal structure of the porous particles prepared through emulsion-solvent evaporation-method can be controlled by tuning the composition of mixed organic solvent before and/or after emulsification. Particle formation mechanism depending on the composition of mixed organic solvent is summarized in Fig. 13. The structure of porous particles changes from D-F to P-FP and finally to P-P by raising the toluene content in TD-OS in the process of emulsification or by quickly raising the toluene content in TD-OS in the process of solvent evaporation. This means that changing the ratio of one solvent which is effective to stabilize w/o emulsions in the mixed organic solvent has predominant effect on particle morphology no matter before or after preparing w/o/w emulsions.

The mechanism for the formation of D-F particles when the spontaneous w/o emulsions are unstable is proposed as follows. When w/o/w emulsions are prepared under condition where the spontaneous w/o emulsions are unstable, inner water droplets frequently agglomerate or diffuse into the outer water phase. Hence, it was assumed that the number of water droplets is higher near the interface between an organic droplet and the outer water phase than the amount in the center of an organic droplet. Therefore, a dense core composed of hydrophobic polymers is easily formed at the center of an organic droplet, while pores are formed only near the particle surface because of the existence of porogens. The gradient in the concentration of organic solvent molecules in a spontaneous o/w emulsion droplet is described using the relationship reported by Sjöström (Eq. 5) [24]. When organic solvent molecules diffuse into the outer water phase from the surface of organic droplets, a concentration gradient occurs in the spontaneous o/w emulsion droplet. The time required to eliminate over 90% of the concentration gradient of toluene molecules in the o/w emulsion droplet (t_{90}) can be calculated using (Eq. 5):

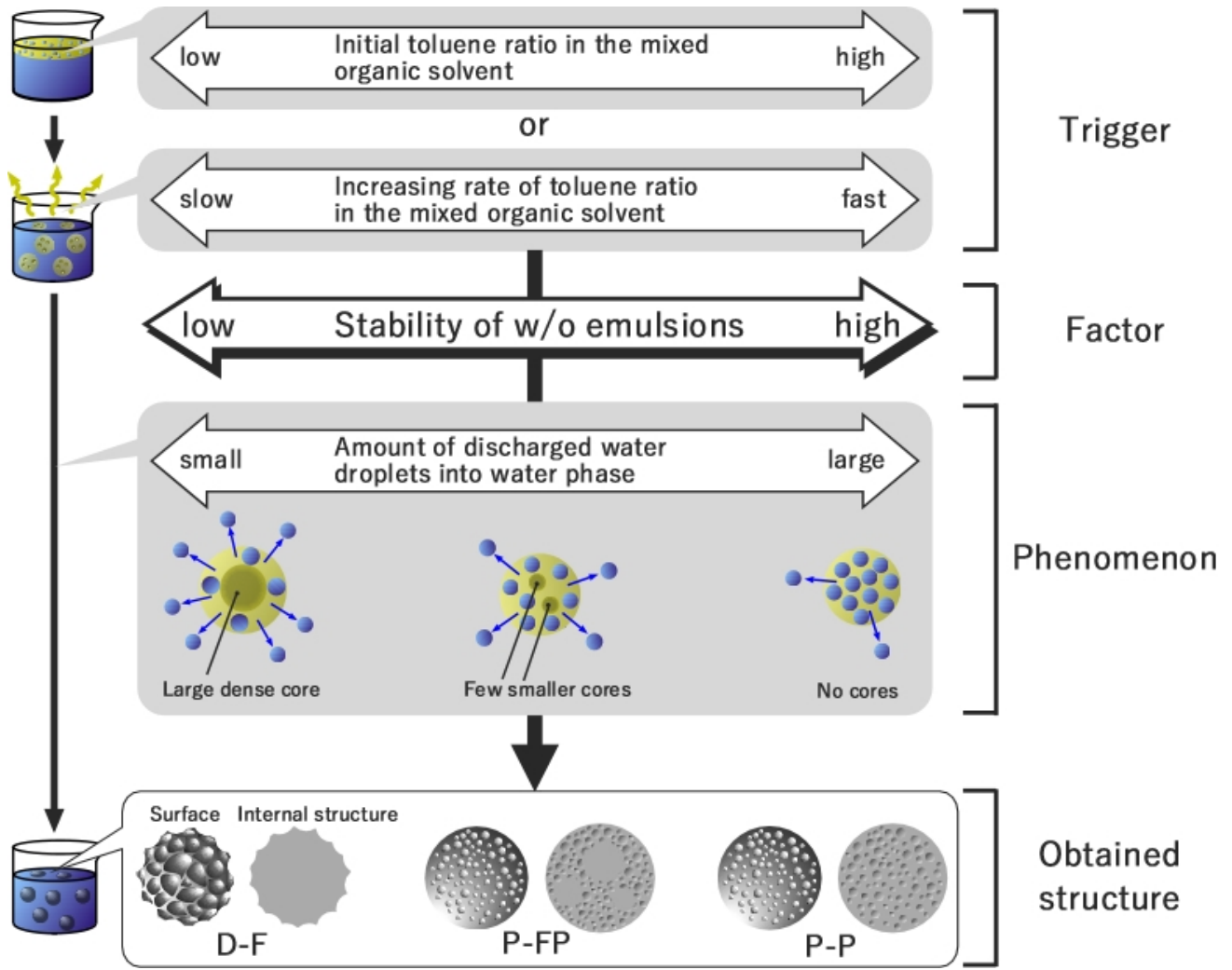


Figure 13. Summary of the effect of the preparation conditions on the morphology of the resulting particles through changing the stability of w/o emulsions.

$$t_{90} = \frac{0.3r^2}{D_{PLGA/toluene}} \quad (\text{Eq. 5})$$

where r is the radius of a droplet and $D_{PLGA/toluene}$ is the mutual diffusion coefficient between PLGA and toluene. PLGA is the main component of the particles in this system. Although $D_{PLGA/toluene}$ has not been reported because toluene is not a good solvent for PLGA, the value has been reported for some other organic solvents; that is, the order of 10^{-8} to 10^{-12} $\text{m}^2 \text{s}^{-1}$ [30–32]. Additionally, the diameter of the porous particles is the order of 10^{-6} m and consequently t_{90} would take the value of 3.0×10^{-5} to 3.0×10^{-1} s. Moreover, the time for the next toluene molecules diffusing into outer phase (t_{dif}) was calculated by using Eq. 6 [24]:

$$t_{dif} = \frac{\rho r^2}{3C_{sol}D_{tol/wat}} \quad (\text{Eq. 6})$$

where ρ is the density of toluene (866.9 kg m^{-3}), C_{sol} is the solubility of toluene in water (0.515 kg m^{-3}), and $D_{tol/wat}$ is the diffusion coefficient of toluene in water ($9.5 \times 10^{-10} \text{ m}^2 \text{s}^{-1}$). By using these parameters and Eq. 6, t_{dif} is estimated as 5.9×10^{-1} s. Hence, since, $t_{90} < t_{dif}$, it was concluded that the concentration gradient of toluene can be cancelled

immediately before the subsequent toluene molecules increase the gradient by diffusing into outer water phase from water-oil interface. Therefore, PLGA is not expected to precipitate close to the water-oil interface because of the micro-Brownian motion of inner water droplets. Consequently, PLGA molecules preferentially precipitate at the center of the organic droplet, forming D-F particles.

In contrast, in the case of a toluene-rich composition, the inner water droplets do not significantly agglomerate or diffuse to the outer water phase. Under such conditions, stable water droplets uniformly exist inside the spontaneous w/o emulsion droplets and there are no localized regions of high PLGA concentrations to form dense cores. Consequently, these emulsions would form P-FP or P-P particles.

4. Conclusion

In this chapter, the way of controlling particle morphology was investigated by changing preparation conditions except for the composition of PEG-PLA. As a result, it was found out that the composition of mixed organic solvent is significantly related to the morphology of the porous particles. concretely, the highly porous structure tends to form by raising the content of an organic solvent which is effective to stabilize porogens (w/o emulsion droplets) no matter before and after preparing w/o/w emulsions. Moreover, the effect of solvent evaporation conditions (liquid-gas interfacial area and temperature) on the changing behavior of the composition of TD-OS over time was consistent to the prediction. The study in this chapter consistently indicates that by controlling the stability of porogens (w/o emulsions) in the organic phase by tuning the composition of the mixed solvent before or after preparing w/o/w emulsions, the particle morphology can be precisely controlled. Furthermore, “organic solvent” is a universal factor for emulsification-solvent evaporation-method as opposed to PEG-PLA, a specific factor for this PEG-PLA-containing-system. Therefore, the way of controlling the morphology of the porous particles shown in this chapter might be applied to other particle preparation systems of emulsification-solvent evaporation-method. The controlling method for particle morphology independent of the concentration and the composition of polymers would be an effective factor to investigate and improve the aerodynamic performance and the release behavior of the drugs of the particles having complicated surface and internal structure.

5 References

- [1] S. Nishimura, T. Takami, Y. Murakami, Porous PLGA microparticles formed by “one-step” emulsification for pulmonary drug delivery: The surface morphology and the aerodynamic properties, *Colloids Surfaces B Biointerfaces*. 159 (2017) 318–326. <https://doi.org/10.1016/j.colsurfb.2017.08.004>.
- [2] J. Herrmann, R. Bodmeier, Biodegradable, somatostatin acetate containing microspheres prepared by various aqueous and non-aqueous solvent evaporation methods, *Eur. J. Pharm. Biopharm.* 45 (1998) 75–82. [https://doi.org/10.1016/S0939-6411\(97\)00125-2](https://doi.org/10.1016/S0939-6411(97)00125-2).
- [3] Y. Yang, T. Chung, X. Bai, W.C.-C.E. Science, U. 2000, Effect of Preparation Conditions on Morphology and

- Release Profiles of Biodegradable Polymeric Microspheres Containing Protein Fabricated By Double-Emulsion ..., *Chem. Eng. Sci.* . 55 (2000) 2223–2236.
- [4] G. Ruan, S.S. Feng, Q.T. Li, Effects of material hydrophobicity on physical properties of polymeric microspheres formed by double emulsion process, *J. Control. Release.* 84 (2002) 151–160. [https://doi.org/10.1016/S0168-3659\(02\)00292-4](https://doi.org/10.1016/S0168-3659(02)00292-4).
- [5] R.H. Ansary, M.M. Rahman, M.B. Awang, H. Katas, H. Hadi, F. Mohamed, A.A. Doolaanea, Y.B. Kamaruzzaman, Preparation, characterization and in vitro release study of BSA-loaded double-walled glucose-poly(lactide-co-glycolide) microspheres, *Arch. Pharm. Res.* 39 (2016) 1242–1256. <https://doi.org/10.1007/s12272-016-0710-3>.
- [6] T.L. Terry, B.E. Givens, V.G.J. Rodgers, A.K. Salem, Tunable Properties of Poly-DL-Lactide-Monomethoxypolyethylene Glycol Porous Microparticles for Sustained Release of Polyethylenimine-DNA Polyplexes, *AAPS PharmSciTech.* 20 (2019) 1–9. <https://doi.org/10.1208/s12249-018-1215-9>.
- [7] F. Gao, Z.G. Su, P. Wang, G.H. Ma, Double emulsion templated microcapsules with single hollow cavities and thickness-controllable shells, *Langmuir.* 25 (2009) 3832–3838. <https://doi.org/10.1021/la804173b>.
- [8] K.F. Pistel, T. Kissel, Effects of salt addition on the microencapsulation of proteins using W/O/W double emulsion technique, *J. Microencapsul.* 17 (2000) 467–483. <https://doi.org/10.1080/026520400405723>.
- [9] B. Patel, V. Gupta, F. Ahsan, PEG-PLGA based large porous particles for pulmonary delivery of a highly soluble drug, low molecular weight heparin, *J. Control. Release.* 162 (2012) 310–320. <https://doi.org/10.1016/j.jconrel.2012.07.003>.
- [10] S. Liu, M. Cai, R. Deng, J. Wang, R. Liang, J. Zhu, Fabrication of porous polymer microparticles with tunable pore size and density through the combination of phase separation and emulsion-solvent evaporation approach, *Korea Aust. Rheol. J.* 26 (2014) 63–71. <https://doi.org/10.1007/s13367-014-0007-3>.
- [11] Q. Zhang, K. Tan, Z. Ye, Y. Zhang, W. Tan, M. Lang, Preparation of open porous polycaprolactone microspheres and their applications as effective cell carriers in hydrogel system, *Mater. Sci. Eng. C.* 32 (2012) 2589–2595. <https://doi.org/10.1016/j.msec.2012.07.045>.
- [12] Y. Hong, C. Gao, Y. Shi, J. Shen, Preparation of porous polylactide microspheres by emulsion-solvent evaporation based on solution induced phase separation, *Polym. Adv. Technol.* 16 (2005) 622–627. <https://doi.org/10.1002/pat.629>.
- [13] Y. Bahl, H. Sah, Dynamic changes in size distribution of emulsion droplets during ethyl acetate-based microencapsulation process, *AAPS PharmSciTech.* 1 (2000). <https://doi.org/10.1208/pt010105>.
- [14] H. Sah, Ethyl formate - Alternative dispersed solvent useful in preparing PLGA microspheres, *Int. J. Pharm.* 195 (2000) 103–113. [https://doi.org/10.1016/S0378-5173\(99\)00379-8](https://doi.org/10.1016/S0378-5173(99)00379-8).
- [15] T. Shao, L. Bai, B. Yan, Y. Jin, Y. Cheng, Modeling the solidification of O/W-emulsion droplet in solvent evaporation technique, *Chem. Eng. Res. Des.* 122 (2017) 233–242. <https://doi.org/10.1016/j.cherd.2017.04.022>.
- [16] R. Jeyanthi, B.C. Thanoo, R.C. Metha, P.P. DeLuca, Effect of solvent removal technique on the matrix characteristics of polylactide/glycolide microspheres for peptide delivery, *J. Control. Release.* 38 (1996) 235–244. [https://doi.org/10.1016/0168-3659\(95\)00125-5](https://doi.org/10.1016/0168-3659(95)00125-5).
- [17] W.I. Li, K.W. Anderson, P.P. Deluca, Kinetic and thermodynamic modeling of the formation of polymeric

- microspheres using solvent extraction/evaporation method, *J. Control. Release.* 37 (1995) 187–198. [https://doi.org/10.1016/0168-3659\(95\)00077-1](https://doi.org/10.1016/0168-3659(95)00077-1).
- [18] W.I. Li, K.W. Anderson, R.C. Mehta, P.P. Deluca, Prediction of solvent removal profile and effect on properties for peptide-loaded PLGA microspheres prepared by solvent extraction/ evaporation method, *J. Control. Release.* 37 (1995) 199–214. [https://doi.org/10.1016/0168-3659\(95\)00076-3](https://doi.org/10.1016/0168-3659(95)00076-3).
- [19] A.W. Porter, On the calculation of surface tension from measurements of capillary rise, *J. Sci. Instrum.* 7 (1930) 197–198. <https://doi.org/10.1088/0950-7671/7/6/306>.
- [20] C.E. Stauffer, The measurement of surface tension by the pendant drop technique, *J. Phys. Chem.* 69 (1965) 1933–1938. <https://doi.org/10.1021/j100890a024>.
- [21] P. Wang, A. Anderko, Modeling interfacial tension in liquid-liquid systems containing electrolytes, *Ind. Eng. Chem. Res.* 52 (2013) 6822–6840. <https://doi.org/10.1021/ie303460c>.
- [22] T. Takami, Y. Murakami, Unexpected and successful “one-step” formation of porous polymeric particles only by mixing organic solvent and water under “low-energy-input” conditions, *Langmuir.* 30 (2014) 3329–3336. <https://doi.org/10.1021/la500324j>.
- [23] T. Hiroshi, Percutaneous absorption of organic solvents, *Ind. Health.* 13 (1975) 227–236.
- [24] B. Sjöström, B. Bergenståhl, M. Lindberg, Å.C. Rasmuson, The Formation of Submicron Organic Particles by Precipitation in an Emulsion, *J. Dispers. Sci. Technol.* 15 (1994) 89–117. <https://doi.org/10.1080/01932699408943545>.
- [25] C. Sigma-Aldrich, R.E. Lenga, K.L. Votoupal, The Sigma-Aldrich Library of Regulatory and Safety Data, (1993).
- [26] K. Sakai, S. Iijima, R. Ikeda, T. Endo, T. Yamazaki, Y. Yamashita, M. Natsuisaka, H. Sakai, M. Abe, K. Sakamoto, Water-in-oil emulsions prepared by peptide-silicone hybrid polymers as active interfacial modifier: Effects of silicone oil species on dispersion stability of emulsions, *J. Oleo Sci.* 62 (2013) 505–511. <https://doi.org/10.5650/jos.62.505>.
- [27] T. Muraoka, K. Adachi, M. Ui, S. Kawasaki, N. Sadhukhan, H. Obara, H. Tochio, M. Shirakawa, K. Kinbara, A structured monodisperse PEG for the effective suppression of protein aggregation, *Angew. Chemie - Int. Ed.* 52 (2013) 2430–2434. <https://doi.org/10.1002/anie.201206563>.
- [28] S. Kawasaki, T. Muraoka, H. Obara, T. Ishii, T. Hamada, K. Kinbara, Thermally driven micrometer-scale aqueous-phase separation of amphiphilic oligoethylene glycol analogues, *Chem. - An Asian J.* 9 (2014) 2778–2788. <https://doi.org/10.1002/asia.201402134>.
- [29] E.N. da C. Andrade, LVIII. A theory of the viscosity of liquids. —Part II, London, Edinburgh, Dublin Philos. Mag. J. Sci. 17 (1934) 698–732. <https://doi.org/10.1080/14786443409462427>.
- [30] H. Eser, F. Tihminlioglu, Determination of thermodynamic and transport properties of solvents and non solvents in poly(L-lactide-co-glycolide), *J. Appl. Polym. Sci.* 102 (2006) 2426–2432. <https://doi.org/10.1002/app.24516>.
- [31] R.F. Willard, N.A. Jeffrey, L.C. Amber, A.B. Paul, Diffusivities of Dichloromethane in Poly(lactide-co-glycolide), *J. Appl. Polym. Sci.* 112 (2009) 1622–1629.
- [32] H. Katou, A.J. Wandrey, B. Gander, Kinetics of solvent extraction/evaporation process for PLGA microparticle fabrication, *Int. J. Pharm.* 364 (2008) 45–53. <https://doi.org/10.1016/j.ijpharm.2008.08.015>.

Chapter 4

Establishment of a novel method for preparing a film-type biomaterial with highly porous structure by using spontaneous emulsification

1. Introduction

In Chapter 2 and 3, the feasibility of the porous particles for the application as a drug carrier for pulmonary delivery and the formation mechanism of the porous structure was revealed. These chapters were concerned about a particle-type porous material. However, the most important point in these reports is that spontaneous emulsification was skillfully used by tuning the compositions of PEG-PLA for preparing a highly porous biomaterial for the first time in the world. Indeed, most precursors of the nano- or microparticles prepared via spontaneous emulsification were o/w emulsions; in other words, spontaneous emulsification was used for formation of the outline rather than the internal structure of the spherical particles [1–4]. Even after the novel technique was reported by Murakami for the first time [5], there are still few reports using spontaneous emulsification for the formation of the porous structure of the particles [6–8].

In this chapter, it was expected that this unique technology, controlling spontaneous emulsification for the preparation of porous structure of the particles, could be also applied to fabricate a film-type material with highly porous structure. Porous two-dimensional materials have been applied to medical fields such as a scaffold for tissue regeneration [9,10], a platform for sustainable drug release [11,12], and a substrate for cell culture [13,14]. Therefore, if a porous film was successfully prepared by using spontaneous emulsification, this porous film could be a useful and novel biomaterial. The scheme proposed in this study to prepare a film-type porous material is shown in Fig. 1. It was expected that a porous film would form on the surface of water in a container by evaporating organic solvents without any mechanical emulsification. this proposal as a novel cost-effective method for preparing a film-type porous biomaterial was tried to established by investigating the effect of various preparation conditions on the surface morphology and internal structure of the polymeric films and considered the feasibility of the films for application as a new biomaterial.

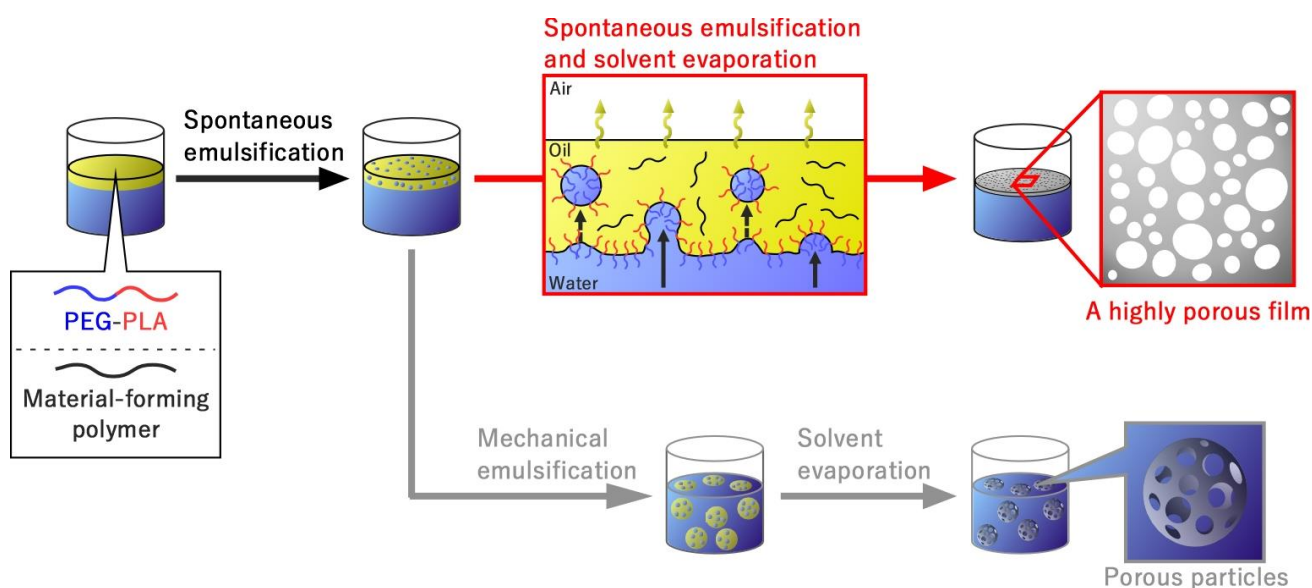


Fig. 1 A novel proposal of preparation method for a highly porous film using spontaneous emulsification.

2. Material and Methods

2.1. Materials

PEG-PLA was continuously used as a polymeric surfactant. In a notation of PEG $_p$ -PLA $_q$, p and q express the M_n of PEG and PLA block, respectively. As a film-forming polymer, PLA (M_w : 75,000-120,000) or poly(ϵ -caprolactone) (PCL) (M_w : 70,000-100,000) was used and they were purchased from Sigma-Aldrich Japan (Tokyo, Japan) and FUJIFILM Wako Pure Chemical Corporation (Osaka, Japan), respectively. Guaranteed reagent of toluene and dichloromethane were used as organic solvent and were purchased from FUJIFILM Wako Pure Chemical Corporation (Osaka, Japan) and used without further distillation.

2.2. Preparation of the polymeric films on the surface of water

a polymeric porous film was tried to obtain by casting polymer solution on the surface of water and subsequent solvent evaporation. 5w/v% solutions of PLA and various compositions of PEG-PLA were prepared in toluene-dichloromethane mixed solvent (8:2 (v/v)). The pre-mixed organic solution (0.2 mL of each solution was mixed) was gently poured onto a glass vessel (inner diameter: 32.4 mm) filled with pure water (5 mL). The vessel was statically placed for 48 h at 25°C in order to spontaneously form w/o emulsions and evaporate the mixed organic solvent. After solvent evaporation, a polymeric thin film was obtained on the surface of water. The wet film was collected and suspended for 12 h in order to naturally dry it. Additionally, a thin film was tried to prepare by using PCL and/or PEG3200-PCL2800 instead of PLA and/or PEG-PLA.

2.3. Observation of the surface morphology of the films

Both sides (the side at liquid-gas interface and water-oil interface) of the obtained films were observed by means of a scanning electron microscope (SEM) (VE-9800, KEYENCE Co., Ltd., Japan, accelerating voltage: 1.0 kV). A naturally dried film was cut and attached onto a fragment of double-sided carbon tape of which the other side was attached to an aluminum plate. The obtained plate was coated with a thin platinum film (in thickness of approximately 10 nm) under a reduced pressure with an MSP-1S ion-coater (Vacuum Device Inc, Ibaraki, Japan).

2.4. Observation of the internal structure of the films

The internal structure of the films was confirmed by observing the cross-section of the films. The film was cut with scissors after freezing it for 1 min in liquid N₂ such that the internal structure would be maintained as it was even after cutting. The fragment of the film was collected and processed as a sample for SEM observation by the same manner described in section 2.3.

2.5. Determination of the composition of the porous films

The composition ratio of each component in the porous films was evaluated by analyzing the ¹H-NMR spectra of the films and each component. The porous films were solved in CDCl₃ and the ¹H-NMR spectrum was obtained. The obtained spectrum includes the specific signals of each component; that is 5.16ppm for alpha hydrogen of carbonyl groups of PLA and 3.64ppm for methylene groups of PEG in PEG-PLA. The molar ratio of PLA and PEG-PLA was determined by comparing the integral ratios of those signals considering the number of ¹H atoms and consequently, the composition ratio of each component (w/w) was determined.

2.6. Evaluation of the effect of temperature and humidity on the morphology of the films

It was predicted that temperature is one of the key factors for controlling the morphology of porous structure because the hydrophilicity of PEG depends on the temperature [15,16]. A PLA film was prepared at 10°C or 35°C by placing a vessel filled with the organic solution on the surface of water in a water bath (relative humidity near the samples was approximately 70%). Additionally, a PLA film was prepared in low humidity at 10°C to investigate the effect of humidity. a plastic box was cooled to 10°C by blowing cold air into the box (relative humidity near the samples was approximately 40%). A vessel containing water and organic solution was put in a small plastic box and the small box was placed in the pre-cooled box such that the airflow would not directly hit the vessel and affect the process of film formation.

3. Results and Discussion

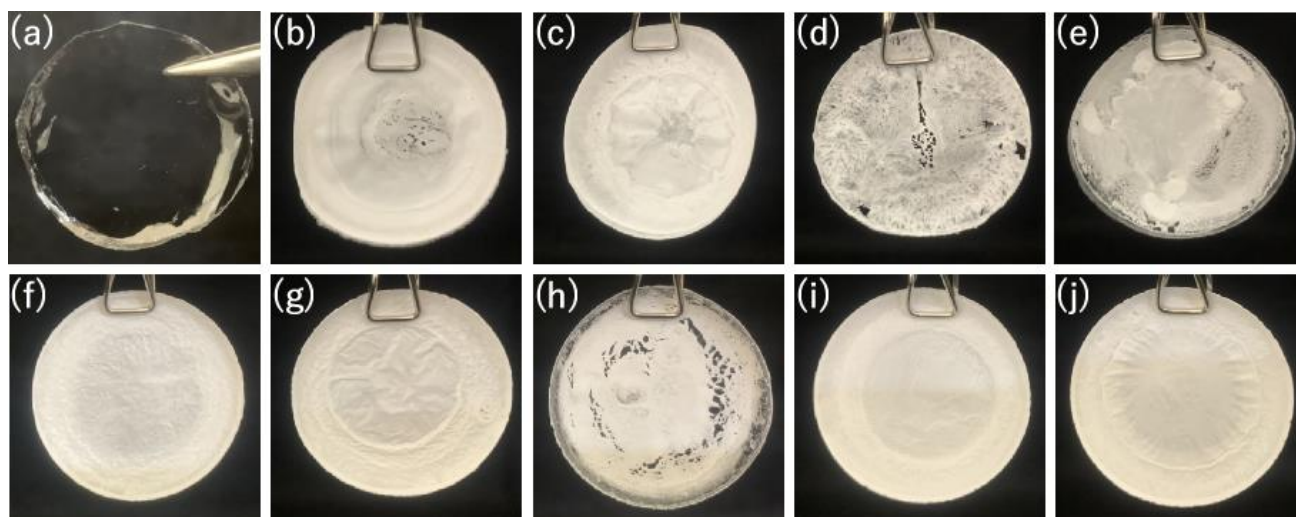


Fig. 2 Appearance of the PLA films. The films were made (a) without PEG-PLA and with (b) PEG3300-PLA3300, (c) PEG3400-PLA5600, (d) PEG3200-PLA9200, (e) PEG5600-PLA2900, (f) PEG6000-PLA6400, (g) PEG6600-PLA8500, (h) PEG9000-PLA3000, (i) PEG9400-PLA6000, and (j) PEG9200-PLA9400.

3.1. Observation of the appearance and the morphology of the films

A vessel containing water and organic solution was placed for 2 days and obtained a polymeric thin film. The appearance of the films is shown in Fig. 2. The film made without PEG-PLA (Fig. 2 (a)) was transparent, whereas most parts of the films made with PEG-PLA (Fig. 2 (b-j)) were white. A transparent film on a glass slide was obtained by casting and evaporating the organic solution of PLA and/or PEG-PLA (data not shown). Thus, the white color of the films (Fig. 2 (b-j)) might result from the structure of the films rather than the components themselves. In the process of solvent evaporation on the surface of water, the organic phase looked white because the light hit spontaneously formed w/o emulsions of which the diameter was 0.5-2 μm [5] and scattered. Therefore, it was expected that the films made with PEG-PLA included the highly porous structure and that their porous structure scattered the light. The white color of the films was deeper in the edge than in the center, which is because of the coffee-ring effect [17]. In a vessel, the evaporation rate of the organic solvent is higher in the edge than in the center of the organic solution. The difference in the evaporation rate of the organic solution caused the capillary flow from the center to the edge of the organic solution. Spontaneously formed water droplets and PEG-PLA orientating on the water-oil interface of the water droplets were moved by that outward flow. As a result, the number of water droplets was higher and the white color was deeper in the edge than in the center.

The surface morphology of both sides of the films is shown in Fig. 3. Fig. 3 demonstrates that numerous pores were formed by using PEG-PLA. It has been reported that by using PEG-PLA as a polymeric surfactant, w/o emulsions are spontaneously formed in an organic phase and they form pores on the surface and the inside of the microparticles [5,18]. The results shown in Fig. 3 and some previous reports indicate that spontaneously formed water droplets worked as the porogens for the obtained materials. This enables us to illustrate the reason for the difference in the morphology of the films between both sides. It has been said with the Stokes equation (Eq. 1) [19]

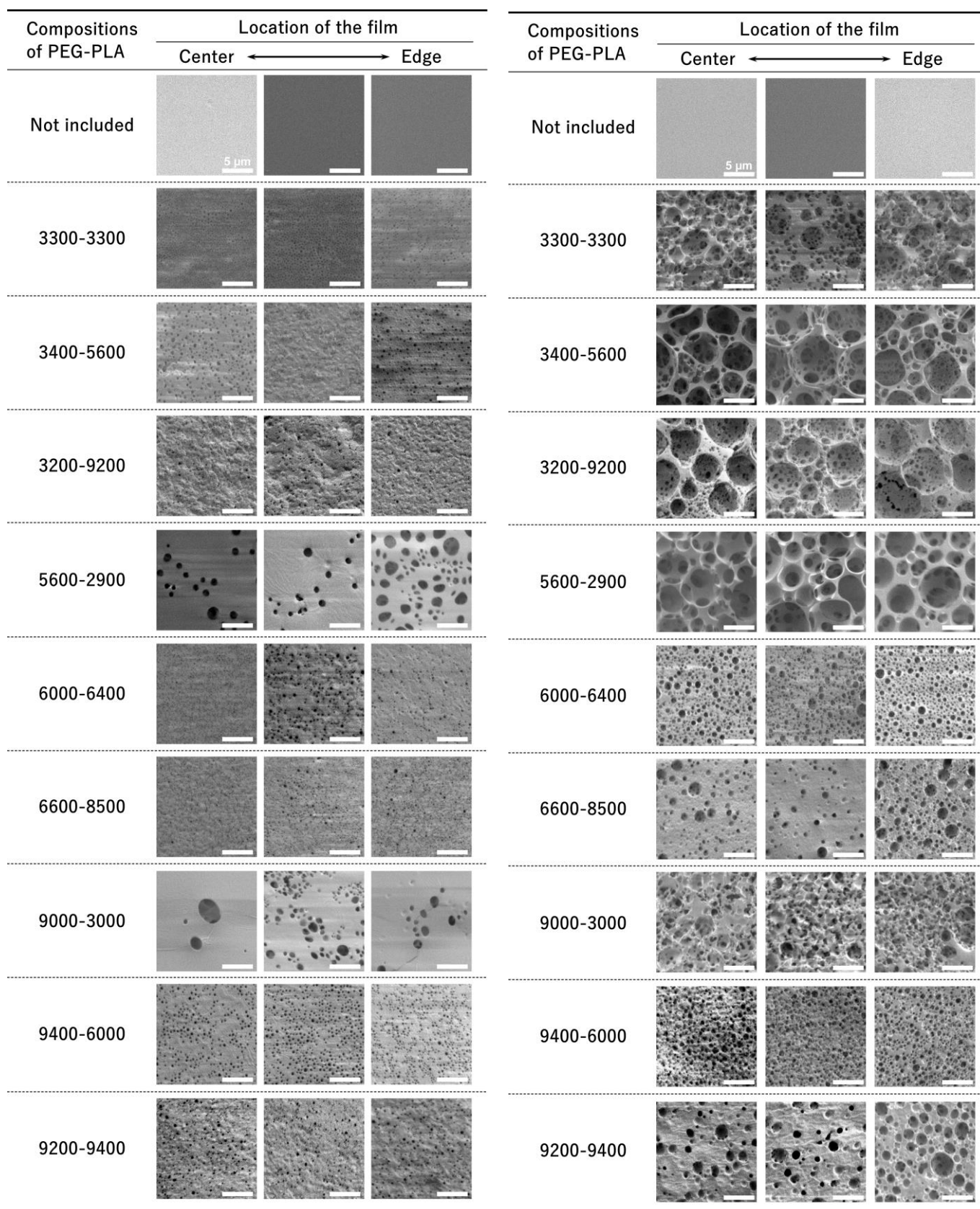


Fig. 3 Effect of compositions of PEG-PLA on the surface morphology of the side of liquid-gas interface (left) and water-oil interface (right) of the PLA films.

that emulsion droplets settle out rapidly as the diameter of a droplet increases:

$$u = \frac{2r^2\Delta\rho g}{9\eta} \quad (\text{Eq. 1})$$

where u is the sedimentation velocity, η is the viscosity of continuous phase, r is the radius of emulsion droplets, $\Delta\rho$ is the difference in the density of dispersed and continuous phase, and g is the gravity acceleration. During porous particle formation, because the organic solvent evaporates during the uniform mixing of an organic solvent and water, the effect of spontaneous w/o emulsion droplets sedimentation does not occur, and pores of approximately the same size formed throughout particles. However, in forming porous films, a polymeric film was prepared on the surface of the aqueous layer by allowing the film to stand without mixing an organic solvent and water. Therefore, it is considered that many large pores derived from spontaneous w/o emulsion droplets with a large diameter were formed on the oil-water interface side, while few numbers of small pores were formed on the gas-liquid interface side. SEM images for a wide range of the locations in the films in Fig. 3 demonstrate that porous structure spreads throughout the films. It was found that on the side of water-oil interface of the films made with a block copolymer of which M_n of PEG block was approximately 3,000 and/or of which M_n of PLA block was approximately 3,000, there were both pores smaller than 1 μm and larger than 3 μm . The reason could be illustrated in terms of the process of spontaneous emulsification and the stability of emulsion droplets according to the previous reports [5,18]. When PEG-PLA of which M_n of PEG block was approximately 3,000 was used, fewer PEG-PLAs orientate on the water-oil interface because of lower hydrophilicity than PEG-PLA of which M_n of PEG block was more than 6,000. The reduction in the number of molecules oriented to the oil-water interface reduces the effect of decreasing interfacial tension, which is the driving force for spontaneous emulsification. The resulting spontaneous emulsion droplets are likely to be large due to their low stability. On the other hand, when PEG-PLA of which M_n of PLA block was approximately 3,000 was used, the emulsion droplets tended to merge with each other by collision because the PLA layer oriented outside of the spontaneous w/o emulsion droplets was thin. In other words, the growth of spontaneous emulsion droplets is thought to increase emulsion droplet size. Furthermore, as shown in Fig. 3, as both sides of the films are porous, it can be expected that the inside of the films will also have a porous structure. Fig.4 shows SEM images of PLA films cross-section, indicating that the films have a porous structure inside them.

3.2. Evaluation of the composition of the porous films

Fig. 5 shows the PEG-PLA fraction and the yield of the porous films. Fig. 5 demonstrates that both values increased as M_n of PLA block of PEG-PLA increased. The results were caused because the hydrophobicity of PEG-PLA is proportional to M_n of the PLA block. A surfactant having PEG chains as the hydrophilic groups spontaneously shifts from organic phase to water phase and this shift causes spontaneous formation of o/w emulsions [1,20,21]. In this system, a slight cloudiness was observed in the water phase as well as cloudy organic phase while placing a vessel. Thus, it was speculated that certain amounts of o/w emulsions were formed in the water phase. However, as M_n of PLA block increased, the entire hydrophilicity of PEG-PLA decreased, thus increasing the number of PEG-PLA molecules distributed to the organic phase. For this reason, the composition ratio of PEG-PLA and the yield of the films was proportional to M_n of the PLA block.

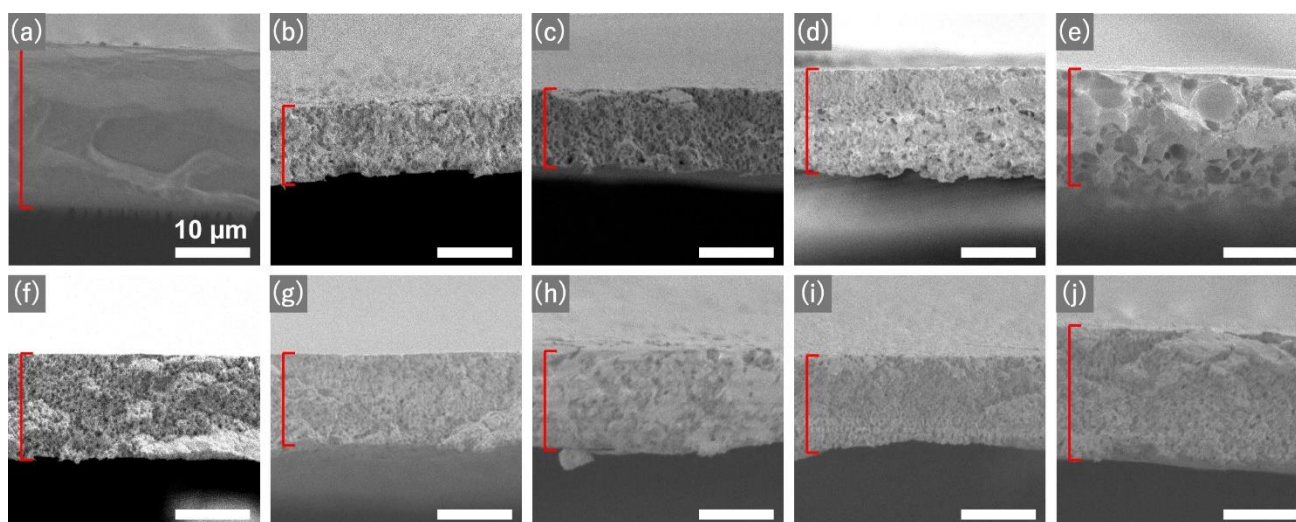


Fig. 4 The cross section of the polymeric films taken by means of SEM. The films were made (a) without PEG-PLA and with (b) PEG3300-PLA3300, (c) PEG3400-PLA5600, (d) PEG3200-PLA9200, (e) PEG5600-PLA2900, (f) PEG6000-PLA6400, (g) PEG6600-PLA8500, (h) PEG9000-PLA3000, (i) PEG9400-PLA6000, and (j) PEG9200-PLA9400.

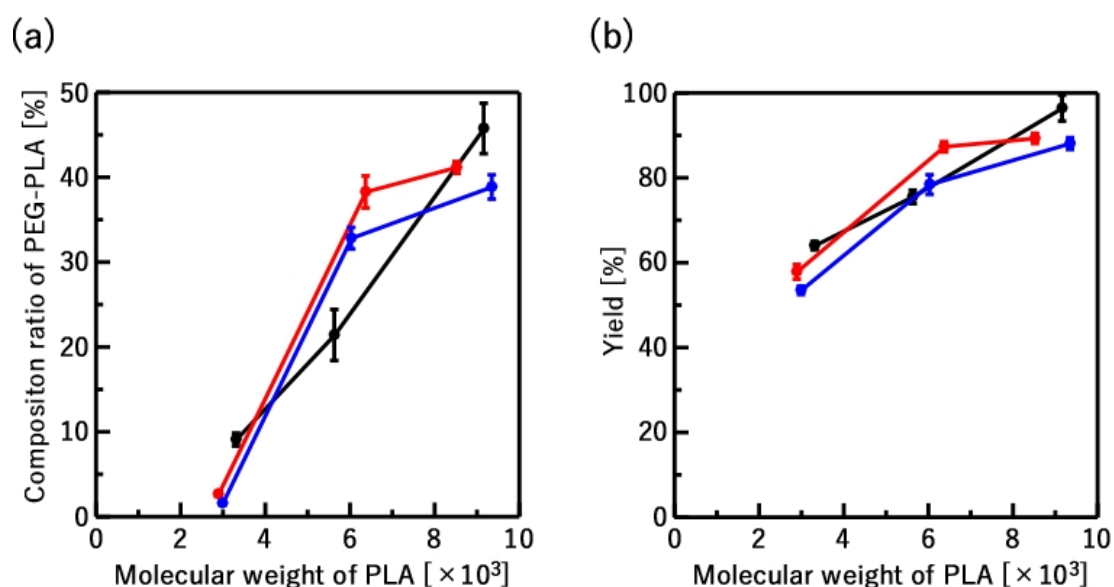


Fig. 5 Effect of the molecular weight of the PLA block of PEG-PLA on (a) composition ratio of PEG-PLA and (b) yield of the porous films. Molecular weight of PEG block was 3200~3400 (black), 5600~6600 (red), and 9000~9400 (blue), respectively.

3.3. Effect of the combination of hydrophobic block and material-forming polymer on the morphology of the materials

Effect of the combination of the hydrophobic block of surfactants and film-forming polymers on the morphology of the films is demonstrated in Fig. 6. Two film-forming polymers (PLA and PCL) and two block copolymers with different hydrophobic blocks (PEG-PLA and PEG-PCL) were examined. When the hydrophobic block of the block copolymer and the film-forming polymer had the same composition (*i.e.*, PEG-PLA and PLA or

PEG-PCL and PCL), the resulting film had a structure in which the pores were interconnected inside the films. By contrast, when the hydrophobic block of the block copolymer and the film-forming polymer had different compositions (*i.e.*, PEG-PLA and PCL), the resulting film had a dimpled surface and no interconnected pores inside the film. Furthermore, for the combination of PEG-PCL and PLA, no films were formed on the water layer after two days. To confirm the generality of these phenomena, the tests were also run using porous particles instead of porous films (Fig. 7) in which almost the same phenomena were observed; particles with porous structures for the combination of PEG-PLA and PLA or that of PEG-PCL and PCL, particles with a dimple surface and densely packed core for the combination of PEG-PLA and PCL, and particles with non-spherical shapes for the combination of PEG-PCL and PLA were obtained. Figs. 6 and 7 strongly suggest that the combination of the hydrophobic block of a surfactant and hydrophobic material-forming polymer greatly affects the morphology of materials. The stability of w/o emulsions increased when hydrophobic molecules having the similar chemical structure to the hydrophobic block of a surfactant coexist in an organic phase [22,23]. In this system, w/o emulsions work as porogens for a polymeric film. Therefore, in the system containing the same hydrophobic block of surfactant and film-forming polymer, a large number of w/o emulsions stayed in an organic phase for a long time and formed the highly porous structure of a film due to the high stability of w/o emulsions.

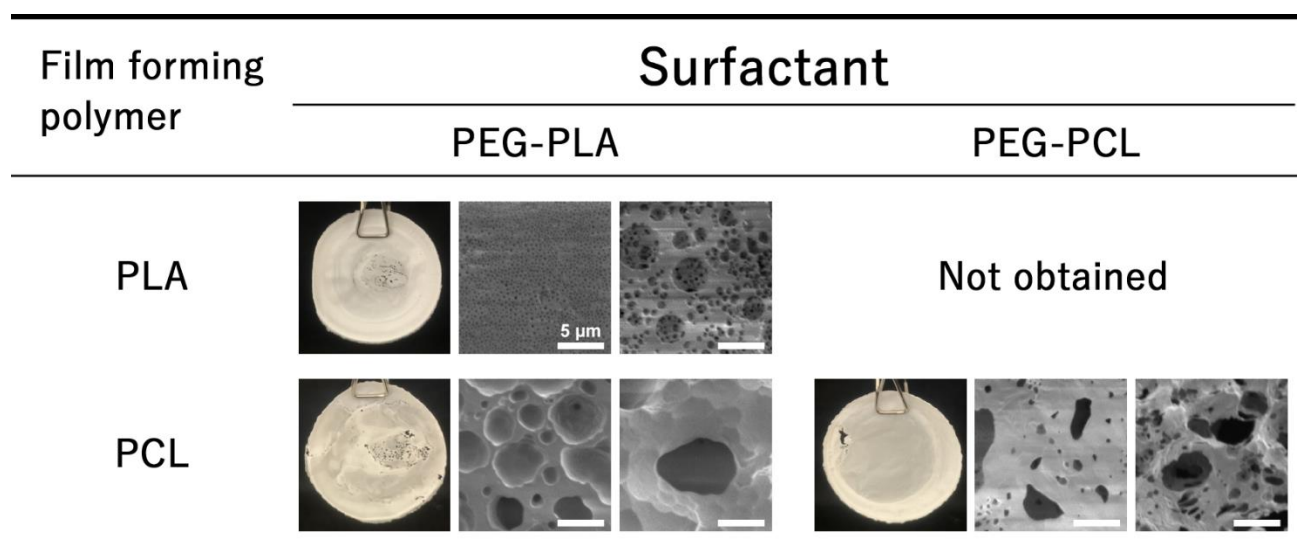


Fig. 6 Effect of combination of surfactant and film-forming polymer on the appearance (left), surface morphology of the side of liquid-gas interface (center), and water-oil interface (right) of the polymeric films.

3.4. Effect of temperature on the morphology of the films

It was speculated that temperature greatly affects the stability of spontaneously formed w/o emulsions and the morphology of the films because hydrophilicity of PEG chains greatly depends on temperature [15,16]. Fig. 8 shows the effect of temperature on the morphology of the films made from PEG-PLA with four different compositions. Firstly, a great change was found in appearance between the films made at 25°C and 35°C. At 35°C, a thin film was not obtained in the system containing PEG3300-PLA3300 and PEG3200-PLA9200, whereas a film of which the center is much thinner than the edge was obtained in the system containing PEG9000-PLA3000 and PEG9200-

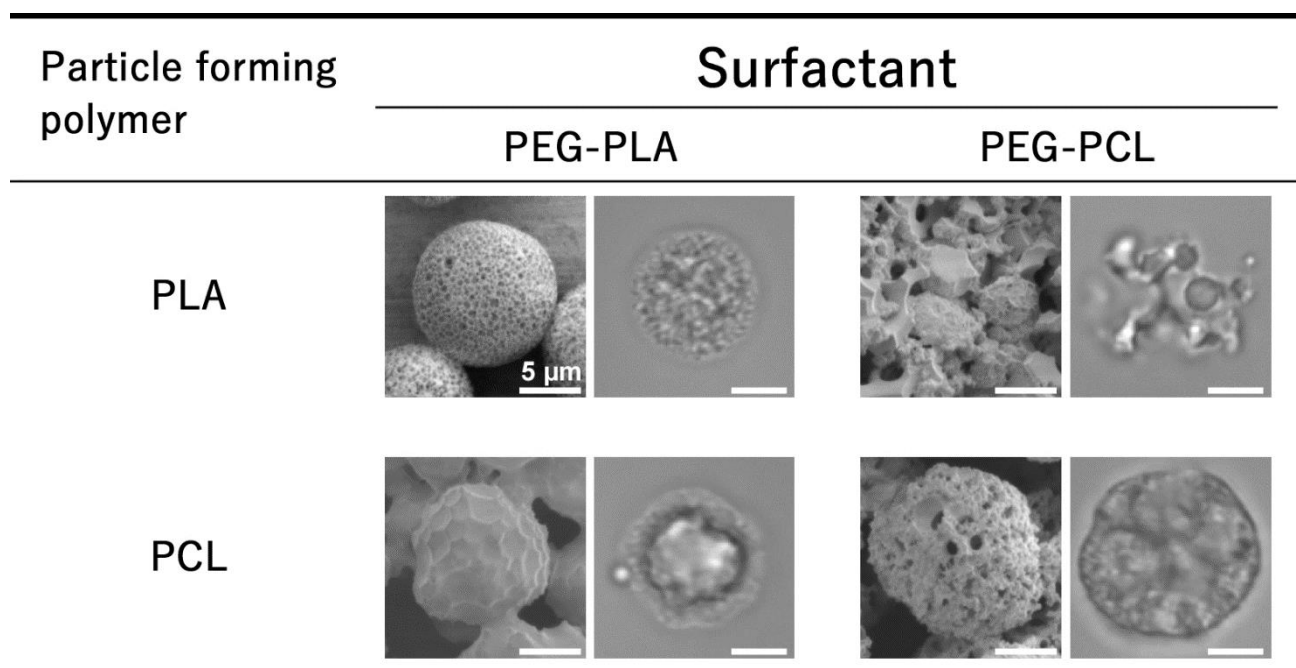


Fig. 7 Effect of combination of surfactant and particle-forming polymer on the surface morphology (left) and internal structure (right) of the polymeric particles.

PLA9400 (Fig. 8 (d, f)). The reason for the results in the system of 35°C was because coffee-ring effect occurred more strongly than in the system of 25°C. In the system where the temperature of a substrate (*i.e.*, the substrate is water in this system) is below 40°C, the direction of Marangoni flow is from the edge to the center [24,25], which means that the direction of Marangoni flow corresponds to the direction of capillary flow described in section 3.1. Therefore, at 35°C, the concentration gradient of the polymers in the organic solution between the center and the edge was larger than at 25°C, thereby forming a film which was thinner in the center and thicker in the edge. The morphology of the side of water-oil interface also changed when the films were made at 35°C. The interconnected pores were observed on the films made at 25°C and 10°C (Figs. 3 and 8 (c, e)), whereas such a structure was not found during the observation of the films made at 35°C (Fig. 8 (d, f)). This is presumably because the hydrophilicity of PEG decreased at higher temperatures, and consequently, the number of spontaneously formed emulsion droplets did not increase as much as the number of pores connected to each other.

On the other hand, an unexpected change was found in morphology of the films made at 10°C. All of the films made at 10°C (Fig. 8 (a, b, c, e)) had many micropores (larger than 5 μm) on the side of liquid-gas interface. These micropores did not exist on all of the films made at 25°C and 35°C and these micropores were found for the first time when the side of liquid-gas interface of the films made at 10°C was observed. It is quite unlikely to consider that these micropores were derived from the spontaneously formed water droplets because large water droplets are presumed to settle out toward water-oil interface and form the large pores on the side of water-oil interface rather than liquid-gas interface as described in Fig. 3. Therefore, Fig. 8 indicates that the micropores on the side of liquid-gas interface were derived from another mechanism. A major possibility is that these micropores were formed by a mechanism similar to that used in the breath figure method. The breath figure method involves preparing a sheet with a honeycomb-like structure and is based on the following procedures [26]: (1) casting of a polymer-dissolving organic

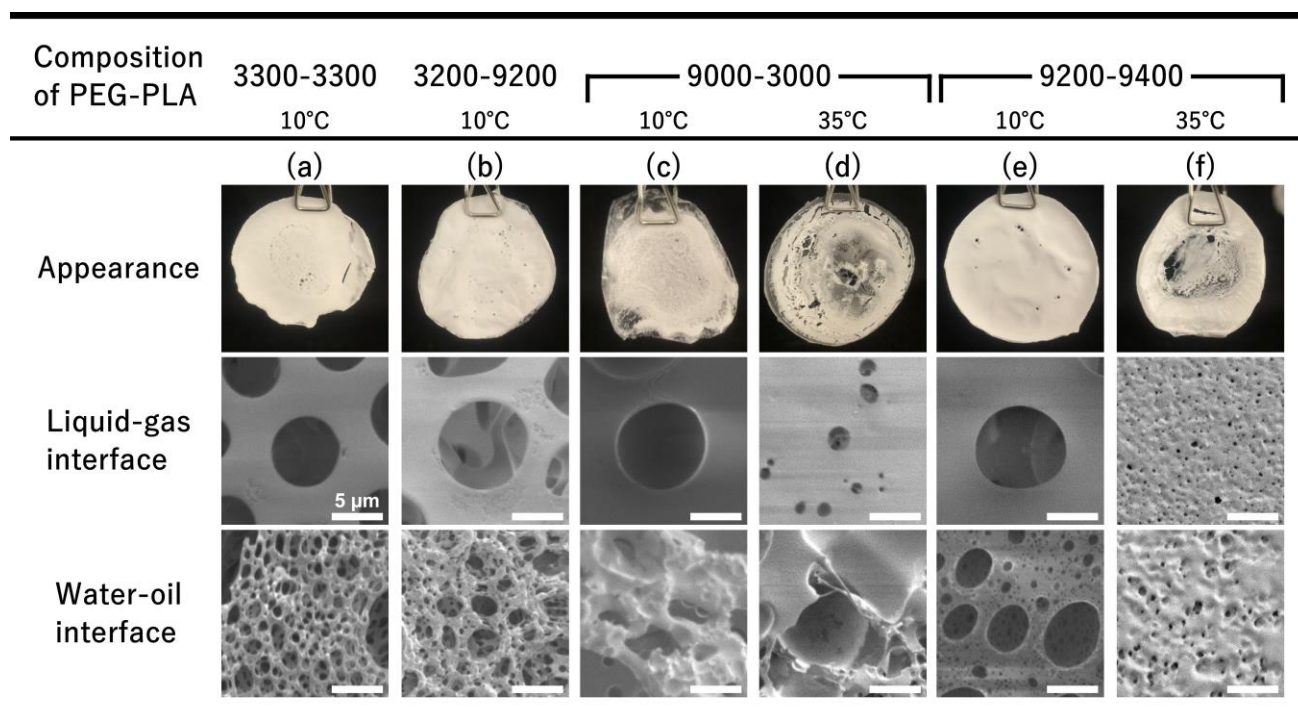


Fig. 8 Effect of the temperature on the appearance and morphology of the PLA films (top: appearance, middle: the side of gas-liquid interface, and bottom: the side of water-oil interface). The films were made with (a) PEG3300-PLA3300, (b) PEG3200-PLA9200, (c, d) PEG9000-PLA3000, and (e, f) PEG9200-PLA9400. The films were made at (a, b, c, e) 10°C and (d, f) 35°C.

solvent on a substrate; (2) evaporation of the organic solvents under high-humidity airflow (generally more than 60% of relative humidity); (3) condensation of water droplets on the surface of the organic solvents by removing the heat due to vaporization; and (4) formation of a polymeric sheet with micropores derived from the water droplets on the side of the liquid-gas interface. In this experimental system, although a high-humidity airflow was not used, the sheet formed under a high relative humidity during the organic-solvent evaporation at 10°C because the vessel where the sheet formed was placed in a water bath with a relative humidity of *ca.* 70%. In addition, as a water bath was set in the environment at such a low temperature, water vapor in the air was likely to be in a state of condensation. Therefore, water droplets condensed in air appeared on the surface of the organic solvent near the air-liquid interface and might have acted as pore-forming agents.

3.5. Effect of humidity on the morphology of the films

It was speculated that the micropores were derived from the water droplets condensed on the liquid-gas interface. In this section, this hypothesis was confirmed by preparing PLA films under the conditions of 10°C and the low relative humidity (approximately 40%). SEM images of both sides of the films are shown in Figs. 9 and 10. It was found that micropores formed on the liquid-gas interface side of the films under high relative humidity conditions, even in the absence of PEG-PLA, which is necessary for the formation of spontaneous emulsions, whereas micropores did not form on the surface under low relative humidity conditions. These results strongly suggest that

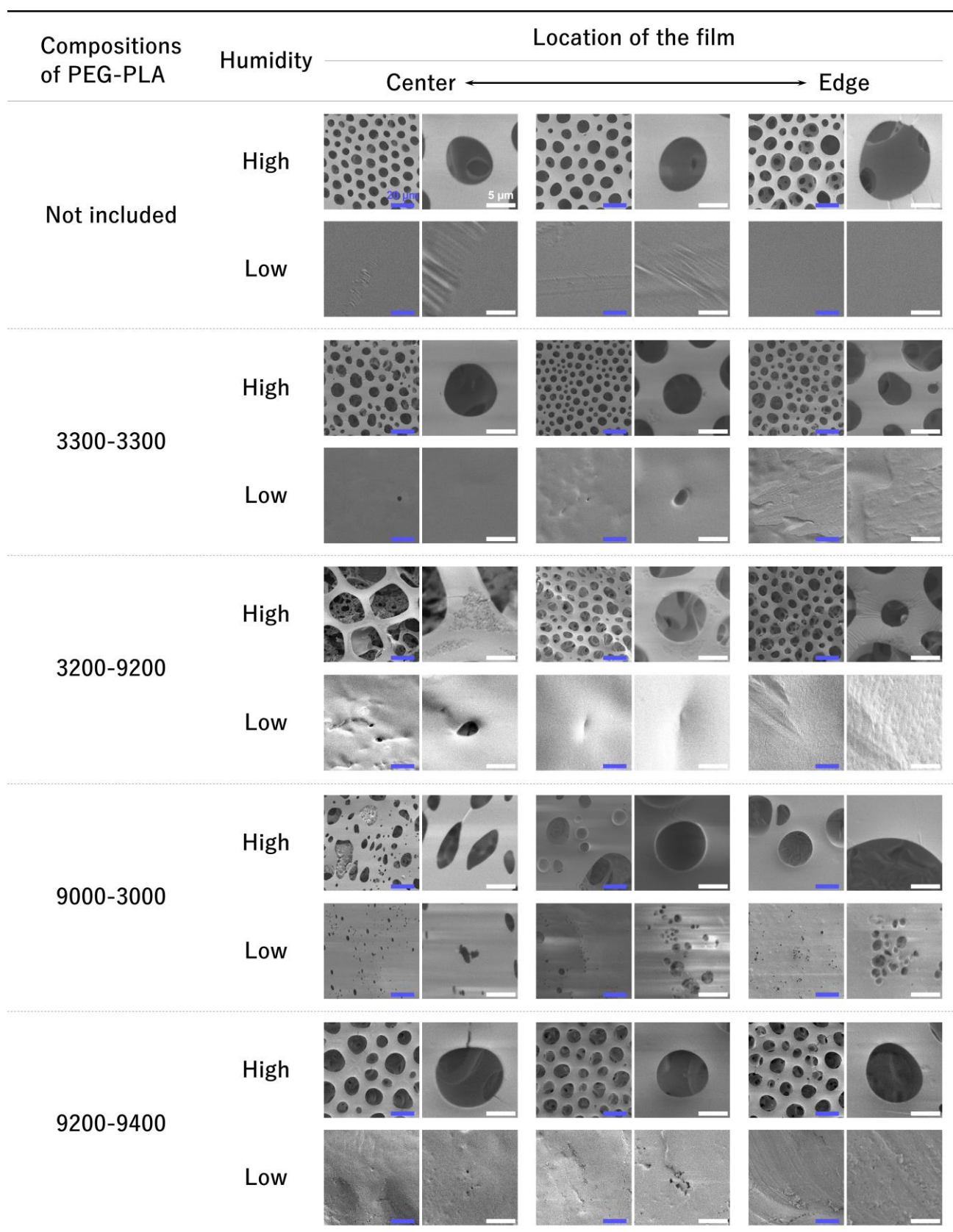


Fig. 9 Effect of the humidity on the morphology of the side of liquid-gas interface of the films.

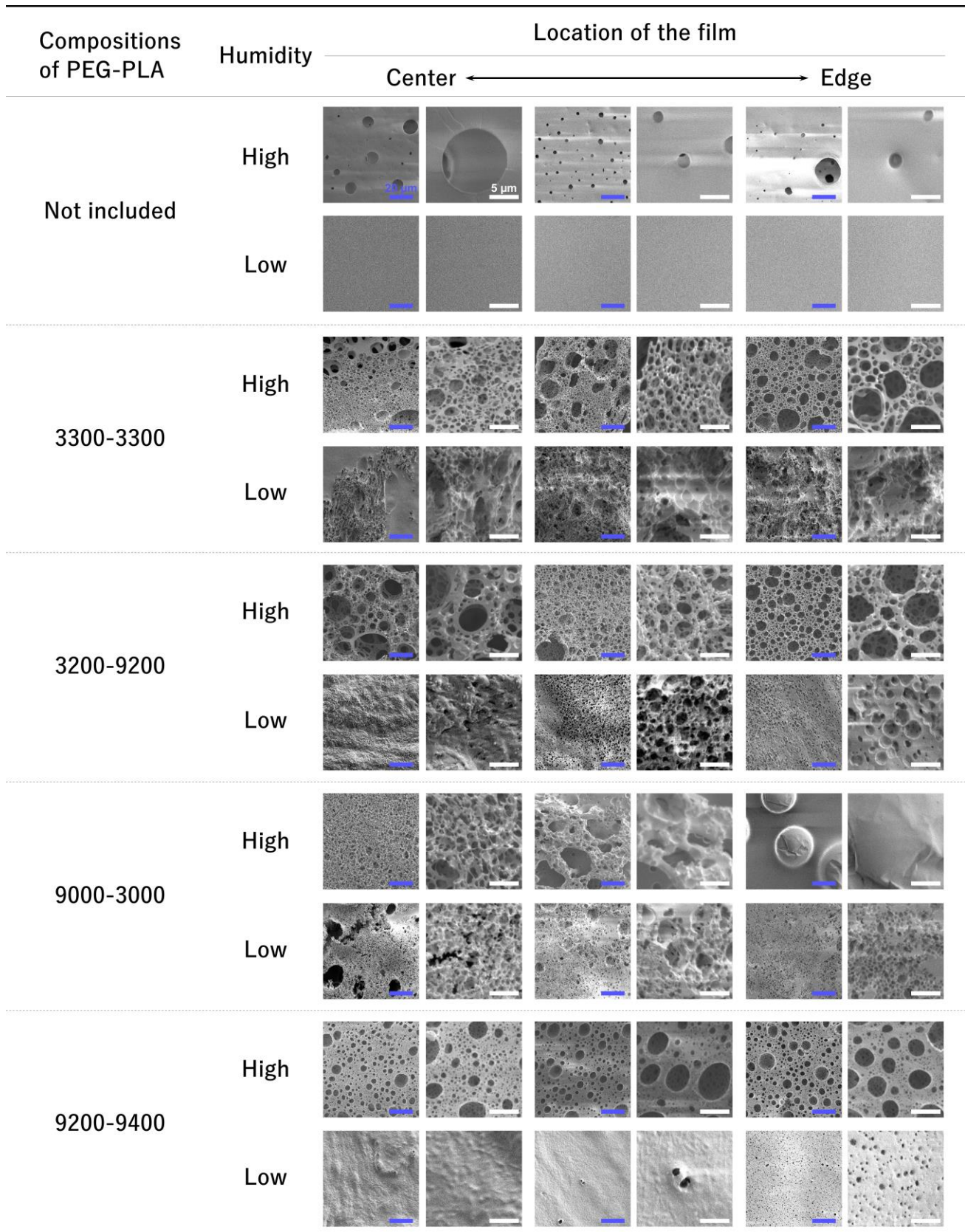


Fig. 10 Effect of the humidity on the morphology of the side of water-oil interface of the films.

the formation of micropores on the liquid-gas interface side of the films is not dependent on the presence or absence of PEG-PLA during film preparation, but it is highly dependent on the relative humidity. Indeed, many reports about the breath figure method revealed that pores could be formed at the relative humidity of more than 60% and that pore diameter was proportional to relative humidity (3-20 μm) [11,12,27–31]. In particular, in the system where PLA was used as a film-forming polymer, the pore diameter was 3-10 μm [31], which was almost the same pore size as this system (Fig. 9). These reports and the results strongly indicate that under the conditions of high humidity and low temperature, micropores could be formed on the side of liquid-gas interface due to condensed water droplets even in the absence of airflow. Besides, the cross section of the films (Fig. 11) shows that there are micropores near the side of the liquid-gas interface, whereas there are small pores (approximately 1 μm) near the side of the water-oil interface. Thus, it was concluded that spontaneous emulsification and condensation could be used at the same time in order to form a porous structure.

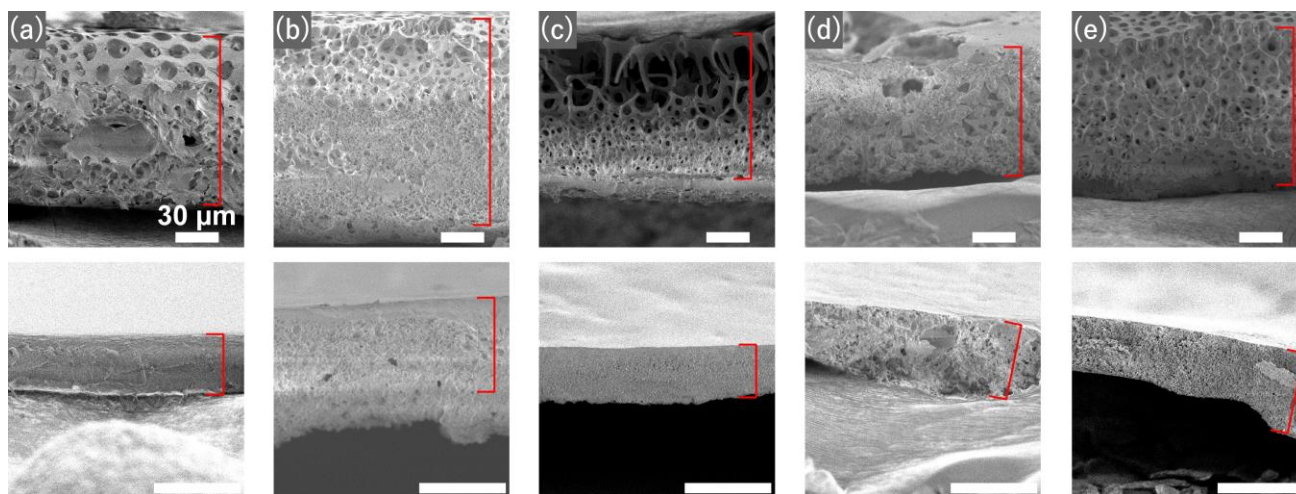


Fig. 11 SEM images of the cross section of the films prepared at 10°C. The relative humidity was approximately (top) 70% and (bottom) 40%.

Fig. 12 shows the pore formation mechanism and the illustration of difference in pore size between both sides of the PLA films. Under the conditions of high temperature (more than 25°C) or both temperature and relative humidity are low (less than 10°C and less than 40%, respectively), only spontaneously formed w/o emulsions, which were formed by PEG-PLA, work as porogens. Water droplets (with a diameter of 0.5-2 μm [5]) tend to settle down and merge near the water-oil interface. Therefore, pore size on the side of the water-oil interface was larger than on the side of the liquid-gas interface. On the other hand, both spontaneously formed w/o emulsions and condensed water droplets work as porogens under the conditions of low temperature (less than 10°C) and high humidity (more than 60%). Spontaneously formed water droplets probably behave similar to the system of high temperature or low temperature and low humidity. Furthermore, water vapor condenses on liquid-gas interface and form micropores. Thus, pore size on the side of water-oil interface was smaller than on the side of liquid-gas interface. By using spontaneous emulsification, a film with unique structure was successfully obtained: different in pore size between both sides of the films. Moreover, condensation of water vapor can be used under the conditions of low temperature

and high humidity, which enables us to control the pore size of the films in a wider range.

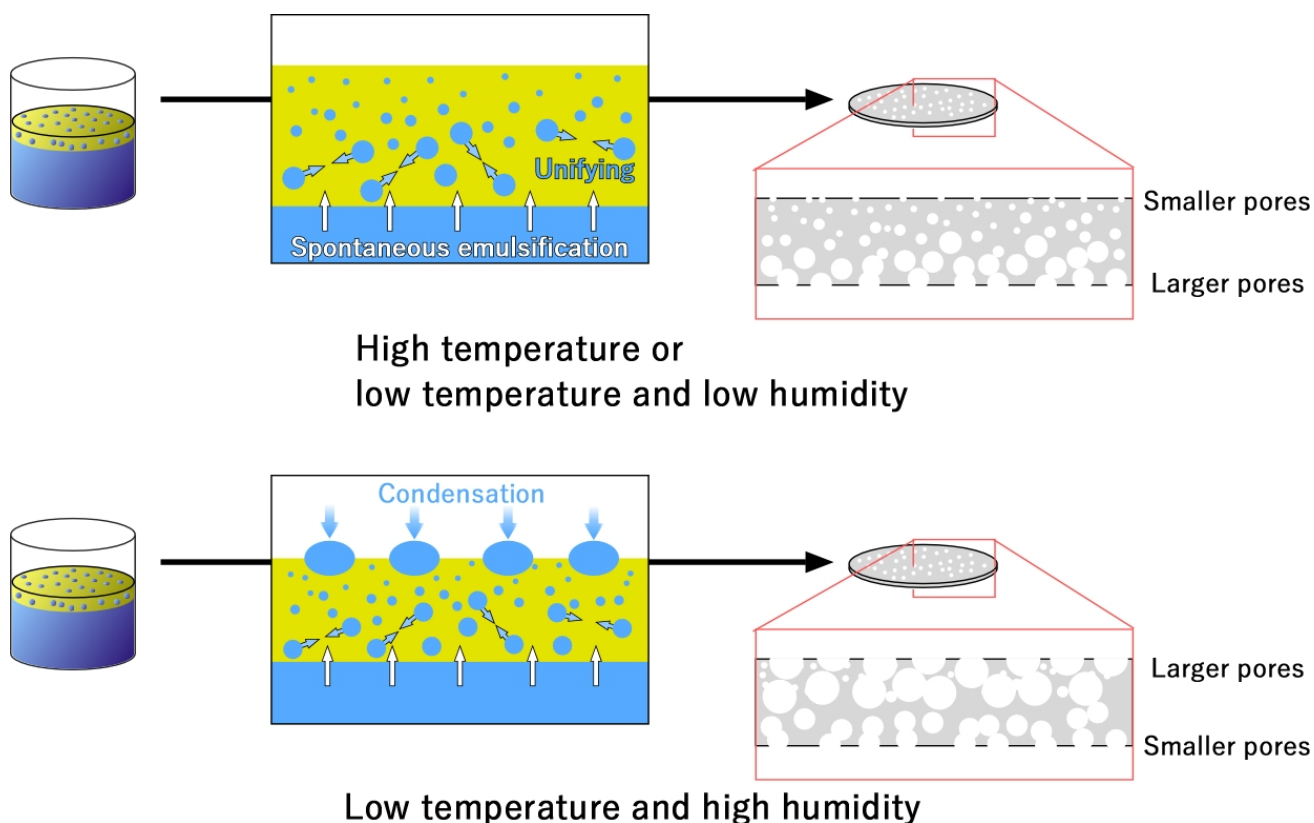


Fig. 12 Pore formation mechanism and illustration of difference in pore size between both sides of the PLA films.

4. Conclusion

An easy and cost-effective method have been established for preparation of the porous particles utilizing spontaneous emulsification [5,18]. It was expected that spontaneous emulsification could be applied to preparation for another shape of porous material. Indeed, a porous film was successfully obtained by utilizing spontaneous emulsification in this study. Moreover, it was revealed that the combination of the hydrophobic block of a surfactant and the hydrophobic material-forming polymer is a dominant factor for the formation and the morphology of a film. the effect of temperature and humidity on the morphology of the films was also investigated. As a result, a film having micropores of more than 5 μm on the side of the liquid-gas interface was unexpectedly obtained under the conditions of low temperature and high humidity. By observing the cross section of the films including a film made without PEG-PLA, it was strongly suggested that both spontaneous emulsification near water-oil interface and condensation of water vapor on liquid-gas interface can be used at the same time for preparing porous structure; in other words, the pore size of the porous film can be controlled in a wide range of about several hundred nm to 10 μm by tuning the composition of the amphiphilic block copolymer, temperature, and humidity. In conclusion, the porous film

should be expected to be applied as a novel biomaterial such as a platform for sustainable drug release and a substrate for cell culture by controlling its porous structure.

5 References

- [1] A.H. Saberi, Y. Fang, D.J. McClements, Fabrication of vitamin E-enriched nanoemulsions: Factors affecting particle size using spontaneous emulsification, *J. Colloid Interface Sci.* 391 (2013) 95–102. <https://doi.org/10.1016/j.jcis.2012.08.069>.
- [2] G. Davidov-Pardo, D.J. McClements, Nutraceutical delivery systems: Resveratrol encapsulation in grape seed oil nanoemulsions formed by spontaneous emulsification, *Food Chem.* 167 (2015) 205–212. <https://doi.org/10.1016/j.foodchem.2014.06.082>.
- [3] M. Beck-Broichsitter, E. Rytting, T. Lehardt, X. Wang, T. Kissel, Preparation of nanoparticles by solvent displacement for drug delivery: A shift in the “ouzo region” upon drug loading, *Eur. J. Pharm. Sci.* 41 (2010) 244–253. <https://doi.org/10.1016/j.ejps.2010.06.007>.
- [4] Y. Weerapol, S. Limmatvapirat, M. Kumpugdee-Vollrath, P. Sriamornsak, Spontaneous Emulsification of Nifedipine-Loaded Self-Nanoemulsifying Drug Delivery System, *AAPS PharmSciTech.* 16 (2014) 435–443. <https://doi.org/10.1208/s12249-014-0238-0>.
- [5] T. Takami, Y. Murakami, Unexpected and successful “one-step” formation of porous polymeric particles only by mixing organic solvent and water under “low-energy-input” conditions, *Langmuir.* 30 (2014) 3329–3336. <https://doi.org/10.1021/la500324j>.
- [6] C. Li, W. Wang, X. Wang, H. Jiang, J. Zhu, S. Lin, Fabrication of porous polymer microspheres by tuning amphiphilicity of the polymer and emulsion-solvent evaporation processing, *Eur. Polym. J.* 68 (2015) 409–418. <https://doi.org/10.1016/j.eurpolymj.2015.05.011>.
- [7] K.H. Ku, J.M. Shin, D. Klinger, S.G. Jang, R.C. Hayward, C.J. Hawker, B.J. Kim, Particles with Tunable Porosity and Morphology by Controlling Interfacial Instability in Block Copolymer Emulsions, *ACS Nano.* 10 (2016) 5243–5251. <https://doi.org/10.1021/acs.nano.6b00985>.
- [8] X. Gao, F. Gao, L. Chen, Y. Yao, T. Chen, S. Lin, Tuning the morphology of amphiphilic copolymer aggregates by compound emulsifier via emulsion–solvent evaporation, *J. Saudi Chem. Soc.* 22 (2018) 297–305. <https://doi.org/10.1016/j.jscs.2016.05.007>.
- [9] K.E. Park, B.S. Kim, M.H. Kim, H.K. You, J. Lee, W.H. Park, Basic fibroblast growth factor-encapsulated PCL nano/microfibrous composite scaffolds for bone regeneration, *Polymer (Guildf).* 76 (2015) 8–16. <https://doi.org/10.1016/j.polymer.2015.08.024>.
- [10] Q. Zhang, H. Lu, N. Kawazoe, G. Chen, Pore size effect of collagen scaffolds on cartilage regeneration, *Acta Biomater.* 10 (2014) 2005–2013. <https://doi.org/10.1016/j.actbio.2013.12.042>.
- [11] T. Ponnusamy, H. Yu, V.T. John, R.S. Ayyala, D.A. Blake, A novel antiproliferative drug coating for glaucoma drainage devices, *J. Glaucoma.* 23 (2014) 526–534. <https://doi.org/10.1097/IJG.0b013e318294869b>.
- [12] G. Daban, C. Bayram, B. Bozdoğan, E.B. Denkbaş, Porous polyurethane film fabricated via the breath figure

- approach for sustained drug release, *J. Appl. Polym. Sci.* 136 (2019) 1–9. <https://doi.org/10.1002/app.47658>.
- [13] M.G. Haugh, T.J. Vaughan, C.M. Madl, R.M. Raftery, L.M. McNamara, F.J. O'Brien, S.C. Heilshorn, Investigating the interplay between substrate stiffness and ligand chemistry in directing mesenchymal stem cell differentiation within 3D macro-porous substrates, *Biomaterials*. 171 (2018) 23–33. <https://doi.org/10.1016/j.biomaterials.2018.04.026>.
- [14] V.H. Fragal, D.M. Catori, E.H. Fragal, F.P. Garcia, C. V. Nakamura, A.F. Rubira, R. Silva, Two-dimensional thermoresponsive sub-microporous substrate for accelerated cell tissue growth and facile detachment, *J. Colloid Interface Sci.* 547 (2019) 78–86. <https://doi.org/10.1016/j.jcis.2019.03.071>.
- [15] T. Muraoka, K. Adachi, M. Ui, S. Kawasaki, N. Sadhukhan, H. Obara, H. Tochio, M. Shirakawa, K. Kinbara, A structured monodisperse PEG for the effective suppression of protein aggregation, *Angew. Chemie - Int. Ed.* 52 (2013) 2430–2434. <https://doi.org/10.1002/anie.201206563>.
- [16] S. Kawasaki, T. Muraoka, H. Obara, T. Ishii, T. Hamada, K. Kinbara, Thermally driven micrometer-scale aqueous-phase separation of amphiphilic oligoethylene glycol analogues, *Chem. - An Asian J.* 9 (2014) 2778–2788. <https://doi.org/10.1002/asia.201402134>.
- [17] D. Mampallil, H.B. Eral, A review on suppression and utilization of the coffee-ring effect, *Adv. Colloid Interface Sci.* 252 (2018) 38–54. <https://doi.org/10.1016/j.cis.2017.12.008>.
- [18] S. Nishimura, T. Takami, Y. Murakami, Porous PLGA microparticles formed by “one-step” emulsification for pulmonary drug delivery: The surface morphology and the aerodynamic properties, *Colloids Surfaces B Biointerfaces*. 159 (2017) 318–326. <https://doi.org/10.1016/j.colsurfb.2017.08.004>.
- [19] K. Sakai, S. Iijima, R. Ikeda, T. Endo, T. Yamazaki, Y. Yamashita, M. Natsuisaka, H. Sakai, M. Abe, K. Sakamoto, Water-in-oil emulsions prepared by peptide-silicone hybrid polymers as active interfacial modifier: Effects of silicone oil species on dispersion stability of emulsions, *J. Oleo Sci.* 62 (2013) 505–511. <https://doi.org/10.5650/jos.62.505>.
- [20] Y. An, X. Yan, B. Li, Y. Li, Microencapsulation of capsanthin by self-emulsifying nanoemulsions and stability evaluation, *Eur. Food Res. Technol.* 239 (2014) 1077–1085. <https://doi.org/10.1007/s00217-014-2328-3>.
- [21] Y. Chang, L. McLandsborough, D.J. McClements, Physicochemical properties and antimicrobial efficacy of carvacrol nanoemulsions formed by spontaneous emulsification, *J. Agric. Food Chem.* 61 (2013) 8906–8913. <https://doi.org/10.1021/jf402147p>.
- [22] E. Sadecka, H. Szeląg, One-step synthesis of W/O and O/W emulsifiers in the presence of surface active agents, *J. Surfactants Deterg.* 16 (2013) 305–315. <https://doi.org/10.1007/s11743-012-1404-6>.
- [23] N. GARTI, G.F. REMON, Relationship between nature of vegetable oil, emulsifier and the stability of w/o emulsion, *Int. J. Food Sci. Technol.* 19 (1984) 711–717. <https://doi.org/10.1111/j.1365-2621.1984.tb01890.x>.
- [24] Y. Li, C. Lv, Z. Li, D. Quéré, Q. Zheng, From coffee rings to coffee eyes, *Soft Matter*. 11 (2015) 4669–4673. <https://doi.org/10.1039/c5sm00654f>.
- [25] A.D. Nikolov, D.T. Wasan, P. Wu, Marangoni Flow Alters Wetting: Coffee Ring and Super-spreading, *Curr. Opin. Colloid Interface Sci.* (2020). <https://doi.org/10.1016/j.cocis.2020.08.012>.
- [26] G. Widawski, M. Rawiso, B. François, Self-organized honeycomb morphology of star-polymer polystyrene films, *Nature*. 369 (1994) 387–389. <https://doi.org/10.1038/369387a0>.

- [27] M.T. Calejo, J. Saari, H. Vuorenpää, E. Vuorimaa-Laukkanen, P. Kallio, K. Aalto-Setälä, S. Miettinen, H. Skottman, M. Kellomäki, K. Juuti-Uusitalo, Co-culture of human induced pluripotent stem cell-derived retinal pigment epithelial cells and endothelial cells on double collagen-coated honeycomb films, *Acta Biomater.* 101 (2020) 327–343. <https://doi.org/10.1016/j.actbio.2019.11.002>.
- [28] B. Yao, Q. Zhu, L. Yao, J. Hao, Fabrication of honeycomb-structured poly(ethylene glycol)-block-poly(lactic acid) porous films and biomedical applications for cell growth, *Appl. Surf. Sci.* 332 (2015) 287–294. <https://doi.org/10.1016/j.apsusc.2015.01.170>.
- [29] C. Huang, X. Shen, X. Liu, Z. Chen, B. Shu, L. Wan, H. Liu, J. He, Hybrid breath figure method: A new insight in Petri dishes for cell culture, *J. Colloid Interface Sci.* 541 (2019) 114–122. <https://doi.org/10.1016/j.jcis.2019.01.074>.
- [30] A. del Campo, C. Echeverría, M. San Martín, R. Cuervo-Rodríguez, M. Fernández-García, A. Muñoz-Bonilla, Porous Microstructured Surfaces with pH-Trigged Antibacterial Properties, *Macromol. Biosci.* 19 (2019) 1–9. <https://doi.org/10.1002/mabi.201900127>.
- [31] H. Abe, Y. Hirai, H. Yabu, Thermally Stable Honeycomb-Patterned Porous Films of a Poly(L-lactic acid) and Poly(D-lactic acid) Stereo Complex Prepared Using the Breath Figure Technique, *Macromol. Mater. Eng.* 301 (2016) 523–529. <https://doi.org/10.1002/mame.201500474>.

Chapter 5

General conclusion of this thesis

This doctoral thesis is a study of the preparation of porous materials using a low energy emulsification method. Emulsions have been used in familiar areas such as food and cosmetics from before. In chapter 1, the usage of emulsions, especially in the medical field, is reviewed. Emulsions used in the medical field are mainly nanometer-sized ones. This means that they require extremely high-energy input such as ultrasound irradiation and high-speed agitation. Therefore, the use of emulsions as carriers for transporting substances encapsulated in the dispersed phase has been a challenge because of the risk of destroying the encapsulated substances. Therefore, a low-energy emulsification method was focused on. The low-energy emulsification method uses intrinsic chemical energy in the system and requires little or no external energy input. Therefore, it has attracted attention as a method for encapsulating drugs in the dispersed phase without destroying their structure. Spontaneous emulsification, one of the low-energy emulsification processes, is considered to occur due to non-uniformity of temperature at the interface or due to non-uniformity in the local concentration of surfactant adsorbed on the interface. Droplets spontaneously form against the continuous phase due to interfacial turbulence that occur to resolve these non-equilibrium conditions. Studies using spontaneous emulsification have mostly dealt with “o/w type” emulsions. This is due to the fact that the emulsion-evaporation method is the predominant method for preparing nanoparticles. That is, it is more convenient to use emulsions in which the organic solvent is the dispersed phase because it is necessary to use volatile solvents that can be removed from the emulsions. Therefore, spontaneous emulsification has been used as a convenient way to shape the outline of “spherical” particles.

On the other hand, Murakami recently discovered by chance that dissolving PEG-PLA in an organic solvent induces “w/o type” spontaneous emulsification. Using this phenomenon, w/o/w emulsions were successfully prepared from spontaneously formed w/o emulsions and pure water in a one-step mechanical emulsification and obtained porous particles using them as precursors. This is the first report on the use of spontaneous emulsification to form a porous structure rather than a particle’s spherical outline. This method is a low-energy consuming and simple preparation method because it can spontaneously complete the preparation of w/o emulsions, which in the conventional method requires the application of extremely high energy. Moreover, because the energy applied is low, the possibility of destruction of the encapsulated material is low. In other words, the application of spontaneous emulsification to the preparation of porous materials is useful.

Porous materials are used in various kinds of applications in the medical field. The second half of chapter 1 reviewed their various forms and applications. Particle type porous materials can be most skillfully used as drug carriers for pulmonary DDS. Drug carriers for pulmonary delivery should have high delivery efficiency to the lungs and even have the ability to avoid phagocytosis by alveolar macrophages. Porous particles are considered to have a

lower particle density than non-porous particles. Therefore, it is expected to have both an aerodynamic particle diameter suitable for pulmonary delivery and a geometric particle diameter suitable for avoiding phagocytosis from alveolar macrophages. Two-dimensional porous materials can be used in many situations such as tissue regeneration scaffolds, drug delivery systems, and biosensors. In other words, two-dimensional porous materials are widely used in the medical field, both inside and outside the body. Microneedles are a patchy material consisting of many small protrusions less than 1 mm in height. By making the surface of non-porous microneedles porous or creating microneedles with a porous structure, new applications are emerging, such as biological fluid collectors using capillary action or stimuli-responsive smart materials, instead of conventional microneedles for drug administration only. possible. As described above, porous materials have a very wide range of applications as biomaterials. In other words, if porous materials can be fabricated by using spontaneous emulsification, which is a low energy emulsification method, they will be very useful in various fields. In later chapters, the preparation of porous materials using spontaneous emulsification, especially for particulate and film materials, is reported.

In Chapter 2, the feasibility of these particles as drug carriers for pulmonary delivery was evaluated based on the basic techniques for porous particles that have been previously reported. Porous particles with different surface morphology and with a geometric diameter of 5 μm or 10 μm were prepared. These particles were then evaluated for their basic properties. The results showed that the porous particles had an extremely low density (about 0.03 g/cm^3). The pulmonary delivery efficiency of the prepared particles was evaluated *in vitro*. The results showed that 5 μm porous particles and even 10 μm porous particles had higher delivery efficiency to the lungs than 5 μm non-porous particles. Particularly high deposition rates were observed in the bronchi, which are difficult to reach with conventional particles. In other words, the porous particles were found to have a high delivery capacity to the deep lung due to their low particle density, while having a geometric diameter that may be advantageous in avoiding phagocytosis. On the other hand, the correlation between the surface morphology and the aerodynamic behavior of the particles was not detailed. One possible explanation for this is that the morphology of the particles changes simultaneously with the modification by PEG on the surface of the particles, which is considered to be involved in the adhesion force of the particles. In this chapter, the surface morphology of the particles was tuned by adjusting the molecular weight of PEG block. Therefore, the simultaneous changes in both the modified state of the particle surface and the particle surface morphology, which are considered to affect aerodynamic behavior, made it difficult to elucidate the effects of each factor on the aerodynamic behavior.

Therefore, in Chapter 3, a method to precisely control the morphology of the porous particles was investigated. The morphology of the porous particles is controlled in a way that is independent of PEG molecular weight. In this chapter, particular attention was paid to the properties of organic solvents. The mixing ratios of toluene and dichloromethane mixtures were varied. It was found that as the mixing ratio of dichloromethane increased, the number of voids inside the particles decreased and cores formed. Further investigation suggested that the internal structure of the particles changed in this experimental system depending on the ratio of favorable (toluene) and unfavorable (dichloromethane) solvents for the stability of the emulsions. That is, the porous structure can be precisely controlled by varying the mixing ratio of organic solvents before and the removal rate of organic solvents after preparation of w/o/w emulsions, respectively. Using this method, it will be possible to independently control the PEG-modified state of the particle surface and the morphology of the particles and to evaluate the aerodynamic

behavior of the porous particles in detail.

In Chapter 4, the incorporation of a porous structure into a film-type material using spontaneous emulsification was investigated. In the preparation of the porous particles, particles of several μm were prepared by applying moderate energy. On the other hand, in this chapter, a polymeric solution is gently dropped onto pure water and the organic solvent is removed without any artificial emulsification. It was expected that a film-like porous material would form on the water surface by this method. The results of the study showed that the porous films with larger interconnected pores on the water-oil interface side than on the gas-liquid interface side were obtained. After further investigation, the film was formed at low temperature (10°C) and high humidity (70%), the unique porous film with a few micrometers of pores derived from spontaneously formed emulsions at the water-oil interface and huge pores of more than $10\ \mu\text{m}$ derived from condensed water droplets at the gas-liquid interface was formed. The structure with both small pores (about $1\ \mu\text{m}$) and large pores (more than $10\ \mu\text{m}$) is greatly advantageous for cell culture, which means that this porous film can be used as a new biomaterial. In other words, this porous film has potential applications as a novel biomaterial.

In the above chapters, the fabrication of porous materials based on spontaneous emulsification and their applications has been discussed. For the porous particles, outstanding results were obtained, showing promise as drug carriers for pulmonary DDS. It was also newly possible to precisely control the porous structure by factors independent of the composition of the block copolymers. As a result of fundamental investigations to prepare the newly proposed porous film materials, the films with unique porous structure were successfully fabricated. In summary, particle and film type porous biomaterials have been successfully fabricated using spontaneous emulsification. This study is a pioneering method for the preparation of low energy emulsions for porous materials with low energy cost and easy encapsulation of materials.

Acknowledgement

I would like to express my gratitude to many people and organizations for their cooperation in conducting this research and writing this doctoral thesis.

I would like to express my sincere gratitude to Professor Yoshihiko Murakami, my primary supervisor, for his guidance in all aspects of my research, including the concept of this research, experimental design, and basic experimental techniques. Thanks to his persistent guidance, I was able to write this doctoral thesis and academic paper. I would like to express my deepest gratitude to him.

In writing this doctoral thesis, I would like to thank my associate referees, Prof. Hiromu Saito, Prof. Toshiyuki Watanabe, Prof. Takeshi Shimomura, and Associate Prof. Koji Nakano, for their many sharp comments and suggestions to improve this research. I would like to express my gratitude to all of them.

I would like to thank the Futaba Foundation for providing me with financial support through a scholarship to carry out this research. It is no exaggeration to say that it is thanks to this support that I have been able to concentrate on my research. I also received financial support for my research from the Japan Science Society. There is no doubt that their expectation for the future of this research has been a great motivation for me to carry out my research. I would like to express my heartfelt gratitude to both organizations.

Finally, I would like to express my gratitude to all the members of Murakami Laboratory. I would like to express my sincere gratitude to all the members of Murakami Laboratory, including my seniors who gave me advice on experiments, my classmates who worked hard together, and my juniors who befriended me not only in experiments but also in private. I would like to express my gratitude to all of them.

Finally, I would like to express my gratitude again to all the people who have helped me in carrying out this research.

March 2021

Shinnosuke NISHIMURA